NSK Technical Journal

Motion & Control

No. 25 September 2015

ISSN1342-3630

NSK

MOTION & CONTROL No. 25
NSK Technical Journal
Printed and Published: September 2015
ISSN1342-3630
Publisher: NSK Ltd., Ohsaki, Shinagawa, Tokyo, JAPAN
Public Relations Department
TEL +81-3-3779-7050
FAX +81-3-3779-7431
Editor: Naoki MITSUE
Managing Editor: Hitoshi EBISAWA
Design, Typesetting & Printing: Kuge Printing Co., Ltd.

NSK Technical Journal
Motion & Control
No. 25
September 2015

NSK

Contents

Technical Articles

Coupled Simulation of Starved Elastohydrodynamic Lubrication and Liquid Film Flow ..... *K. Shibasaki* 1
Differences in Preventive Mechanisms for Fretting Wear between Oil and Grease Lubrication ..... *T. Maruyama, T. Saitoh* 11
Development of a Robot Substitute for a Guide Dog ..... *K.Tobita, H. Ogawa, K. Sagayama* 19
Technological Trends of Jet Aircraft Engine Bearings ..... *M. Kawada, K. Hara* 25
Technology Development and Future Challenge of Machine Tool Spindle ..... *S. Nakamura, H. Kawamura, Y. Katsuno* 30
Electrical Erosion of Motor Bearings ..... *K. Yasunaga* 39
Development of Long-Life Planetary Shaft (SHX3 Steel) for Planetary Gears of Automotive Transmissions ..... *K. Yamamoto, H. Takemura* 45

New Products

Shinkansen Axle Cylindrical Roller Bearings for E5 Series Bullet Train 51
High-Performance Standard NSKHPS Large-Size Spherical Roller Bearings 53
Energy-Saving HALFRICTION Ball Bearings for High-Efficiency Motors 55
High-Performance, Shielded Double-Row Angular Contact Ball Bearings for Industrial Water Pumps 57
NSKROBUST Series Type E of Angular Contact Ball Bearings for Machine Tools 59
SPACEA Series—Highly Corrosion Resistant and High-Hardness Stainless Steel ESZ Bearings 61
Ultrahigh-Speed, Large-Diameter Ball Bearing for Hybrid Car Motors 63
Highly Reliable, Lower Frictional Torque Ball Bearings for Belt-Type CVTs 65
Silent Needle Roller Bearing for Automotive Electrical Components 67
Automotive Transmission Thrust Needle Roller Bearings with Integrated Washer and Oil-Flow Control 69
HMS Series of Ball Screws for High-Speed Machine Tools 71
Miniature Large-Lead Series of High-Speed, Low-Noise Ball Screws 73
Precision-Grade, Medium-Preload, Random-Matching NSK Linear Guides 75
Random-Matching, Miniature PU and PE Series of NSK Linear Guides 77
Highly Durable, Highly Rigid, Slidable Intermediate Shaft for EPS 79
Wedge Gear of New Positive-Lock Mechanism for Steering Column 81
Megapositioner of Highly Rigid, Ultralarge-Torque-Output, Rotary Positioning Units 83
PX Series of High-Acceleration Megatorque Motors 85

Coupled Simulation of Starved Elastohydrodynamic Lubrication and Liquid Film Flow

Kenichi Shibasaki
Corporate Research & Development Center

ABSTRACT

Minimal quantity lubrication (MQL) on rolling element bearings facilitates the reduction of bearing friction and environmental impact. However, excessive reduction of the amount of oil leads to a shorter bearing life because the elastohydrodynamic lubrication (EHL) oil film becomes thinner than the surface roughness. Therefore, it is important to elucidate the relationship between oil flow rate and oil film thickness. A new numerical method has been developed to couple simulations of starved EHL and oil liquid film flows outside the EHL to provide information on the above relationship. The present method has an advantage in that it can solve the inlet boundary conditions of the EHL domain, such as meniscus length and inlet oil distribution. The effects of the numerical grid type and resolution on the simulation of a ball bearing were investigated. Ball-on-disk tests under steady-state starved lubrication were also carried out experimentally to validate the newly developed method.

1. Introduction

Lubricating the rolling bearings with a minimal quantity of oil (Minimal Quantity Lubrication, MQL) produces the following benefits:

- Energy saving[1] by reducing rolling viscous resistance and agitation resistance
- Reduction of environmental load by reducing waste oil

To prevent bearing damage caused by direct metal contact, however, an elastohydrodynamic lubrication (EHL) oil film that is thicker than the surface roughness should be maintained. Therefore, predicting the interaction between supply oil quantity and oil film thickness becomes the key to realizing MQL.

A method for predicting the relationship between oil supply and oil film thickness has not yet been proposed. Assuming that the oil quantity existing at the inlet of the rolling contact area (inlet oil quantity) is known, oil film thickness can be calculated in accordance with conventional methods[2)–4)], but inlet oil quantity is currently unknown.

Thus, this research was conducted to propose a method to couple the micro flow at the contact area with the outside macro flow, to solve the problem of the inlet oil quantity.

2. Analytical Method

The object of this research is the starved (oil film thickness is affected by oil quantity) lubrication conditions with a minute quantity of supply oil. It is thought that oil adheres to the surface of components (outer ring, inner ring, rolling elements) due to its minute quantity, and flows as a liquid film (LF). From flowing into a bearing through draining from the bearing, oil follows three steps:

(a) Oil flows into the bearing by traveling along the outer ring and inner ring surfaces.
(b) Oil that reaches the contact area forms an EHL oil film.
(c) Oil flows on component surfaces again and drains out of the bearing.

Since the features of the physical phenomenon differ greatly between EHL ((b)) and LF ((a), (c)) as shown below, both are achieved by modeling the suitable equations respectively.

- EHL: Elastic deformation and viscosity increase by high pressure
- LF : Free surface flow

As shown in Figure 1, the boundary between the oil supply and oil drain is established in the LF area. By determining the variable for the amount of oil at the oil supply boundary, the inlet oil quantity and EHL oil film thickness can be calculated simultaneously.

2.1 Analytical method of starved elastohydrodynamic lubrication

The dominant equation for the EHL area is as follows.

A cavitation algorithm[5] is included to treat the starved lubrication in Reynolds's lubrication equation, which is:

$$\nabla\cdot\left(\frac{\theta h^3}{12\eta}\frac{dp}{d\theta}\nabla\left(s(\theta-1)\right)\right)=\nabla\cdot(\theta h\boldsymbol{u})+\frac{\partial\theta h}{\partial t} \quad \cdots (1)$$

Load balance equation;

$$\iint_{\Omega} p\,dx\,dy = w_0 \quad \cdots (2)$$

Pressure dependence equation of viscosity;

$$\eta=\eta_0 e^{\alpha p} \quad \cdots (3)$$

Pressure dependence equation of density;

$$\rho=\rho_0\frac{0.59\times10^9+1.34p}{0.59\times10^9+p} \quad \cdots (4)$$

Surface elastic deformation equation;

$$d=\frac{2}{\pi E}\iint_{\Omega}\frac{p}{\sqrt{(x-x')^2+(y-y')^2}}dx'dy' \quad \cdots (5)$$

Interfacial distance equation;

$$h=g+d-\delta \quad \cdots (6)$$

Where,

∇ : Bidimensional nabla
θ : Non-dimensional density (= ρ/ρ_0)
h : Interfacial distance (in EHL)
η : Viscosity
η_0 : Viscosity at atmospheric pressure
p : Pressure
Ω : Contact area
x : Rolling direction, origin is the center of contact area
y : Rolling orthogonal direction, origin is the center of contact area
s : Switch function
$\boldsymbol{u}$: Rolling speed vector
t : Time
w_0 : Load
e : Exponential
α : Pressure viscosity coefficient
ρ : Density
ρ_0 : Density at atmospheric pressure
d : Surface elastic deformation
E : Interfacial equivalent longitudinal coefficient
x' : Rolling direction, origin is the center of contact area
y' : Rolling orthogonal direction, origin is the center of contact area
g : Interfacial distance under no load
δ : Approach distance

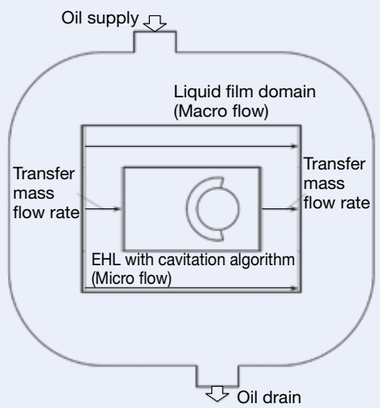

Fig. 1 Schematic view of the coupled simulation of starved EHL and liquid film flow

The cavitation algorithm is the method to solve both the full film area ($\theta \geq 1$) filled with oil and the cavitation area ($\theta < 1$) at the same time by replacing pressure ρ with non-dimensional density θ (= ρ/ρ_0).

The finite difference method was used for space discretization, and the implicit method was used for time discretization. To calculate the elastic deformation at high speed, the FFT method[6] was used. The independent variable was non-dimensional density θ and approach distance δ, and the relaxation method was used for the correction.

2.2 The analytical method of liquid film flow

The dominant equation of the LF area is as follows.

Equation for conservation of mass;

$$\frac{\partial h}{\partial t}+\nabla\cdot\left(h\left(-\frac{h\boldsymbol{\tau}}{6\eta}+\frac{2\boldsymbol{u}_h}{3}+\frac{\boldsymbol{u}_w}{3}\right)\right)=0 \quad \cdots (7)$$

Equation for conservation of momentum;

$$\begin{aligned}&\frac{2h}{3}\frac{\partial\boldsymbol{u}_h}{\partial t}+\frac{1}{3}\left(\boldsymbol{u}_w+2\boldsymbol{u}_h-\frac{h\boldsymbol{\tau}}{\eta}\right)\frac{\partial h}{\partial t}\\&+\frac{8}{15}\nabla\cdot\left(h\boldsymbol{u}_h\boldsymbol{u}_h\right)+\frac{2}{15}\nabla\cdot\left(h\boldsymbol{u}_h\boldsymbol{u}_w\right)\\&-\frac{7}{60\eta}\nabla\cdot\left(h^2\boldsymbol{u}_h\boldsymbol{\tau}\right)+\frac{2}{15}\nabla\cdot\left(h\boldsymbol{u}_w\boldsymbol{u}_h\right)\\&+\frac{1}{5}\nabla\cdot\left(h\boldsymbol{u}_w\boldsymbol{u}_w\right)-\frac{1}{20\eta}\nabla\cdot\left(h^2\boldsymbol{u}_w\boldsymbol{\tau}\right)\\&-\frac{7}{60\eta}\nabla\cdot\left(h^2\boldsymbol{\tau}\boldsymbol{u}_h\right)-\frac{1}{20\eta}\nabla\cdot\left(h^2\boldsymbol{\tau}\boldsymbol{u}_w\right)\\&+\frac{1}{30\eta^2}\nabla\cdot\left(h^3\boldsymbol{\tau}\boldsymbol{\tau}\right)\\&=-\frac{h}{\rho}\nabla p_l+2\frac{\eta}{\rho}\left(\frac{\boldsymbol{\tau}}{\eta}-\frac{\boldsymbol{u}_h}{h}+\frac{\boldsymbol{u}_w}{h}\right)+\boldsymbol{a}_l h\end{aligned} \quad \cdots (8)$$

Where,

∇ : Bidimensional nabla
h : Oil film thickness (in LF)
$\boldsymbol{\tau}$: Shearing stress vector on liquid film surface
$\boldsymbol{u}_w$: Wall speed vector (= ($\boldsymbol{u}_w$, $\boldsymbol{v}_w$))
$\boldsymbol{u}_h$: Surface speed vector (= ($\boldsymbol{u}_h$, $\boldsymbol{v}_h$))
p_l : Pressure
$\boldsymbol{a}_l$: Acceleration vector

Equations (7) and (8) are derived from the equation of continuity in three-dimensional non-compressible fluid and the Navier-Stokes equation, respectively. Using the assumption of enabling speed distribution in the direction of film thickness with thin film to approximate by quadratic function, a bidimensional equation is obtained by integrating in the direction of film thickness.

The bidimensional finite volume method of the surface of a three-dimensional object was used for space discretization, and the implicit method was used for time discretization. The independent variable was oil film thickness h and surface speed vector $\boldsymbol{u}_h$ (= ($\boldsymbol{u}_h$, $\boldsymbol{v}_h$)), and the relaxation method was used for corrections.

2.3 Coupling method

The coupling of EHL and LF is achieved by transferring a mass flow of liquid film at their boundary. If the transferred mass flow is not preserved, the calculation diverges. Therefore the preservation method precisely shown in Figure 2 was used.

For these calculation procedures, successive iteration was adopted, which solved for EHL and LF alternately, and sequentially updated information on the transferring mass flow rate.

3. Application of the Analysis Method to Ball Bearings

This method was applied to ball bearings, and it was confirmed that the relationship between volume flow of oil and the oil film thickness could be calculated, in addition to investigating the effect of the shape and resolution of the LF calculated grid.

The object of our analysis was deep groove ball bearings with seven balls and a bore diameter of 8 mm. Outer ring, inner ring, and ball surfaces were considered; the nut cage was ignored. To shorten calculation time, one ball was solved for by using the periodic boundary condition.

The rolling element load was 100 N, and the rolling speed was 10 m/s. The shearing stress of air flow affecting a liquid film surface of 1 kPa was given in an axial direction. This sharing stress becomes the driving force of fluid film flow; oil is supplied from one side of the bearing and drains from the other side. Additionally, centrifugal force and Coriolis force are taken into consideration.

3.1 Effects of grid shape

Effects of the LF grid shape on the calculation result were investigated. Grid shapes used for calculation were the triangle and quadrangle (upper area in Figure 3), with cells numbering 43 988 (triangle) and 13 960 (quadrangle).

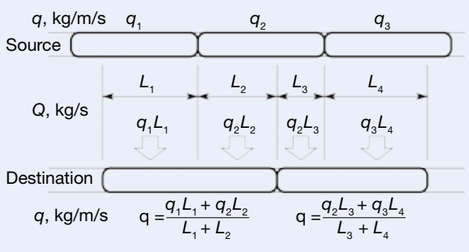

Fig. 2 Schematic diagram of transfer of mass flow rate

Figure 3 (middle) shows the calculation results of liquid film mass per unit area. Thin liquid film (blue) on the ball rolling tracks gradually becomes blurry (the liquid film becomes flat) in the triangle, but this does not happen in the quadrangle. It is thought that this is because of quasi-diffusion caused by non-orthogonalization of the triangular grid line and the speed vector. Increasing the number of cells would likely improve this issue, but quasi-diffusion does not appear in the quadrangle even if the number of elements in the grid is reduced. From this point, use of a quadrangular grid is assumed.

Figure 3 (lower) shows the distribution of the non-dimensional density θ and oil film thickness h at EHL. It is asymmetric in the quadrangular grid, and the full film area on the supply oil side (fulfilled oil area, orange) is wider than that on the drain oil side, and the oil film on the supply oil side is thicker. Because flattening the liquid film by quasi-diffusion uniformizes inlet oil quantity in the triangular grid, distribution is thought to become symmetrical.

Figure 4 shows the relationship between the inlet meniscus m and EHL central oil film thickness $h_{c,S}$. m is the distance from the center of the osculating circle to the end of the inlet-side full film (upper right in Figure 4). m* is m of the boundary line between fully lubricated condition and starved lubrication condition. This is different from the shape of the full film area of conventional research[4] (lower right in Figure 4), but the relationship between meniscus length and oil film thickness almost matches the results from conventional research, and the validity of the EHL analysis area in this research was confirmed.

Figure 5 shows the distribution of EHL oil film thickness at the center of an osculating circle (x = 0). The supply side of the EHL oil film is thicker than that of the drain side in the quadrangular grid (right). Also, the condition of increasing oil film thickness can be calculated with increasing oil supply.

According to the calculating equation for the EHL central oil film thickness h_c and assuming full lubrication under the Hamrock-Dowson model[3], the oil film of the outer ring side is calculated to be thicker than that of the inner ring side; for example, h_c = 1.34 µm at the outer ring side and h_c = 1.09 µm at the inner ring side. Central oil film thicknesses of the outer-ring side and inner ring side almost agree in this method, however; furthermore, the central oil film shape of the inner ring side is similar to that of the outer ring. It is thought that this is due to a transfer of liquid film through the ball surface between the outer-ring-side EHL and the inner ring side EHL.

3.2 Effects of grid resolution

To investigate the effects of grid resolution, a calculation was conducted with the number of elements changed on two levels of the quadrangular grid shape. Grid (fine grid) in Clause 3.1 and a double-width (rough) grid were used. Figure 6 (a) and (c) show the EHL oil film thickness, and Figure 6 (b) and (d) show the relationship between volume flow of oil supply and oil film thickness. The difference in EHL film thickness by grid resolution is a maximum 3.3 %, and the rough grid can be said to have a sufficient resolution in this condition.

The following equation is proposed as an index for an unconditional grid resolution.

$$n_f = \frac{m - b}{\Delta x} \quad \ldots (9)$$

Where,

n_f : Grid resolution index
m : Inlet meniscus length
b : Short radius of contact ellipse
Δ_x : Grid width in the rolling direction

The principal factor for determining the starved EHL oil film thickness is inlet oil quantity (size of full film area). n_f becomes the index of whether or not inlet oil quantity can be resolved. The rough grid n_f used in this instance was 1.8. Therefore it will be sufficient if inlet oil quantity can be resolved by using two grids.

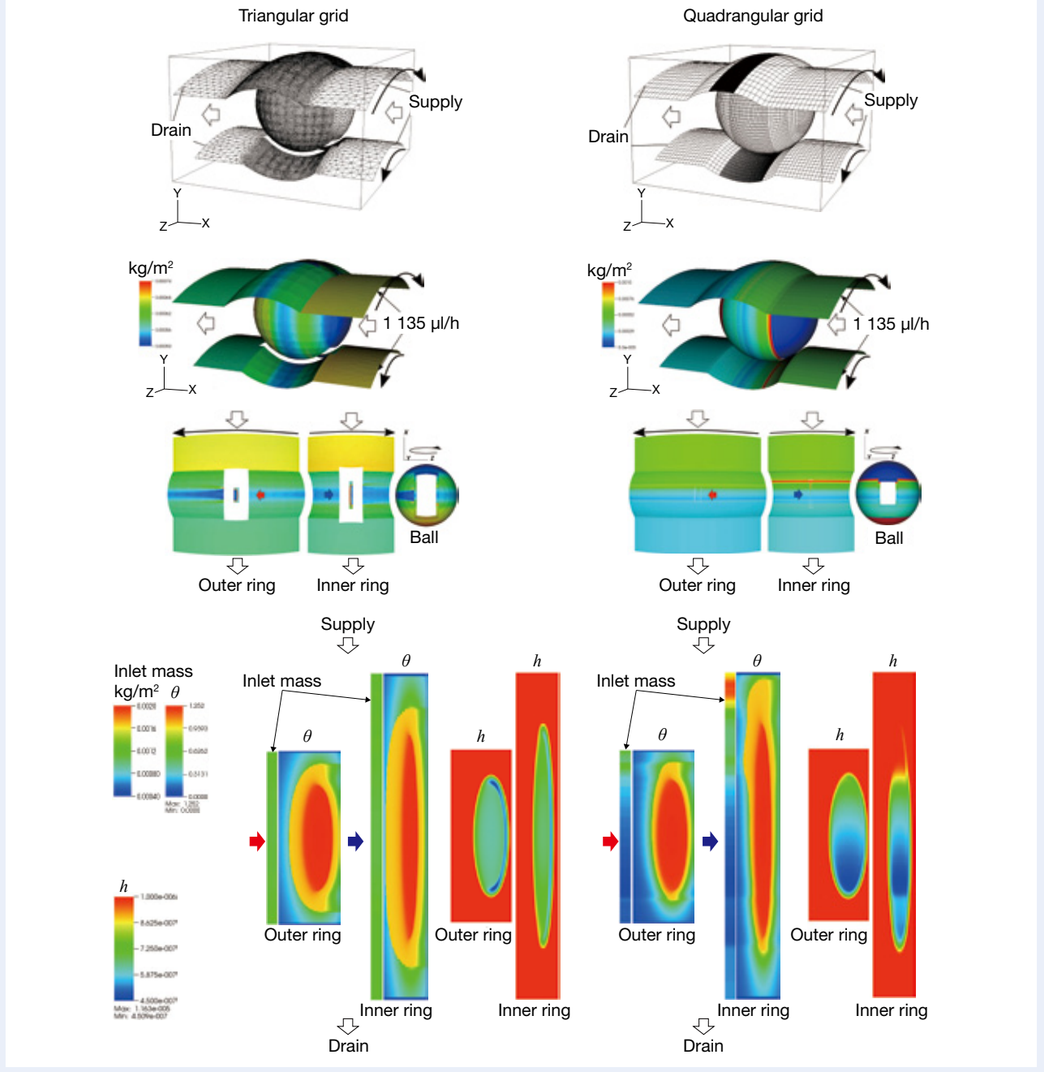

Fig. 3 Comparison between the triangular grid and the quadrangular grid

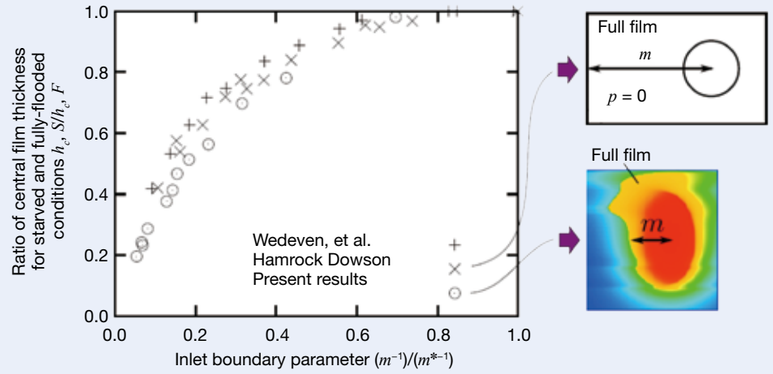

Fig. 4 Relationship between the inlet meniscus length and the EHL film thickness

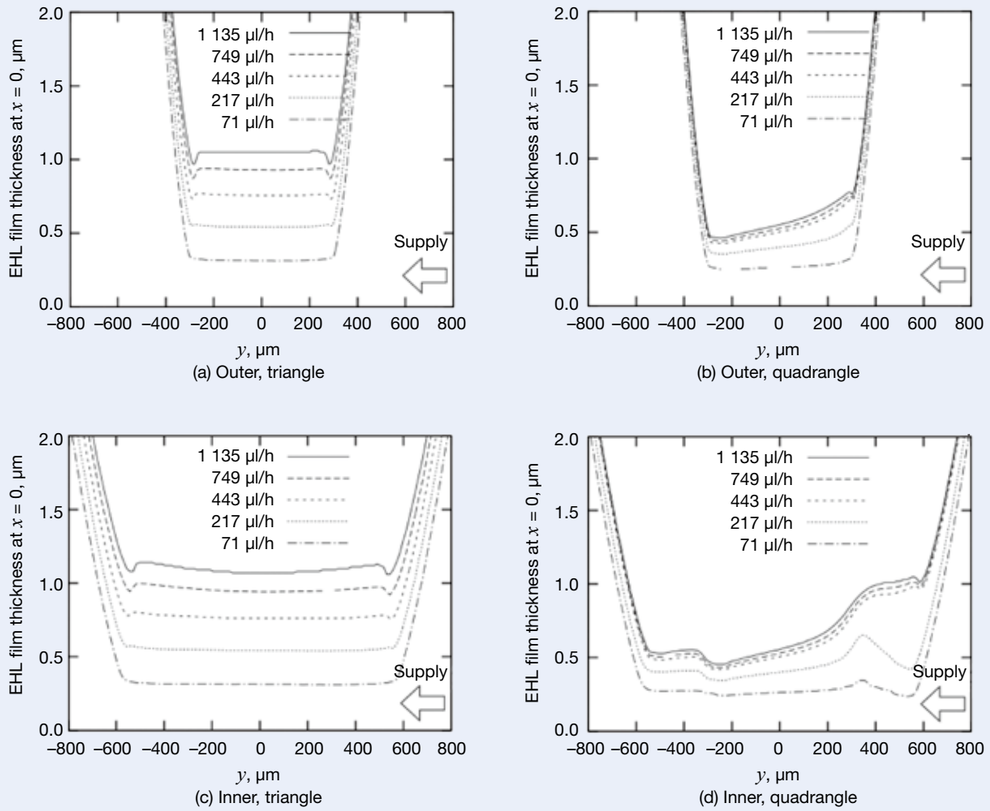

Fig. 5 EHL film thickness at $x = 0$

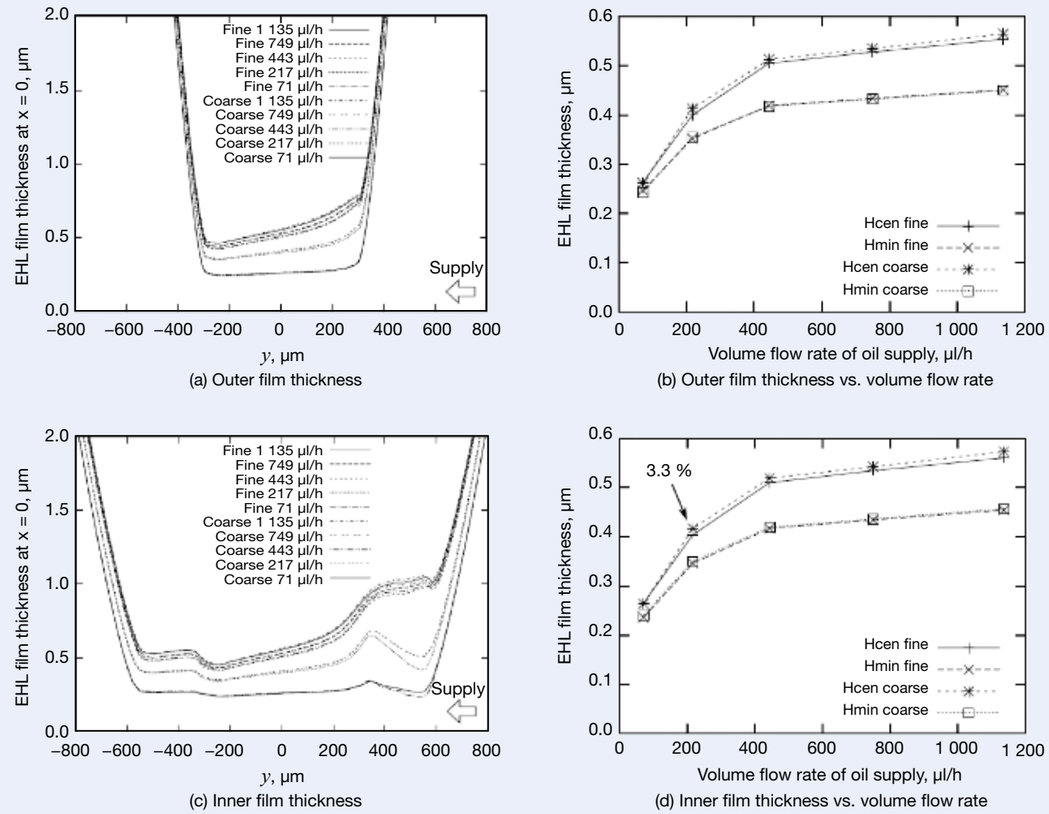

Fig. 6 The influence of grid density on EHL film thickness

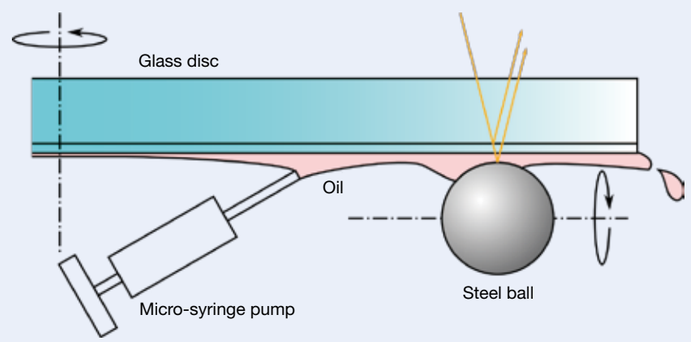

Fig. 7 Steadily starved lubrication using a micro-syringe pump

4. Experimental Verification Using Ball-on-disc

Experimental verification of this method was tried. It is difficult to measure distribution of oil film thickness and inlet oil quantity in rolling bearings. Next, the test and calculation were compared by using a ball-on-disc device to simulate a bearing.

For steadily starved lubrication on the contact area, lubrication oil was supplied to the inside of the disc at a constant flow volume using a micro-syringe pump, as shown in Figure 7.

When the disc's rotation is used to make centrifugal force the driving power, liquid film flows toward the outside, lubricates the contact area, and drains from outside of the disc. The conditions of this test were: ball diameter of 25.4 mm, disc diameter of 100 mm, rolling speed of 1.8 m/s, maximum surface pressure of 0.49 GPa, and viscosity of 19 mm²/s.

Figures 8 (a), (b), and (c) show the distribution of the full film area. "Inlet" shows the EHL inlet side and "Inside" shows the inside of the disc in these figures. For full film area broadening to both sides of an osculating circle, the inside of the disc is larger than the outside. Also, the EHL inlet full film area increases with increasing oil supply.

Figure 8 (d) shows the distribution of EHL oil film thickness measured by optical interferometry. Oil film thickness on the outside of the disc decreases when the oil supply is reduced, but the thickness on the inside of the disc rarely decreases, thus demonstrating the asymmetric distribution of oil film thickness.

4.1 EHL oil film thickness

This calculation was conducted under the same conditions as the test.

Figure 9 (a), (b), and (c) show the distribution of non-dimensional density. It is different from the test in that the full film area on the outside of the disc is small, and a full film area does not exist at the EHL inlet area.

Figure 9 (d) shows the EHL oil film thickness. The oil film in this calculation was thinner than it was in the test result.

The proximate cause of the calculation of a thin oil film is a small quantity of inlet oil. Generally, the oil that is lost in the course of rolling will flow again into the area (track) of the osculating circle passing at some place while the disc is making a circuit. That is, it is possible to have underestimated this re-flow for the purpose of calculation.

On the other hand, when observing EHL from the back, it was found that full film existed (Figure 8) at the contra-wedge area stretching out into space, and oil moved round to the back of the contact area.

The places where this backward movement of oil originates are located within the EHL analysis area, but the movement was not taken into consideration in the present cavitation model.

Therefore, oil movement was modeled as an experimental formula, and its effects on calculation results were investigated. From the shape of the full film area of EHL behind the contact area, as shown in Figure 8, distribution of liquid film thickness at the EHL outlet was calculated, and an experimental formula for oil movement was prepared. By modifying liquid film distribution at the EHL outlet using an experimental formula at every repeated calculation, the oil moving to the back of the contact area was reproduced for simulation purposes.

Figure 10 shows the calculation results considering the oil movement. Full film area (Figure 10 (a), (b), and (c)) and EHL oil film thickness (Figure 10 (d)) matched the test in regard to the following features.

- Existence of a full film area at both ends of the contact area
- A wider full film area on the inside of the disc than on the outside
- An increasing full film area at the EHL inlet with the increase in oil supply
- Tip of the cavitation area around the inlet slides to the outside.
- Asymmetric distribution of EHL oil film thickness (Figure 10 (d))

Figure 11 shows the relationship between oil supply and minimum EHL oil film thickness. Except for two instances where the amount of oil was small, the tendency of the oil film to become thinner with reduced flow volume of oil matched the test result qualitatively. Because the index of the grid resolution is $n_f = 3.5$ at 30 µl/h, and exceeds the value of 1.8 in section 3.2, grid density is said to be sufficient for over 30 µl/h. From the above results, it was found that oil moving around to the back of the contact area was the important factor for forming oil film under starved lubrication conditions.

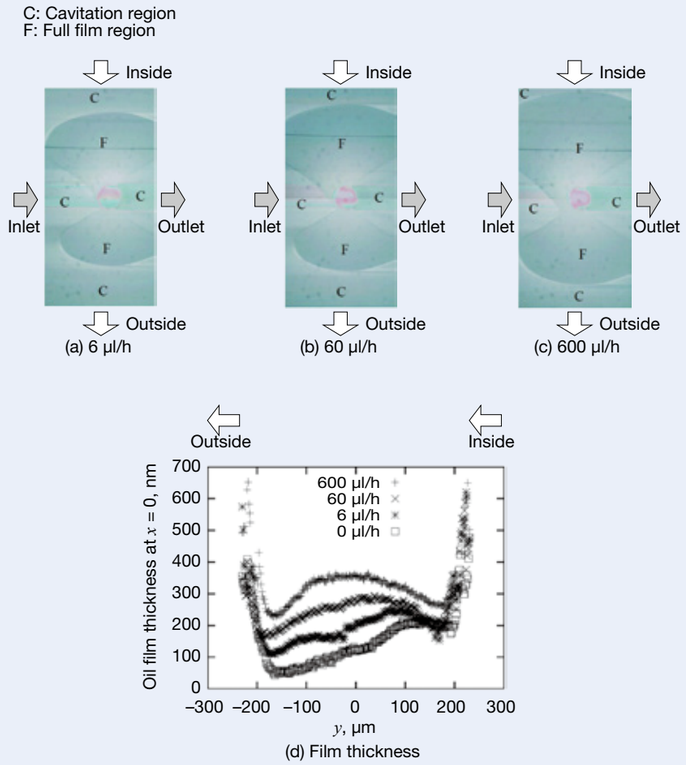

Fig. 8 Experimental results

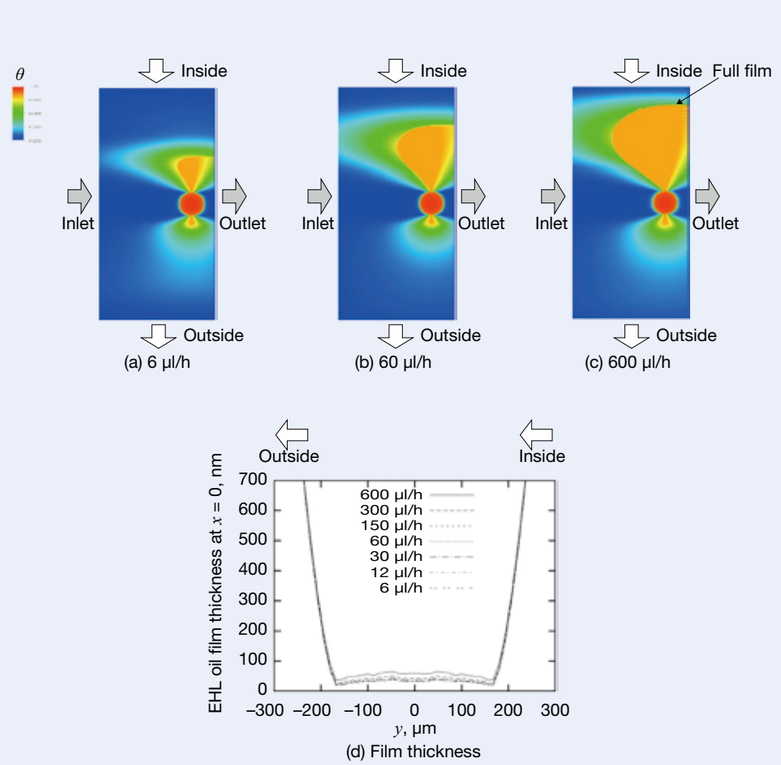

Fig. 9 Computational results

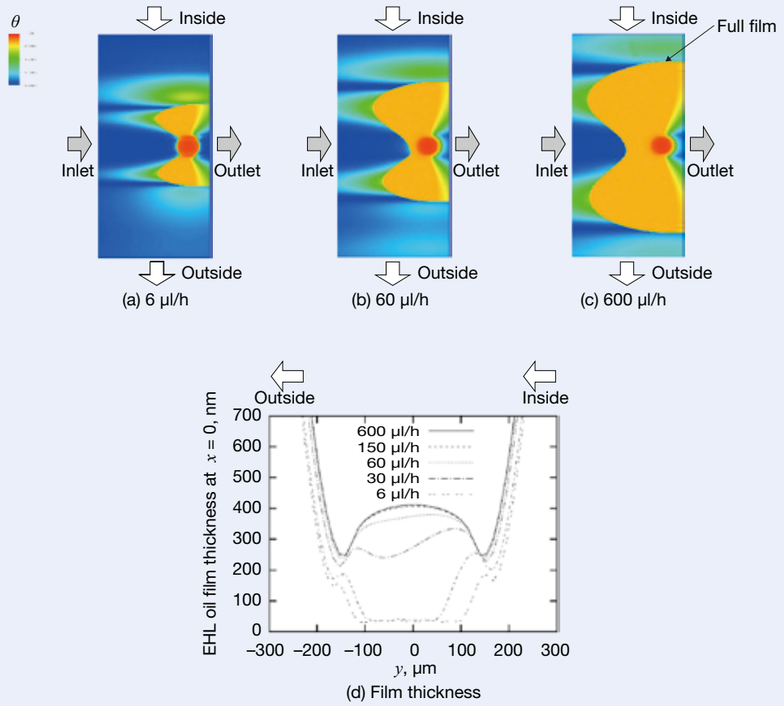

Fig. 10 Computational results with oil replenishment model

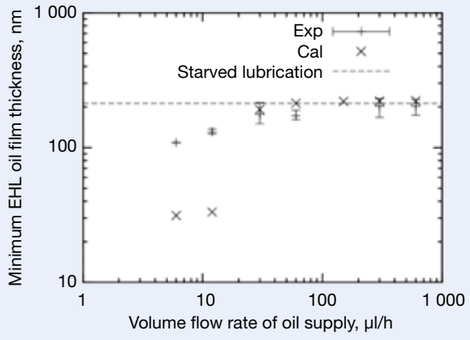

Fig. 11 Relationship between oil supply and EHL oil film thickness

4.2 EHL inlet oil quantity

Distribution of liquid film thickness on the disc surface at the EHL inlet was measured and compared with the calculation result (considering the movement pattern of the oil). Measurement was conducted at nine positions, as shown by lines in Figure 12 (a). Figure 12 (b) shows the results.

Because the calculated result and test result matched up well, it was confirmed that oil quantity at the EHL inlet could be calculated by this method.

5. Conclusion

To predict the relationship between oil supply and oil film thickness, a coupled simulation method of starved elastohydrodynamic lubrication and liquid film flow was proposed. It has previously been necessary to assume the oil quantity at the inlet of the rolling contact area, but this method enables the user to calculate the oil quantity and maintain oil film thickness at the same time.

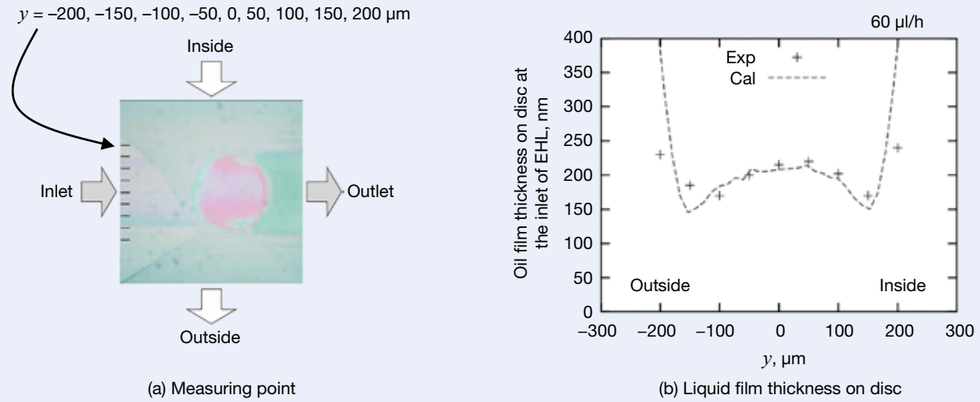

Fig. 12 Liquid film thickness at EHL inlet on disc

References

1) H. Aramaki, “Low Frictional Torque Technology of Rolling Bearings,” NSK Technical Journal, No. 677 (2004) 32–38.
2) F. Chevalier, A. A. Lubrecht, P. M. E. Cann, F. Colin, G. Dalmaz, “Film Thickness in Starved EHL Point Contacts,” J. Tribol., 120 (1998) 126–133.
3) B. J. Hamrock, D. Dowson, “Ball Bearing Lubrication: Elastohydrodynamics of Elliptical Contacts,” (1981), John Wiley & Sons Inc.
4) D. Dowson, B. J. Hamrock, “Isothermal Elastohydrodynamic Lubrication of Point Contacts Part IV — Starvation Results,” J. Lub. Tech., Trans. ASME, 99 (1977) 15–23.
5) F. Sahlin, A. Almqvist, R. Larsson, S. Glavatskih, “A Cavitation Algorithm for Arbitrary Lubricant Compressibility,” Tribol. Int., 40 (2007) 1294–1300.
6) S. Liu, Q. Wang, G. Liu, “A Versatile Method of Discrete Convolution and FFT (DC–FT) for Contact Analyses,” Wear, 243 (2000) 101–111.

Kenichi Shibasaki

Differences in Preventive Mechanisms for Fretting Wear between Oil and Grease Lubrication

Taisuke Maruyama and Tsuyoshi Saitoh
Corporate Research & Development Center

ABSTRACT

Rolling bearings may suffer from fretting wear on the rolling element or raceway surface as a result of an oscillatory motion. The fretting wear on a bearing surface can result in excessive noise, an increase of torque, flaking, and so on. Previously, the degree of oscillation was expressed as a non-dimensional parameter of the amplitude ratio. The amplitude ratio is now expressed as A / D, where A is the amplitude during oscillation, and D is the Hertz contact diameter. Oil film behavior was then observed during minute oscillation in EHL (elastohydrodynamic lubrication) point contact, and the critical amplitude at which oil film could not be formed was measured. This paper investigates the relationship between kinematic viscosity and fretting wear by using the thrust bearing when the amplitude ratio was changed and comparing oil lubrication with grease lubrication. Fretting wear decreased when high-viscosity oil was used during oil lubrication and when low-viscosity oil was used during grease lubrication.

Translated and reprinted with permission from JAST, Journal of Japanese Society of Tribologists Vol. 56, No. 12, (2011)

1. Introduction

Rolling bearings are used in various machines. Using these bearings in a mode where minute oscillatory motion occurs often results in fretting wear on the raceway surfaces of the bearings. This wear has a wide variety of adverse effects on the performance of the bearing such as degradation of the acoustic characteristics of the bearing, a rise in bearing torque, and peeling starting from a fretting wear track.

The authors[1] conducted minute oscillatory elastohydrodynamic lubrication (EHL) oil film measurements under oil lubrication and found that there was a critical amplitude where the oil film could not be formed, and at that amplitude or above, the oil film thickness increased with an increasing kinematic viscosity.

Mitjan et al[2] had been carrying out fretting wear tests on a pure slip point contact under oil lubrication to examine the fretting resistance of the Diamond-Like Carbon (DLC) film. They indicated that, when amplitude is small, specimens with DLC film had better wear resistance than untreated specimens, but in large amplitudes, there was no significant difference, and that both specimens with DLC film and untreated specimens experienced little damage, which demonstrated the existence of oil films.

In contrast, Kita et al.[3] conducted oscillatory tests to investigate the fretting resistance of lithium soap grease using thrust ball bearings. They stated that low-viscosity grease could reduce fretting wear.

Kimura[4] also conducted standardized fretting tests (American Society of Testing and Materials, ASTM-D4170) under grease lubrication, and reported that the fretting wear under grease lubrication could be reduced by decreasing the base oil viscosity.

Yano et al.[5] stated that in an oscillatory test, grease with lower viscosity exhibited less fretting wear, but in the case of a fretting test that applied fluctuation loads, the results were reversed, and grease with higher viscosity had better fretting resistance.

Thus, the relationship between kinematic viscosity and fretting resistance inverts between oil and grease lubrication, and between different test methods. However, the reason for the inversion of fretting resistance and its mechanism are still unclear.

In this research, fretting wear tests were performed in minute oscillation under oil and grease lubrication to examine the effects of kinematic viscosity on fretting wear, and it was considered the mechanism for improving fretting wear resistance.

2. Test Method

2.1 Definition of amplitude ratio

This research used a parameter called an amplitude ratio to represent the degree of oscillatory movement[6]. Given that the amplitude is A and the diameter of the Hertz contact area is D, the amplitude ratio = A/D. As Figure 1 shows, if the amplitude ratio is 1 or smaller, minute oscillation takes place in the range where the contact circle overlaps.

2.2 Method for evaluating fretting wear

In fretting wear, it is not easy to evaluate the amount of wear (volume of wear), because wear particles adhere repeatedly without being displaced from the contact area. Therefore, in this research, the degree of adhesion is represented by using the maximum height roughness. To accurately measure the maximum height roughness of a fretting wear track, a mirror-finished lower disc specimen (material: SUJ2, HV = 725) was used and the area including the entire wear track was measured with an optical interference microscope. Figure 2 shows an example of measurement using the optical interference microscope. The figure on the left is an image of a wear track observed with a metallurgical microscope and the figure on the right shows the result of roughness measurement of the wear track with the optical interference microscope. In addition, the damage ratio was defined as the ratio of maximum height roughness of the test specimen after testing to before testing (approx. 0.1 µm) with the intention of quantifying damage. In this research, the number of rolling elements of the test bearing was 3, and the damage ratios of the wear tracks were averaged and plotted on a graph.

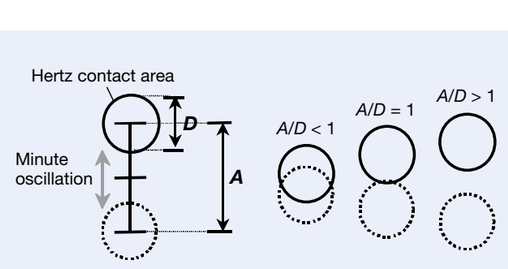

Fig. 1 Example of amplitude ratio

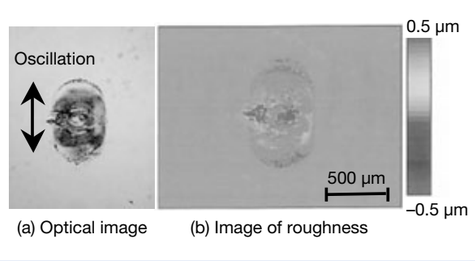

Fig. 2 Example of fretting wear

2.3 Test equipment and conditions

2.3.1 Fretting wear test

A fretting test rig was used as illustrated in Figure 3 to investigate the difference between oil and grease lubrication. The bearing used for testing was a thrust ball bearing 51305, and a minute oscillation angle of 0.6 to 2.5 degrees was applied to the top specimen using a mechanism with a crank and an eccentric cam. Table 1 lists the test conditions. The maximum oscillating speed was kept constant at 20 mm/s to maintain the ability of oil film formation as uniform as possible under the varying amplitude ratios.

2.3.2 Minute oscillating EHL test

A minute oscillating EHL test rig was used as illustrated in Figure 4 to observe the contact area of grease lubrication. The interference fringes of the contact area were observed using a high-speed camera every 5 minutes. Table 2 lists the test conditions. However, since the equipment applies a minute oscillation only to a ball specimen, it is a test under pure slide conditions, which are different from the fretting wear test that used a thrust bearing.

3. Test Results

3.1 Oil lubrication

3.1.1 Transitions of fretting wear

First, the test machine shown in Figure 3 was used to examine the transitions of fretting wear under oil lubrication. Polyalphaolefin oil (PAO: 30 mm²/s at 40 °C) was used as the test oil to compare the transitions of the damage ratios at amplitude ratios of 0.8 and 1.6. Figure 5 indicates the test results. The results demonstrated that almost no wear occurs up to 6×10^2 cycles, then the damage ratio rapidly increases up to 2×10^3 cycles. In addition, beyond 2×10^3 cycles, the damage ratio does not increase very much and almost remains steady. The lower the amplitude ratio, the higher the damage ratio in the steady state becomes and the longer the steady state is. It was considered that when the amplitude ratio is lower than 1, the wear particles adhere repeatedly without being removed from the contact area. After that, it was confirmed that the damage ratio increases again after 3×10^6 cycles if the amplitude ratio is low and after 6×10^4 cycles if the amplitude ratio is high.

Engel et al.[7] conducted fretting wear tests under fluctuation load conditions. As a result, a trend similar to that shown in Figure 5 was identified. It is considered that is difficult removing wear particles from the contact area, and wear particles are continually adhered to the contact surfaces during a fluctuation load test.

In this study, fretting wear tests were conducted with the test number fixed at 1×10^4 cycles to compare the damage ratios in the steady state.

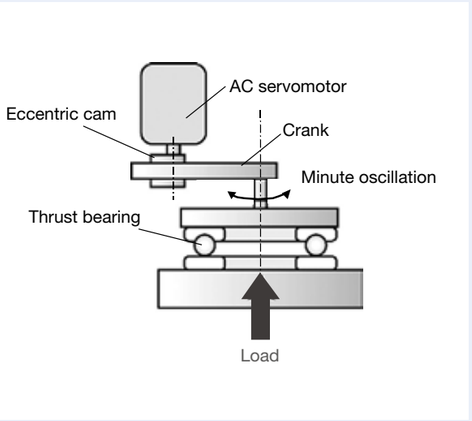

Fig. 3 Fretting test rig

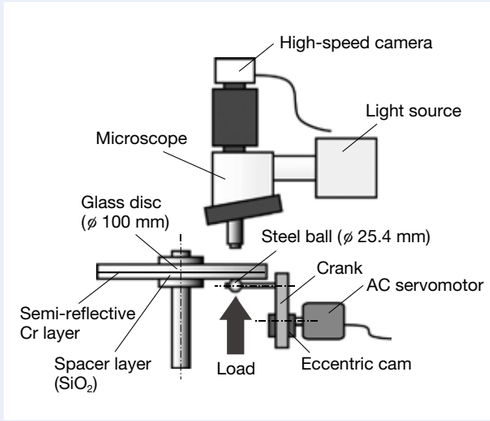

Fig. 4 EHL ball-on-disk test rig

Table 1 Conditions of fretting wear tests

Temperature, °C	25
Test bearing	51305
Maximum oscillating speed, mm/s	20
Maximum contact pressure, GPa	3.24
Load, N	882
Basic dynamic load rating, N	4655
Contact area radius, mm	0.21

Table 2 Conditions of minute oscillatory EHL tests

Temperature, °C	25
Test bearing	51305
Maximum sliding speed, mm/s	20
Maximum contact pressure, GPa	0.37
Contact area radius, mm	0.13
Amplitude ratio	2.0
Camera frame rate, frames/s	500

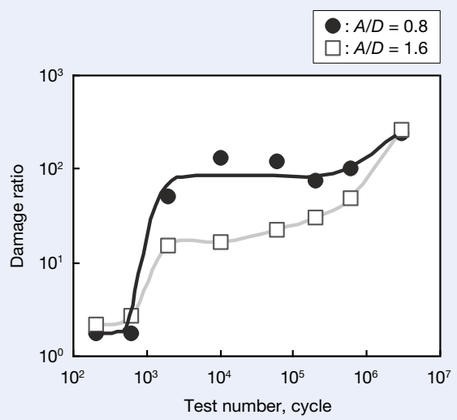

Fig. 5 Relationship between test number and damage ratio

3.1.2 Effects of kinematic viscosity

A minute oscillating EHL test has already been carried out under oil lubrication[1], and it is found that if the amplitude ratio is 1.6 or higher, an oil film can be formed by increasing the kinematic viscosity. To confirm that a similar tendency is found in real bearings, a fretting wear test was carried out under oil lubrication. In this test, the effects of the kinematic viscosity on fretting wear were investigated under different amplitude ratios. Moreover, the test used two types of PAOs with different kinematic viscosities (30 mm²/s at 40 ºC and 396 mm²/s at 40 ºC).

Figure 6 shows the wear track on the lower disc specimen observed with a metallurgical microscope. If the amplitude ratio is 0.7 or lower, ring-shaped fretting wear is found, which is thought to be generated by Mindlin slip. Shima et al.[8] have also discovered the generation of a ring-shaped wear track similar to Figure 6 when the oscillation angle of a rolling bearing is small. In addition, Figure 6 shows that when the amplitude ratio is 1.6 or higher, there is almost no wear by increasing the

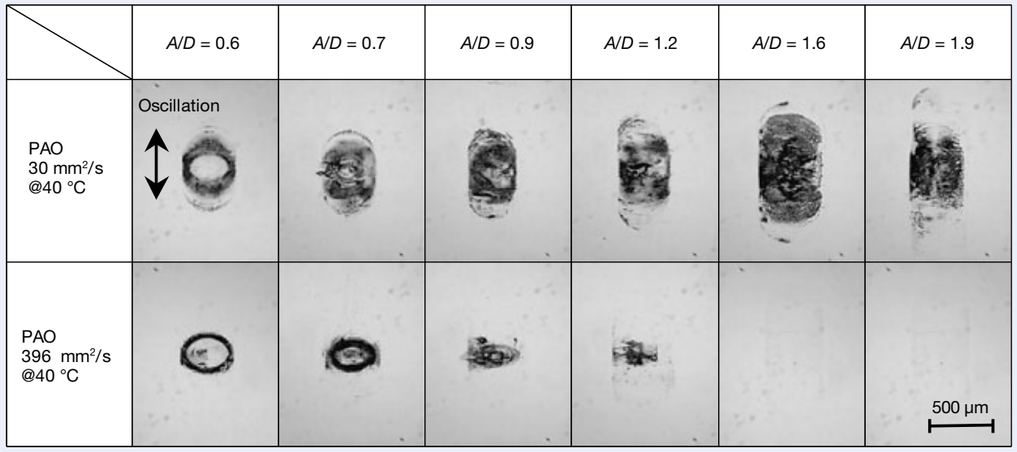

Fig. 6 Photographs of specimens after fretting tests (PAO; 30 mm²/s at 40 °C, 396 mm²/s at 40 °C)

kinematic viscosity of oil. Mitjan et al.[2] also carried out a fretting wear test under oil lubrication and considered that an oil film could be formed by increasing the amplitude.

Figure 7 shows the relationship between the amplitude ratio and damage ratio. The figure suggests that if the amplitude ratio is in a range between 0.6 and 1.2, the damage ratio is scarcely affected by the kinematic viscosity, which means that an oil film cannot be formed. If the amplitude ratio is increased from 0.9 to 1.2, the damage ratio decreases irrespective of the kinematic viscosity. This may be because when the amplitude exceeds the contact circle, the wear particles can be removed from the contact area. It has also become clear that if the amplitude ratio is 1.6 or higher, increasing the kinematic viscosity of oil decreases the damage ratio. As higher kinematic viscosity oil can reduce wear, an oil film is considered to be formed in the contact area. The relationship between the amplitude ratio and oil film thickness has also been confirmed by the result of the minute oscillating EHL test[1].

The above results demonstrate that oil film can be formed if the amplitude ratio is 1.6 or higher and fretting resistance can be improved by increasing the kinematic viscosity of oil, in the case of oil lubrication.

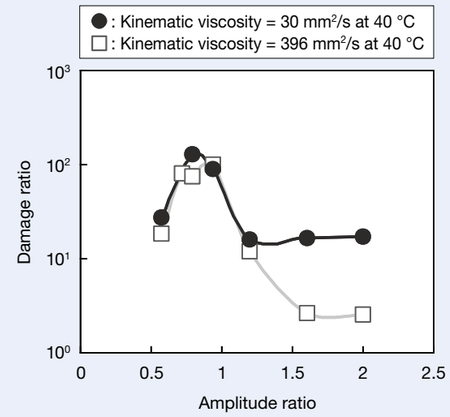

Fig. 7 Relationship between amplitude ratio and damage ratio

3.2 Grease Lubrication

3.2.1 Effects of kinematic viscosity

Table 3 lists the properties of the test greases. In this study, nothing was added to the grease to exclude the effect of additives. In addition, worked penetration was made constant at approximately 200 in order to simplify the effect of the kinematic viscosity of the base oil. In this case, the oil separation of the low-viscosity grease was 1.9 mass%, and that of the high-viscosity grease was 0.1 mass%.

Figure 8 shows the results of a fretting wear test under grease lubrication. If the amplitude ratio is 0.8 or lower, the kinematic viscosity of base oil has only limited effects and the results have a similar tendency to the case of oil lubrication. This may be because the contact circle is oscillating within the range where it overlaps and the wear particles are less likely to be removed from the contact area. On the other hand, it has been found that if the amplitude ratio is high, decreasing the kinematic viscosity greatly reduces the damage ratio. This is the opposite result of the tests under oil lubrication.

Figure 9 is an enlarged photo of the lower disc specimens after testing cleaned with petroleum benzine. White accretion was found around the contact area under low base oil kinematic viscosities and no accretion was found under high viscosities. Figure 10 shows the results of the analysis of the white accretion using a Fourier transform infrared spectrophotometer (FT-IR). As the figure indicates N-H absorption near 3300 cm^{-1}, the accretion is estimated to be a urea compound.

From these results, it is considered that in grease lubrication, a protective film of a urea compound is formed in the contact area, which could reduce wear. Next, the effects of the amount of the thickener in the grease on the damage ratio was examined.

Table 3 Grease properties

Base oil	Poly-α-olefin oil
Kinematic viscosity, mm^2/s at 40 °C	19 and 396
Thickener	Urea
Worked penetration	200
Contact area radius, mm	0.21

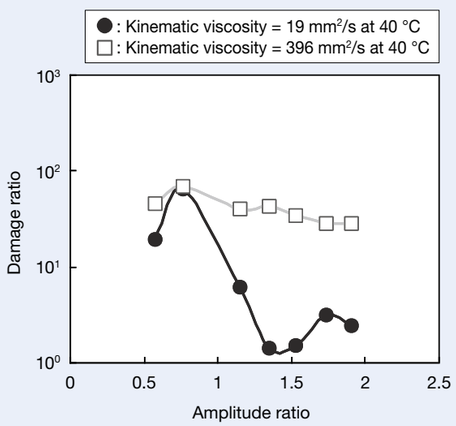

Fig. 8 Relationship between amplitude ratio and damage ratio

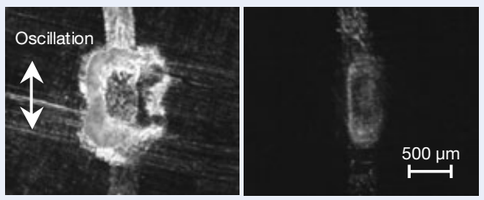

(a) 19 mm^2/s @ 40 °C (b) 396 mm^2/s @ 40 °C

P_{max} = 3.24 GPa, V_{max} = 20 mm/s, A/D = 1.9
Test number = 10^4 cycle, Worked penetration ≈ 200

Fig. 9 Photographs of specimens after fretting tests

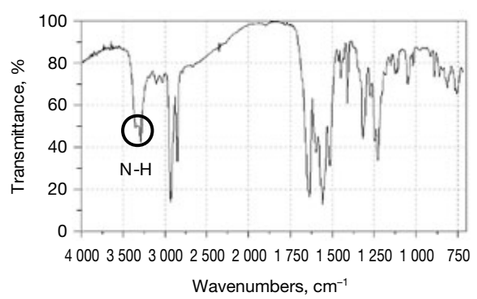

Fig. 10 Analysis result using FT-IR

3.2.2 Effects of worked penetration

The amount of the thickener affects the worked penetration of grease. Figure 11 shows the relationship between the worked penetration and oil separation. The figure indicates that the higher the worked penetration, the higher the oil separation is, and if the worked penetration is constant, decreasing the base oil kinematic viscosity increases oil separation. Figure 12 indicates the relationship between the worked penetration and the damage ratio where the amplitude ratio is A/D = 1.9. The figure demonstrates that the higher the worked penetration, the lower the damage ratio is, and degreasing the kinematic viscosity of base oil enhances fretting resistance. Kita et al.[3] have also found that higher worked penetration increases oil separation, which results in better fretting resistance.

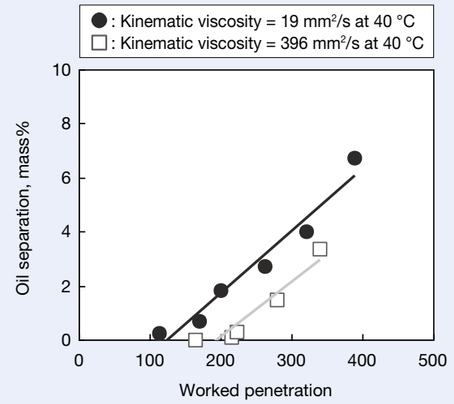

Fig. 11 Comparison of worked penetration and oil separation

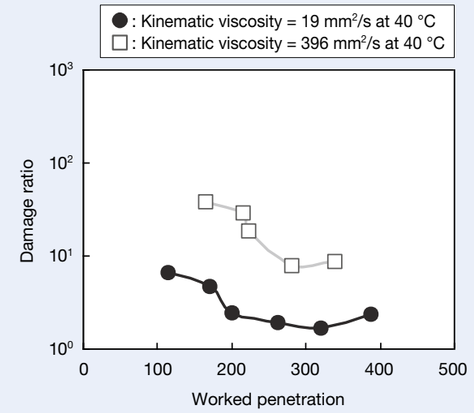

Fig. 12 Comparison of worked penetration and damage ratio at A/D = 1.9

3.2.3 In-situ observation of the contact area

To confirm that this urea protective film (the thickener layer) is formed within the contact area, in-situ observation was conducted. A minute oscillating EHL test was performed using the two types of grease listed in Table 3. Figure 13 shows the interference fringes in the contact area observed every 5 minutes. If the kinematic viscosity of base oil is high, the size of the interference fringes does not change. However, if the viscosity is low, the interference fringes gradually shrink and disappear after 10 minutes. It is considered that as the contact circle becomes smaller, the thickener layer begins to form at the circumference of the contact area. Because of the disappearance of the interference fringes, the thickener layer thickness is at least 700 nm, which is the upper measurement limit of this test rig. The interference fringes re-appeared 25 minutes and 35 minutes after the beginning of the test, which indicates that the reason for disappearance is not the wear of the glass disc specimen.

After testing, the surface of the glass disc specimen was cleaned with petroleum benzine. Figure 14 is an enlarged photo of the surface after cleaning. Similar to Figure 9, it was confirmed that when the kinematic viscosity of base oil is low, the thickener layer is formed in the contact area.

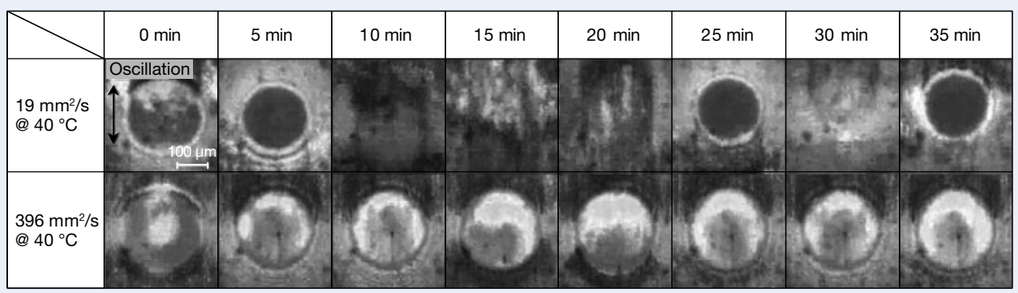

P_{max} = 0.37 GPa, V_{max} = 20 mm/s, A/D = 2.0

Fig. 13 Observation of interference fringes

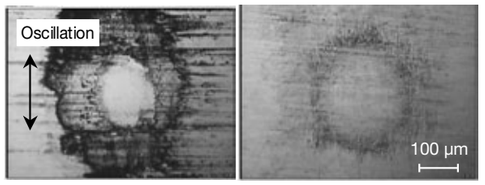

(a) 19 mm²/s @ 40 °C (b) 396 mm²/s @ 40 °C

Fig. 14 Photographs of specimens after fretting tests

4. Discussion

Figure 15 shows the relationship between the kinematic viscosity of base oil and oil separation, and Figure 16 shows the relationship between the kinematic viscosity and damage ratio at an amplitude ratio of 1.9 as a graph that compares the results under oil and grease lubrication. In this situation, the worked penetration is kept constant at approximately 200. Figure 16 indicates that under oil lubrication, increasing the kinematic viscosity decreases the damage ratio. This is because the oil film becomes thicker by increasing the kinematic viscosity[1].

In case of grease lubrication, contrary to oil lubrication, the fretting can be reduced by decreasing the kinematic viscosity. In addition, Figure 15 indicates that decreasing the kinematic viscosity of base oil increases the oil separation, which demonstrates a correlation with the damage ratio. Similar results have already been reported in past references[3)–5)]. In fact, it is widely accepted that fretting wear can be reduced at high oil separation because of the increase in the bled oil supply. However, as Figure 16 indicates, at low viscosities, the damage ratios under grease lubrication are lower than those under oil lubrication. This demonstrates that conventional thinking cannot explain the phenomenon. Therefore, it has been estimated from this research that under grease lubrication, the urea compound itself, a thickener, can contribute to lubrication. The results in Figure 9 are reflected in Figure 16 and indicate that the grease with high oil separation easily forms the thickener layer. Sato et al.[9] have stated that a urea compound, which is used as a thickener, has shorter fibers than lithium soap and inferior shear stability, which results in relatively easy introduction into the contact area. Yano et al.[5] and Kimura et al.[10)–11)] have estimated that the urea grease can form a protective film in the contact area.

This follows that higher oil separation means easier removal of base oil from the contact area rather than easier supply of oil to the contact area, and the urea compound remaining in the contact area forms a thickener layer, which enhances fretting resistance. On the other hand, in the case of lower oil separation, the thickener is removed from the contact area with the base oil, which results in starved lubrication, increasing the damage ratio.

The results in Figure 11 and Figure 12 demonstrate that increasing worked penetration enhances fretting resistance. Increasing worked penetration means decreasing the amount of thickener in grease. Therefore, these results indicate that a thickener layer can be formed; nevertheless, the amount of thickener in grease is decreased. However, if the amount of thickener is reduced further, which means that there is almost no thickener in grease, the damage ratio under grease lubrication is expected to approach that under oil lubrication in the end.

Finally, Figure 17 shows the relationship between the oil separation and damage ratio at A/D = 1.9 for various viscosity and worked penetration levels. The results show a correlation between the oil separation and the damage ratio. The arrow in the graph indicates the damage ratio under dry condition. From this result, it can be seen that the damage ratio with low oil separation approaches the case of dry condition. This is because grease with low oil separation cannot be replenished in the contact area, resulting in the starved lubrication.

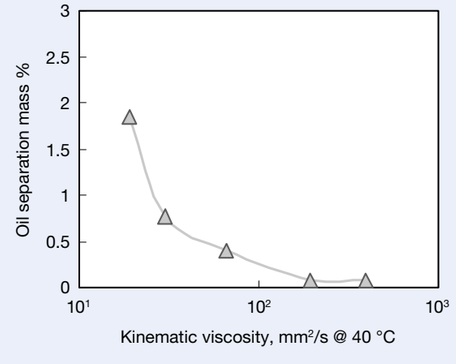

Fig. 15 Comparison of kinematic viscosity and oil separation

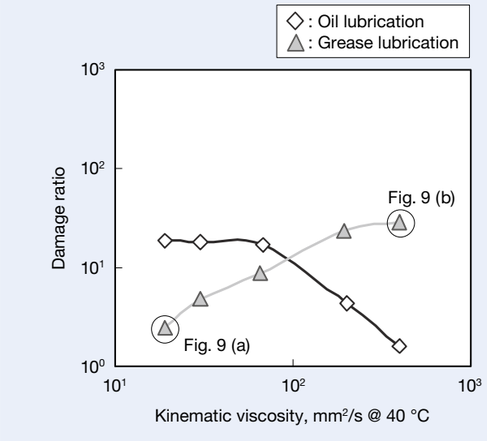

Fig. 16 Comparison of kinematic viscosity and damage ratio at A/D = 1.9

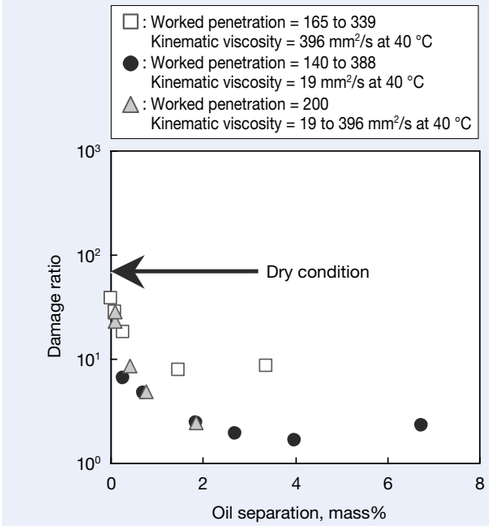

Fig. 17 Comparison of oil separation and damage ratio at A/D = 1.9

5. Conclusion

Fretting wear tests were conducted on thrust bearings in minute oscillation under oil and grease lubrication (base oil: PAO; thickener: urea compound) to investigate the effects of kinematic viscosities on fretting wear. It was also considered how worked penetration affects fretting wear. In addition, in-situ observations were performed on the contact area using an EHL test rig to explore the formation of a thickener layer. The following is a summary of the knowledge gained from this research.

1. Whether under oil or grease lubrication, if the amplitude ratio is low, the kinematic viscosity has little effect on the damage ratio.
2. Under oil lubrication, if the amplitude ratio is 1.6 or higher, and high viscosity oil is used, fretting resistance is improved. This is because of the increase of the oil film thickness.
3. Under grease lubrication (base oil: PAO; thickener: urea compound), with an increasing amplitude ratio, the effects of the base oil viscosity become apparent and decreasing the base oil viscosity increases oil separation, easily removing base oil from the contact area. This results in the formation of a thickener layer, which is expected to enhance fretting resistance.
4. The in-situ observations of the contact area using a minute oscillating EHL test rig revealed that if grease with low kinematic viscosity is used, a thickener layer begins to form at the circumference of the contact area and then covers the entire area.
5. There is a correlation between the damage ratio and oil separation. Grease with low oil separation cannot be replenished in the contact area, resulting in the starved lubrication.

References

1) Maruyama, T., and Saitoh, T., “Oil Film Behavior under Minute Vibrating Conditions in EHL Point Contacts” Tribology Int., 43, 8 (2010) 1279.
2) Kalin, M., and Vizintin, J., “The Tribological Performance of DLC Coatings under Oil-lubricated Fretting Conditions”, Tribology Int., 39, 10 (2006) 1060.
3) Kita, T., and Yamamoto, Y., “Fretting Wear Performance of Lithium 12- Hydroxystearate Greases for Thrust Ball Bearing in Reciprocating Motion,” Tribologist, 42, 6 (1997) 492. (in Japanese)
4) Kimura, H., “Grease as a Functional Lubricant and Its Trend,” Junkatsu Keizai, 7, 6 (2002) 2. (in Japanese)
5) Yano, A., Noda, Y., Akiyama, Y., Watanabe, N., and Fujizuka, T., “Evaluation of Fretting Protection Property of Lubricating Grease Applied to Thrust Ball Bearing,” Tribologist, 54, 1 (2009) 64. (in Japanese)
6) Sakagami, K., and Maruyama, T., “Method of Evaluation Fretting of Extra Small Ball Bearings,” NSK technical journal, 680 (2006) 19. (in Japanese)
7) Engel, P. A., and Yang, Q., “Impact Wear of Multiplated Electrical Contacts,” Wear, 181-183, (1995) 730.
8) Shima, M., Li, Q., Yamamoto T., and Sato, J., “Study on Fretting Wear of Rolling Bearing (Part 3),” Tribologist, 40, 9 (1995) 755. (in Japanese)
9) Sato, J., “Fretting Wear and Prevention in Rolling Bearing (13),” Science of Machine, 56, 1 (2004) 39. (in Japanese)
10) Kimura, H., Tsuchiya, M., Suda, T., and Endo, M., “A Research on the Rolling Surface of Bearing Lubricated by Urea Grease,” 1, Proceedings for the 31st Spring Meeting of Japanese Society of Tribologists, (1987) 325. (in Japanese)
11) Kimura, H., Tsuchiya, M., Suda, T., and Endo, M., “A Research on the Rolling Surface of Bearing Lubricated by Urea Grease,” 2, Proceedings for the 32nd General Meeting of Japanese Society of Tribologists (Osaka), (1987) 53. (in Japanese)

Taisuke Maruyama

Tsuyoshi Saitoh

Development of a Robot Substitute for a Guide Dog

Kazuteru Tobita, Hironori Ogawa and Katsuyuki Sagayama
NSK Ltd.

ABSTRACT

We have been developing a robot that can be used in place of a guide dog to assist the visually impaired, with the goal of implementing robot technology in the field of assisted living. We identified the roles that guide dogs perform and incorporated those roles into the robot's functions as we developed the prototype robots.

This paper explains those developments. Firstly, we explain the basic technology of a robot that leads a person while avoiding obstacles and introduce our prototype robot for this purpose. We also describe some methods for reducing typical risks, which were carried out for this prototype robot in consideration of safety. In addition, we will describe another prototype robot, which has been designed to overcome the barrier of stairs.

Translated and reprinted with permission from Japan Industrial Publishing Co., Ltd., Image Laboratory, 2013. Feb.

• Introduction

The momentum of robot technology as a method of supporting people and their livelihoods has been increasing in recent years against the background of a declining birth rate, an aging society, and a labor shortage; research and development of nursing-care robots or welfare robots have been actively carried out at both research institutes and companies. We are aiming to create a robot that can, as a welfare application, replace the guide dog, guiding the user (a visually impaired person) to a destination safely and securely based on the user's will.

The number of visually impaired persons in Japan is estimated to total 310 thousand[1], including Class 1 through Class 6, according to statistics gathered by the Ministry of Health, Labour and Welfare. When the Japan Ophthalmologists Association calculated using the American Standard (less than 0.5 of corrected vision in the better eye), the number they arrived at was 1.64 million persons in Japan with vision loss or low vision[2]. According to the World Health Organization, there are estimated to be 285 million visually impaired persons in the world[3]. Though the actual number of guide dog used in Japan is 1 067[4], the estimated number of applicants is 13 500. Surveys have shown[5] many cases of people who would prefer not to have to take care of a dog or to live with one, and we consider that the application of robot technology would be an effective way to resolve the imbalance of supply and demand.

In the past, examples of research and development into robots serving as guide dogs have included MELDOG[6] by S. Tachi et al., and the walking guide robot[7] by H. Mori et al.; research including obstacle avoidance and point-to-point guidance has been developed. The navigation function is important, but we have aimed to develop a robot that a user can operate intuitively from the beginning and feel in control of the situation, not as if he is "being walked" by the robot. The robot goes basically in the direction that a user wants, but it should have an "intelligent non-obedience" such as for avoiding surrounding obstacles or stopping when necessary.

We are developing the technology to realize such a robot which can both be driven and move under its own power, recognize obstacles, and communicate with the user as the core of human-assisting technology. This paper mainly introduces a prototype for an obstacle-avoidance leading robot.

• Classification of Main Roles of a Guide Dog

According to documents from the Japan Guide Dog Association and interviews with guide dog users, the main roles of a guide dog are classified as described below.

(1) Avoiding obstacles
  Move in the direction indicated by the user but avoid obstacles and stop when necessary
(2) Notifying the user when the floor level changes
  (a) Help the user to avoid falling due to a change in floor levels
  (b) Inform the user of the need to go up or down stairs
(3) Informing the user of a street corner (intersection)
  Verified by the user's mental map
(4) Guiding the user to the nearest instance of the desired target type
  Door, ticket wicket, postal drop box, etc.

A robot serving as a guide dog must be able to fulfill these roles.

• Obstacle-avoiding Leader Robot NWR002

Outline

Figure 1 shows the appearance of the prototype of obstacle-avoiding leader robot NWR002. The outside dimensions of the robot are 520 mm wide, 660 mm long, and 1 200 mm high; it weighs 40 kg.

When this prototype robot acts as a guide dog, it:

(1) Avoids obstacles
(2) Notifies the user when the floor level changes
  (a) Helps the user to avoid falling due to a difference in floor levels

To facilitate intuitive operation, the robot communicates with the user by its movement or lack of movement. The travelling direction is communicated by movement in that direction, and the robot stops if it is headed toward an obstacle. We have aimed for intuitive input and smooth operational feeling.

Move and drive technologies

This wheeled robot has independent two-wheel drive, which moves rotationally or straight by applying rotation to the right- or left-drive wheels. Force that is transmitted through the grip (force sensor) indicates the rotational velocity and forward velocity. Figure 2 shows the grip, which can fit in the right or left hand of the user.

A moving robot equipped with this grip interface helps the user feel confident in the robot, knowing that the robot has passed through the area ahead, and the velocity can be controlled by the user. On the other hand, the force sensor value sometimes results in the robot sending vibrations through the user interface. We have solved this problem by adopting a model where virtual mass M and virtual viscous resistance η are added to calculate the best velocity for smooth operation, using the following formula:

$$V_{dir} = \int \frac{F - \eta V}{M} dt \quad \ldots (1)$$

V_{dir} : Velocity indicating value
F : Force applied to a grip
V : Current velocity

Obstacle detection and avoidance technologies

Figure 3 shows the areas in which objects are detectable by the robot's sensors. The sensors focus forward, relying mainly on the laser range finders, with an ultrasonic sensor also on board to detect transparent bodies such as glass objects.

As a technology for obstacle avoidance, NSK took the strategy of generating a repulsive force between the robot and the user, using a potential method and giving the positive potential to an obstacle[8]. However, we found that, in narrow spaces such as doorways and ticket wickets, it became impossible for the robot to move, due to the repulsive forces it received from both sides.

Therefore, we developed and implemented the following collision prediction avoidance algorithm. First, the algorithm predicts the trajectory of obstacle P from the

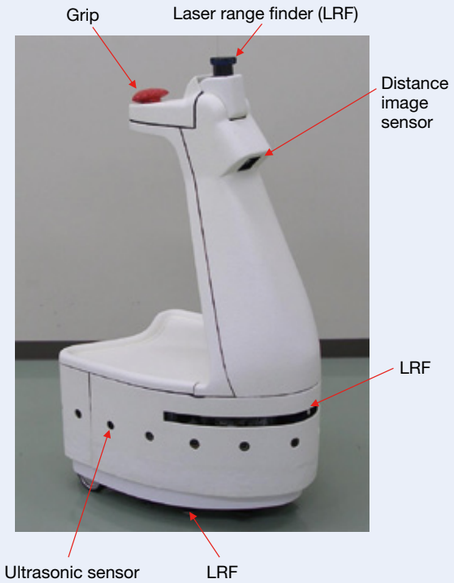

Fig. 1 The NWR002 robot substituting for a guide dog for assisting the visually impaired

Fig. 2 The grip as an interface between the NWR002 robot and the user

user-determined velocity (translation v, rotation ω) of the robot itself, as shown in Figure 4, and determines that a collision is likely if the obstacle's trajectory intersects with the robot's footprint. Risk degree u is determined in response to the distance d until collision. Risk degree u is 0 when at a long distance and moves toward 1 as it grows closer, as shown in the following formula.

$$d > D_u : u = 0$$

$$d < D_u : u = \frac{D_u - d}{D_u} \quad \ldots (2)$$

D_u: Threshold distance

Risk degrees are calculated for various translations v and rotations ω. When there are several obstacles, the degree of risk is calculated for each obstacle and a risk map (Figure 5) is produced, showing the highest calculated degree of risk for each area. Because the risk map is determined by the ratio of translations v and rotations ω, however, the risk degree is radially the same centering around the origin; the risk degree can be expressed by the angle θ.

When the A in the risk map of Figure 5 is the point of velocity instruction, the user's velocity instruction is adopted as being effective, because the degree of risk is low. When the user's velocity instruction is point B or point C, the angle θ is adjusted toward an area with a lower degree of risk because the user's instructions carry a higher degree of risk; that is, the robot does calculations to adjust the velocity instructions.

By the above collision prediction avoidance algorithm, the motion leading a user will avoid obstacles even in narrow doorways and gates.

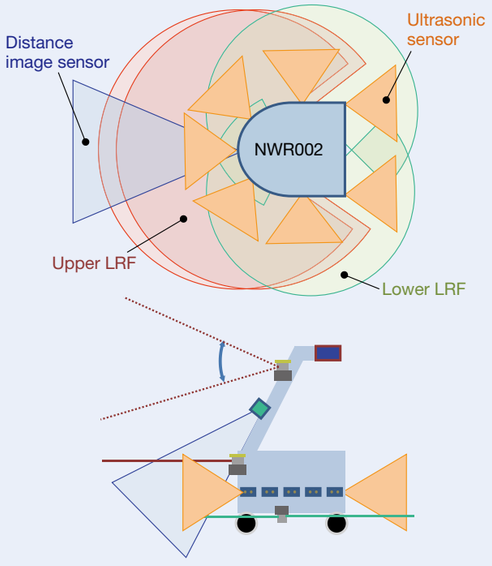

Fig. 3 Detectable area with the NWR002 robot's multiple sensors

Risk reduction measures

Outline

When taking the robot's safety into consideration, risk evaluation becomes necessary. A risk assessment based on the basic safety standards for machinery ISO 12100 determines that tipping over when on an incline, falling from a step, or being damaged in a collision are the biggest dangers to the robot. We have investigated to determine the best countermeasures for these dangers and have implemented our findings, as described below.

Risk of fall

Because a falling robot could injure the user or another person, we included countermeasures not only to prevent damage to the robot but also to prevent it from falling.

As a countermeasure to avoid falling, we installed an attitude control system that helped to keep the upper part of the robot in a horizontal position. We installed a drive mechanism that consisted of a two-axis (roll, pitch) arc guide and a direct drive unit to the lower part of the robot and also installed an attitude sensor to the upper part. Driving these mechanisms so that the roll angle, and also the pitch angle, become 0°, the upper part is kept in a horizontal position, as shown in Figure 6.

An incline of 1/8 (7.1°) was assumed in accordance with Article 26 of the Order for Enforcement of the Building Standards Act, and the movable range of the attitude control system was set at ± 8°. But it is less than 1/12 (4.8°), in accordance with the "Act for Promoting Easily Accessible Public Transportation and Facilities for the Aged and the Disabled" (Barrier-Free Transportation Act), and a 5° incline indoors or around buildings is not a problem.

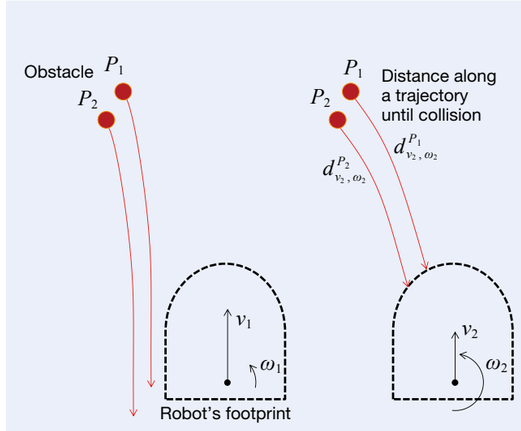

Fig. 4 Collision prediction algorithm of the NWR002 robot

Risk of falling down

If a robot falls down one or more steps, the user will fall with it and be injured. They could also potentially injure someone standing nearby. To reduce these risks, we added countermeasures to prevent a fall, as shown in Figure 7.

When the control device is in a normal position, the robot observes the ground with the forward distance image sensor (obliquely downward and forward) and the laser range finder at the back of its neck and takes action to avoid a difference in floor levels, as it would when avoiding a wall. But when the control device or the above sensor is in an abnormal position, and output of close-range sensors provided around the wheels exceeds the predetermined distance, the robot assumes the ground is not beneath it, shuts down the drive system circuit power and brakes the wheels. The sensors are pointed obliquely downward and forward instead of vertically downward in order to prevent issues in close quarters, such as an elevator entrance.

Additionally, if a wheel runs off the ground in spite of these measures, the robot has a structure for preventing a fall with stoppers located around the wheels.

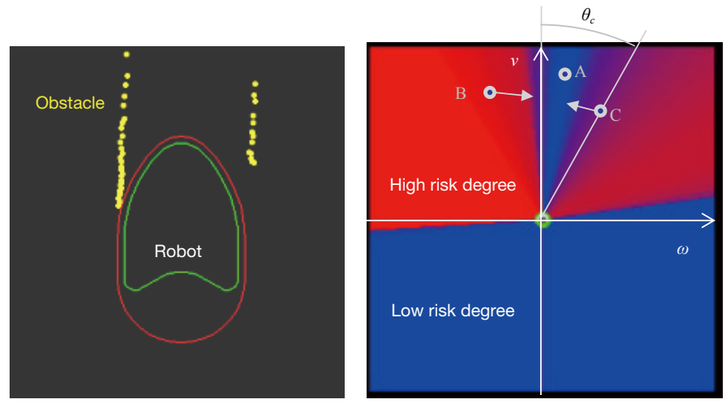

Robot and obstacle point cloud — Cautionary map

Fig. 5 An example of cautionary mapping of a safer path for collision avoidance

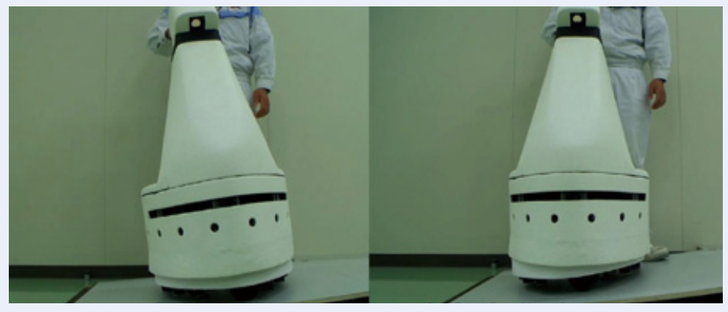

Without attitude control — With attitude control

Fig. 6 Action of the stability-control algorithm for reducing the risk of tipping over

Impact risk

Adopting a soft material with silicon coating on the robot's FRP exterior reduces impact in the event of a collision.

• Guide Dog Robot NR003

The operating environment of the NWR002 stated above mainly targets level and inclined areas. Because a guide dog must also (b) help the user go up and down stairs and (2) let the user know the difference from one step to the next, NSK is also developing a four-legged wheel robot that can recognize stairs and go up and down them, as shown in Figure 8[9]. The robot travels with the wheels on its feet in flat, level areas, and walks and goes up and down stairs utilizing its leg structure on stairs. For the technology of recognizing the outside world, such as recognition of stairs, we are aiming at higher recognition capability by incorporating the results cultivated by our collaborative research with The University of Electro-Communications[10]. NR003 was the third prototype achieved to enable guiding on stairs at a realistic speed together with the user.

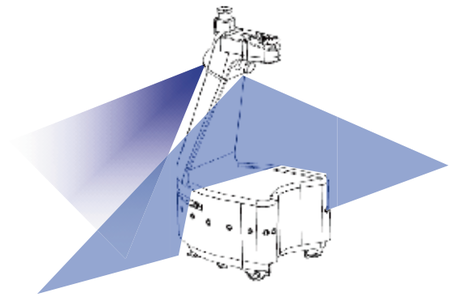

(1) Detection of difference in floor levels by LRF through the control device

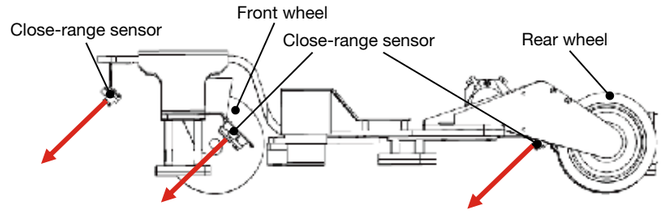

(2) Detection of difference in floor levels by close-range sensors without using the control device

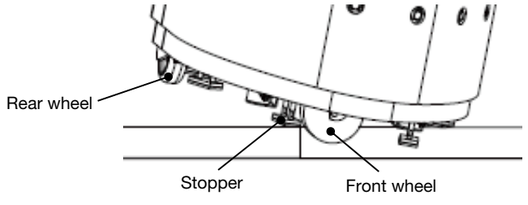

(3) Avoidance of fall by a stopper at a time when the wheel runs off the floor

Fig. 7 Systems for avoiding falls and components for reducing such risks

Fig. 8 The NR003 robot substituting for a guide dog for assisting the visually impaired

• Conclusion

This paper has described the technological development and prototype developmental status of robots to be used in place of guide dogs. Especially for the obstacle-avoiding leader robot, know-how on risk evaluation methods and risk reduction methods was accumulated with an emphasis on safety. These robots were exhibited at the 2011 International Robot Exhibition and received a great response. Additionally, there were several requests for demonstrations at events for the visually impaired, and in response we are collecting comments from the potential users.

We will address the challenges of functional integration of these two types of robots, obtaining feedback for market introduction by going out to give demonstrations and get feedback, expanding the area of activity, and considering additional functions (such as navigation functions) while moving toward accomplishing our goals.

References

1) "Fact-finding investigation results of disabled children and disabled persons 2006," Ministry of Health, Labour and Welfare, 2008.
2) "8.8 trillion yen of social loss caused by impaired vision," Japan Ophthalmologists Association, 2009.
3) "Visual impairment and blindness," World Health Organization, October 2011.
4) Japan Social Welfare Facility Council of the Blind, Independence Support Division, Guide Dog Committee Investigation, as of end of fiscal year 2010.
5) Investigation result report of "Investigation of guide dog," Nippon Foundation, 1998.
6) S. Tachi and K. Komoriya, "Guide Dog Robot," Robotics Research: The Second International Symposium 1984, The MIT Press, pp. 333–340, 1985.
7) H. Mori, K. Matsumoto, S. Kobayashi and A. Mototsune, "Research and development of walking guide robot for practical use," Journal of Robotics Society of Japan, Vol. 19, No. 8, pp. 26–29, 2001.
8) H. Ogawa, K. Sagayama and K. Tobita: Development of guide dog robot using force sensor, The Japan Society of Mechanical Engineers, Proceedings of the 2009 JSME Conference on Robotics and Mechatronics, 1P1-L12, 2009.
9) K. Sagayama, K. Tobita, H. Ogawa and S. Sugita: Going up and down stairs by four-legged wheel robot with two wheels per leg, The Japan Society of Mechanical Engineers, Proceedings of the 2011 JSME Conference on Robotics and Mechatronics, 2A2-C01, 2011.
10) K. Tobita, C. Kanamori, Y. Ookubo, H. Ogawa and S. Sugita: Recognition of stairs by multiple area conical scanning, The Japan Society of Mechanical Engineers, Proceedings of the 2011 JSME Conference on Robotics and Mechatronics, 1P1-E08, 2011.

Kazuteru Tobita

Hironori Ogawa

Katsuyuki Sagayama

Technological Trends of Jet Aircraft Engine Bearings

Masakazu Kawada and Kazuhiro Hara
Industrial Machinery Bearing Technology Center

ABSTRACT

In recent years, in addition to the longstanding demands for high reliability and high performance, jet aircraft engines have also been required to be environmentally friendly and operate more quietly, at lower operating costs. Demand for bearings has varied along with the structural change of the next-generation small-to-mid-size jet aircraft engines.

This article describes an integrated cylindrical roller bearing and discusses the results of testing under actual operating conditions using an integrated bearing with high-speed, counter-rotating inner and outer rings, and the results of calculations for verification.

1. Introduction

Modern jet aircraft must not only meet the long-established goals of remaining highly reliable and developing the highest technology; they are also expected to reduce emissions of CO_2 and NOx (to conform to environmental regulations, particularly in Europe and the USA) and be fuel efficient and save energy amid rising oil prices and the depletion of fossil fuels. Additionally, the requirements for improved maintenance performance (in terms of economy efficiency), electrical operation of the hydraulic pump, and low noise have led to developments that have resulted in a wide range of new technologies being put into practical use[1].

In addition, efforts have been made to improve cabin comfort and the economic efficiency of flight, resulting in a new jet engine mounting and the most advanced aerodynamic design, make planes using composite materials to reduce the weight, and reduce fuel consumption in the development of next-generation small-to-mid-sized civilian aircraft. This includes regional jets that are expected to be in great demand when they go into production in the near future.

As can be seen from the new environmental requirements described above, technical requirements for bearings change. This paper introduces technological trends in the aircraft industry and corresponding examples at NSK.

2. Trends in Bearing Design and Corresponding Examples

Conventionally, high performance and high reliability have been expected of jet aircraft engine bearings, and improvements have been made in material cleanliness for longer life and processing accuracy. NSK has developed bearings with a phosphate modified film treatment (Photo 1) with the goal of improving seizure resistance, and they continue to win acclaim[2].

In addition, for the cage of a jet aircraft engine bearing, the bearing ring riding method has been conventionally applied while taking into consideration the bearing's strength and lubrication properties during high-speed rotation, and it has been endowed with a self-lubricating silver-plated surface. On the other hand, bearings with TiN coating on the cage riding surface of the bearing ring, sliding under high temperature and high speed conditions, have recently been developed for improving wear resistance and are currently being supplied by NSK.

In order to meet requirements for reduced fuel consumption and airplane weight, each engine manufacturer has started to adopt an integrated bearing that is fixed with an outer-ring flange as well as an integrated bearing with a spring structure for absorbing vibration; NSK has started to supply such bearings (Figure 1).

Options under consideration to lower fuel consumption include a structure that would reduce the aerodynamic load on the low-pressure turbine stator vane and reduce the number of vanes by reversing the low-pressure and high-pressure systems for the improvement of aerodynamics inside an engine and to reduce weight, and also omission of the housing by supporting the space between two shafts with the bearing itself. For bearings used with this structure, one concern is abnormal wear on the roller end face and bearing ring rib surface, due to higher speed of rolling element revolution and skidding damage on the raceway surface, because the inner and outer rings rotate at high speed in opposite directions. NSK has carried out a series of development tests of cylindrical roller bearings (differential counter-rotating roller bearing) used for jet engines of next-generation small aircraft, with inner and outer rings rotating at high speed in opposite directions. With these tests, NSK has established the bearing specifications and confirmed performance. They are reported in the next section[3].

It is worth noting that this development was carried out in partnership with IHI Corporation[4] as part of "Research and development of an environmentally compatible type of small aircraft engine (ECO engine project)" with financial assistance from the New Energy and Industrial Technology Development Organization (NEDO) based on the aerospace industry innovation program and energy innovation program of the Ministry of Economy, Trade and Industry (Figure 2).

Photo 1 Chemically modified bearing resulting in phosphate surface films (test bearing)

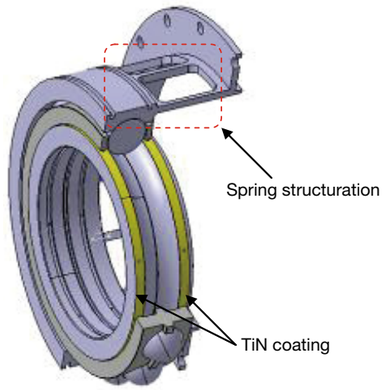

(a) Cylindrical roller bearing with outer ring flange (b) Integrated bearing with outer ring flange

Fig. 1 Integrated bearings with outer ring flange

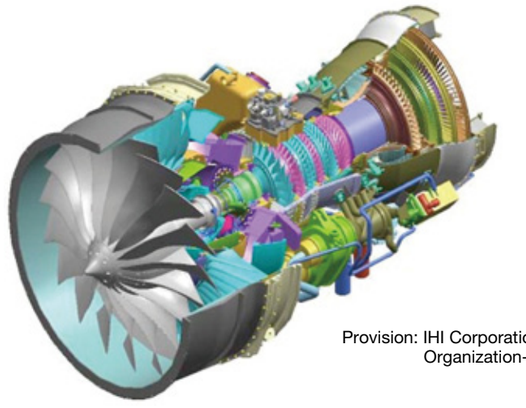

Provision: IHI Corporation, NEDO Technology Development Organization-subsidized project results

Fig. 2 Cutaway view of a small, environmentally-friendly jet engine[4]

3. Development of Differential Counter-rotating Roller Bearings

3.1 Purpose of this development

For the differential counter-rotating roller bearing whose inner ring and outer ring rotate in opposite directions at high speed, the bearing ring rib surface and roller end face reach a high relative speed because the revolving speed of rolling elements becomes much higher than that of a normal cylindrical roller bearing whose inner ring or outer ring only rotates. We are concerned that this leads to abnormal wear.

Additionally, we fear that abnormal wear (skidding damage) is generated between the roller rolling contact surface and raceway surface (especially the inner ring) when the difference in speed between the inner and outer rings becomes larger (higher relative speed).

We carried out bearing design and development tests that focused on these phenomena.

3.2 Test bearing and test method

3.2.1 Test bearing

The test bearing has specifications that take into consideration the following three items[5].

(1) Optimization of bearing internal clearance
(2) Optimization of rib height and control of clearance between roller and rib
(3) Lower heat generation by optimizing roller dimensions and accuracy

Table 1 shows test bearing specifications (refer to Photo 1 for test bearing appearance).

3.2.2 Test rig and test contents

We made a special stand test rig for this test. Photo 2 shows the appearance of the test rig, and Figure 3 shows a schematic view of the test rig around the test bearing.

The test bearing is positioned between the inner ring drive shaft end and the facing outer-ring drive shaft end. It is possible to drive each shaft at an arbitrary speed that is independent of electric motors. Additionally, the test rig has a structure that enables the application of an arbitrary load to test the bearing by loading the outer-ring drive shaft using hydraulic control. The amount of oil supplied and the temperature of the lubrication oil are variably controllable, and the test rig has a structure that enables the simulation of various operating conditions of jet engines. Table 2 shows the test conditions.

Also, we carried out the evaluations while making simultaneous multipoint recordings of the speeds of the inner ring, outer ring and cage; radial load; supply oil amount and temperature of lubrication oil; bearing temperature; drain oil temperature; and shaft displacement. In addition, we carried out comparative verification of the test results and analysis results using NSK's Rolling Bearing Kinetic Friction Analysis Program Package "BRAIN"[6].

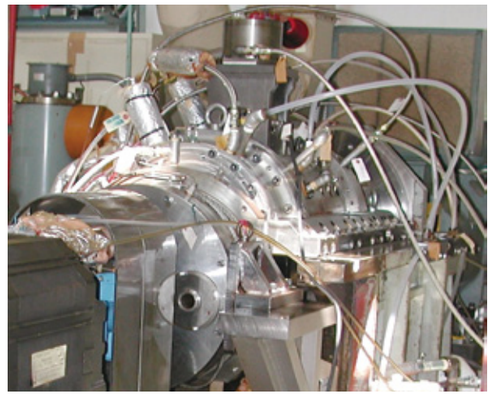

Photo 2 Rotational bearing test rig for high-speed bearing rings

Table 1 Test bearing specifications

Inner ring bore diameter	ø 136 mm
Outer ring outside diameter	ø 181 mm
Inner ring width/outer ring width	25 mm/29 mm
Number of rollers (pcs)	36
Cage riding type	Inner ring riding
Lubrication method	Inner ring shaft hole lubrication
Bearing material	AMS6278 conforming material/ AMS6491 conforming material
Cage material	AMS6414 conforming material
Surface treatment	Inner ring, outer ring, roller: Phosphate modified film treatment (NSK's developed treatment) Cage: Silver plating (AMS2410)

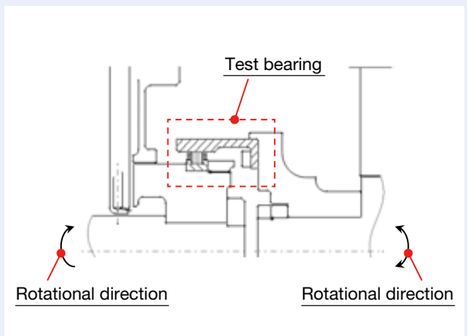

Fig. 3 Schematic view of test rig

Table 2 Test conditions

Test rig	Rotational bearing test rig for high-speed bearing inner and outer rings (NSK's independently-developed test rig for special use)
Maximum inner ring rotational speed/ Maximum outer ring rotational speed	30 000 rpm/±10 000 rpm (Minus sign denotes a rotational direction opposite to that of the inner ring. Plus sign denotes the same rotational direction as the inner ring.)
Radial load (Max)	2 500 N
Lubrication oil quantity	5 L/min to 15 L/min
Lubrication oil temperature	Ambient temperature to 120 °C
Lubrication oil	Conforming oil to MIL-PRF-23699

3.3 Test results and discussion

3.3.1 Bearing temperature and cage speed

Figure 4 shows the recorded bearing temperature and cage speed along with the varying inner ring speed when the outer ring speed is –5 600 rpm in the reverse direction, the radial load is 1 176 N, the supply oil amount is 10 L/min, and the supply oil temperature is 100 °C.

No big change in the inner ring temperature was observed, but the outer ring temperature increased along with the inner ring speed, and it tended to increase the difference in temperature between the inner and outer rings. While there are numerous factors to take into consideration, it seems that the method of lubrication has a large effect. Along with the increase of relative speed between the inner and outer rings, heat generation is increased by the friction between the bearing rings and rolling elements. However, the inner ring receives a supply of constant-temperature lubrication oil through the shaft hole, and we observed that it remained much cooler than the outer ring.

Additionally, as the difference in temperature between the inner and outer rings also tends to be smaller than that recorded in another test in which only the amount of supplied oil was increased (Figure 5), we suggest that there is a relationship between oil amount, method of lubrication, and the temperatures of the inner and outer rings.

3.3.2 Comparison of test result and analysis result of bearing heat generation

Figure 6 shows the relationship between outer-ring speed (forward or reverse direction) and bearing heat generation when the inner ring speed is 11 000 rpm in the opposite direction, radial load is 490 N, the amount of oil supplied is 6.5 L/min, and the temperature of the supplied oil is 70 °C. Figure 7 shows the measurements of cage speed. Also, analysis results by BRAIN are compared in each figure.

As shown in Figure 6, there is greater heat generation when the outer ring is rotating in the opposite direction (minus sign) compared to when the rotational direction of the inner and outer rings is in the same direction (plus sign). So we found that heat generation depended on roller revolution speed.

In addition, we obtained test results similar to the analysis results generated by BRAIN as shown in Figure 6 and Figure 7, and we were able to confirm that it is possible to predict by analysis. As a slight difference is observed in a few parts, we plan to improve the precision of the analysis tool by improving the testing and measuring technologies while continuing to accumulate data going forward.

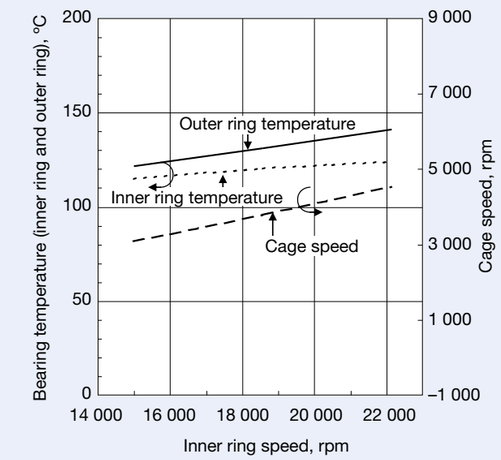

Fig. 4 Relationships between inner ring speed and bearing temperature, and between inner ring and cage speeds

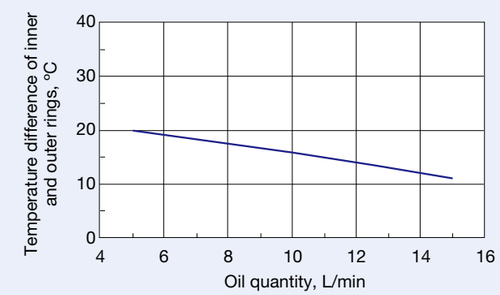

Fig. 5 Relationship between oil quantity and the bearing temperature difference of the inner and outer rings

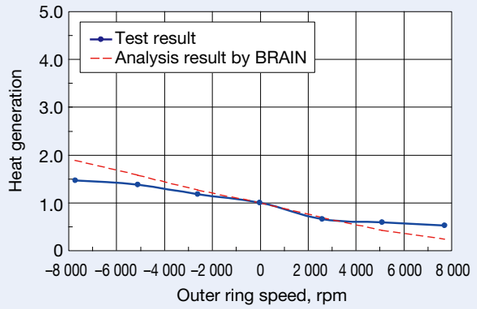

Fig. 6 Relationship between outer-ring speed and heat generation

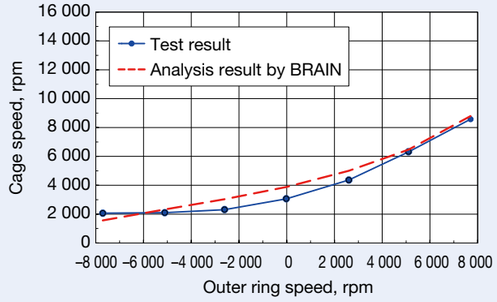

Fig. 7 Relationship between outer-ring speed and cage speed

4. Conclusion

Our observations suggest that other requirements that differ from those of the past will arise in accordance with the changes in use conditions and structure for future jet aircraft engine bearings. Additionally, we predict that it will be necessary to improve comprehensive technological capability for responding to the requirements of tapered roller bearings, which have rarely been used for jet aircraft engines, and other rolling bearings. We aim to continue to improve mass production and quality, along with improving comprehensive technological capability.

References

1) Investigative report of technology development trends in aircrafts in fiscal 2011, (March 2012) 2–17, International Aircraft Development Fund.
2) Y. Ohura and T. Yuruzume, Development of Jet-Engine Bearings, NSK Technical Journal, 663 (1997) 8–17.
3) Y. Osada, M. Kameko, M. Kawada, H. Yoshimoto and A. Itou, Research of differential counter-rotating bearings for jet engines, Tribology conference proceedings, (Fukui 2010–9) 259–260.
4) S. Yamawaki, T. Fujimura and M. Yamamoto, Summary of Research and Development in the ECO Engine Project, IHI Engineering Review, 47–3 (2007–9) 91–95.
5) Y. Morita and Y. Ohura, Development of High-Speed Cylindrical Roller Bearings, NSK Technical Journal, 671 (2001) 14–20.
6) H. Aramaki, Rolling Bearing Analysis Program Package “BRAIN”, NSK Technical Journal, 663 (1997) 1–7.

Masakazu Kawada

Kazuhiro Hara

Technology Development and Future Challenge of Machine Tool Spindle

Shinya Nakamura, Hisashi Kawamura and Yoshiaki Katsuno
NSK Ltd.

ABSTRACT

In this paper, the history of main spindle speeding up and future technological challenge are described, at the same time, the latest main spindle technology is introduced.

Reprinted with permission from SME Tokyo Chapter, Journal of SME Japan Vol. 1

1. Introduction

The machine tool spindles have been developed with a focus on high-speed technology as the reason behind that they aimed the improvement of cutting efficiency by the development of machining center on 1975 or later, in accordance with the demand of speeding up was increased rapidly.

After that the wide range of needs such as higher accuracy, higher stiffness, and improvement of reliability etc. are come out. In addition, the needs in response to environment, saving energy, 5-axis machine, multitasking machine and intelligent machine are come out. In this article, the history of spindle speeding up and future technological challenge are described, at the same time, the latest spindle technology is introduced.

2. Speeding Up of Spindle

2.1 History of spindle speeding up

Figure 1 shows the history of spindle speeding up. The $d_m n$ value of spindle bearing has been increased spectacularly in response with the cutting needs with the times. As the key technologies making progress of speeding up, the improvement of lubrication method such as grease lubrication, oil-air lubrication, and jet

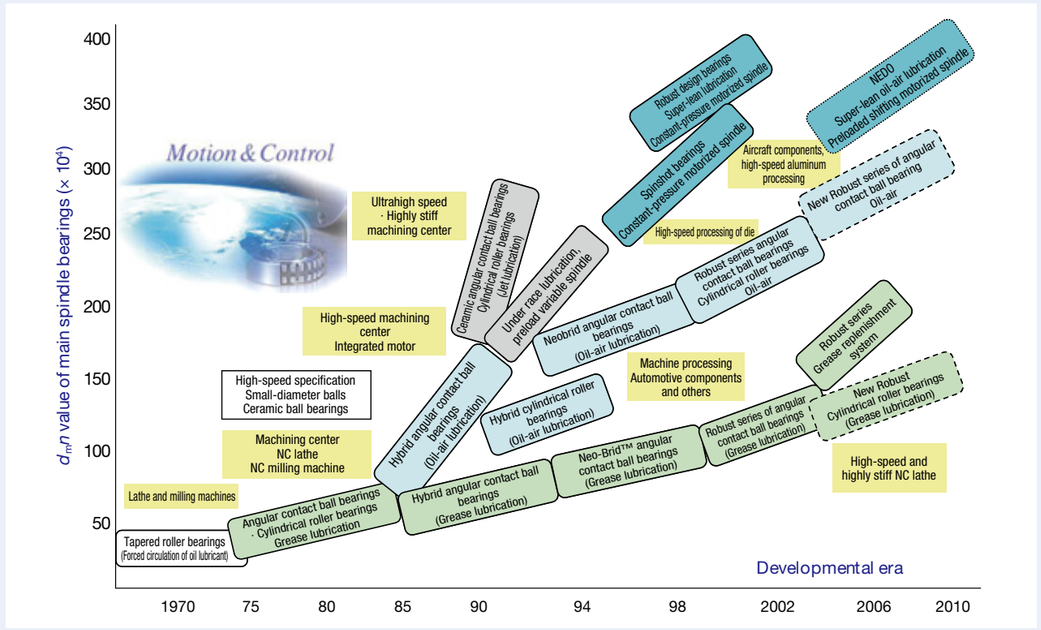

Fig. 1 Transition of speeding up of machine tool spindles

lubrication, the application of new material to bearings (rolling elements, inner and outer rings and cage) such as ceramic balls, and the advancement of design approach and technique of analysis are mentioned.

Figure 2 shows the investigation results of high-speed spindle (10 000 rpm over) displayed in Japan International Machine Tool Fair (JIMTOF) since 1982. In JIMTOF2012, the progress of speeding up is standstill in recent years, and the maximum rotating speeds are focused on around 12000 rpm and 20000 rpm. As the features of whole machines, speaking of machining center, the exhibits of 5-axis machining center which has the turning mechanism of spindle (tool side) and table (work side) are increased, and in the case that they are used as processing machine of aircraft components or dies, in order to attain high-efficiency process, high-speed spindle is equipped. In the case of multitasking lathe, the trend toward speeding up of milling spindle is remarkable.

The so-called built-in motor spindle which the driving motor is integrated inside the spindle is become regular use as it is indispensable technology for high-speed spindle, for the attainment of ultrahigh-speed rotation, further speeding up, high output, and downsizing of the rotor and stator are expected. Recently in response to environment and saving energy, additional speeding up and improvement of reliability of grease lubrication begin to be required.

2.2 High-speed bearing technology

As for the high-speed spindle of recent machine tool, in order to make the inertia of rotating parts, the adoption of built-in motor spindle which integrates compact and high output rotor is increasing. However, for such kind of spindle structure, at the transition period of rapid rotational fluctuation, ambient environmental variation (heat generation change of motor and outer cylinder cooling) becomes significant, and the bearing of spindle is exposed under the harsh thermal fluctuation condition. For the spindle bearing, it is the most important to have the characteristics of seizure resistance under such environmental condition, and it is necessary to have temperature robust performance (against thermal load fluctuation, the bearing itself shows small fluctuation of heat generation value, more specifically, against the thermal disturbance, the bearing has a characteristic of thermal insensitivity). For these high-speed spindles, to respond the demands described above, the ultrahigh-speed bearings “ROBUST Series”, whose bearing internal design was optimized as described below are adopted[1]. (Refer to Figure 3)

Under the processing conditions with various cutting conditions and rotational fluctuation, the temperature change inside the spindle is significant and the temperature difference between inner and outer rings involved, it causes the decrease of bearing internal clearance, the contact angles between balls and raceway groove of inner and outer rings change rapidly, and the internal preload of bearing increases, the *PV* value (*P*: Contact surface pressure, *V*: Sliding speed) of rolling contact area between the raceway groove of inner and outer rings and balls increases. The internal specification of ROBUST Series bearings is that the change of *PV* value is minimized under the conditions described above on the basis of analytical results by the computer as the affectors such as ball diameter, raceway groove curvature of inner and outer rings, and contact angle etc. are considered the parameters. And the application of special carbonitrided steel (SHX steel) and the adoption of high-strength plastic cage of special configuration that has excellent heat resistance and wear resistance improve seizure resistance additionally. Also, the Spinshot bearings that the lubricating oil is replenished effectively under the condition of high-speed operation by optimizing the bearing configuration are developed.

3. Technical Challenge of Spindle

Figure 4 shows the technologies required from the machine tools in Japan in the future. To begin with, the technologies required from the machine tools, secondly the technologies required from the spindle and the bearings were summarized. Until recently the development of high speed, high accuracy, and high stiffness was focused but recently the durability and the improvement of reliability are required, especially in the past several years, the environmental responsiveness, saving energy, and advanced grease lubrication for maintenance-free operation are required. And the requirement of Intelligent and Smart by applying the sensor is increasing. This article introduces a method to achieve reduced torque without reducing basic performance, halving both bearing internal torque and seal torque, and provides examples of the aforementioned.

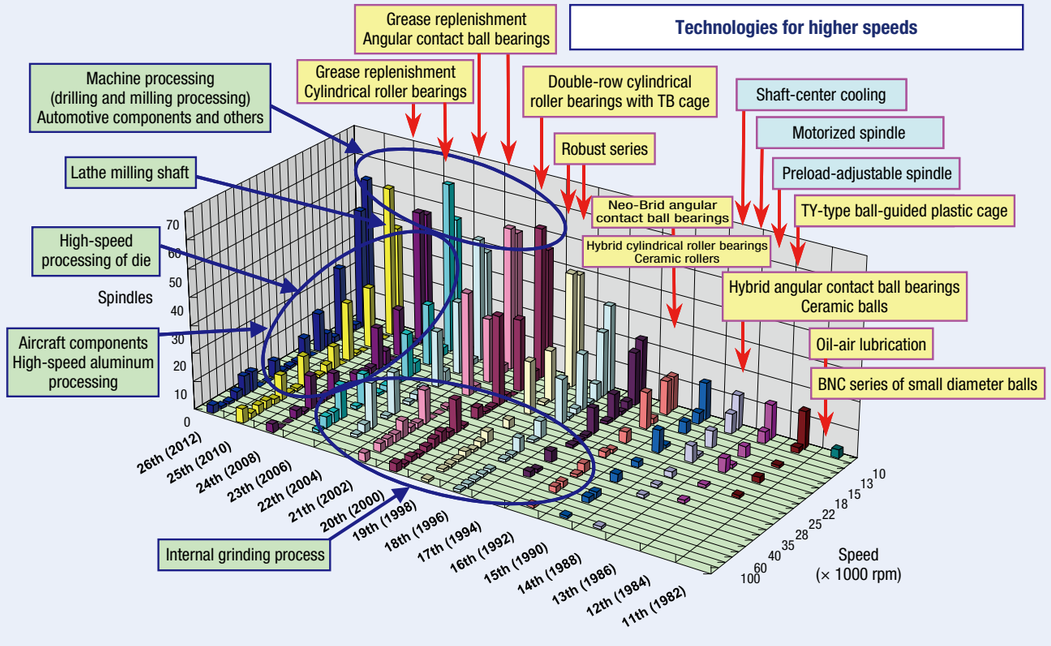

Fig. 2 JIMTOF High-speed spindle display situation (10 000 rpm over) Investigated by NSK

Ultrahigh-speed angular contact ball bearing

Spinshot II bearing

Ultrahigh-speed single-row cylindrical roller bearing

Fig. 3 Examples of various ROBUST Series

	Needs for machinery	Needs for main spindles	Needs for of bearings
Processing of die	Improved processing of surface quality	Higher speeds and higher accuracy of main spindles	Improved accuracy of bearings exclusively
Processing of automotive components	Tough main spindle	Improved durability and anti-shock characteristics	Improved indentation resistance and seizure resistance of bearings
Processing of aircraft components	Processing technology for difficult-to-machine materials	High capacity, high stiffness, and high torque	Highly rigid, anti-shock, anti-vibration bearings High accuracy of large bearings
General-purpose processing	Measures for the environment	Reduced energy consumption Maintenance-free performance	Technological advances in grease lubrication · Ultralong-life grease · Highly reliable life calculation formula
Common technologies	Intelligent	Fusion of main spindle and peripheral technologies Intelligent main spindle	Intelligent stand-alone bearings · Bearing with sensor · Establishment of sensing technology

Fig. 4 Future technology requirement of machine tools in Japan

3.1 Measures for high speed and high accuracy

As the lubrication method used generally for spindle of machine tool, grease lubrication, oil-air lubrication and oil mist lubrication etc. are quoted. Depending on the method of supplying or retaining the lubrication oil or the difference of quantity, their features are different respectively. For the spindle of machine tools, from the aspect of the improvement of machining accuracy, as the basic characteristics, low heat generation and low temperature rise are required.

(1) Oil-air lubrication

The oil-air lubrication was developed and put to practical use as the suitable lubrication method for ultrahigh-speed rotation by adopting advantages of grease lubrication and oil mist lubrication and by eliminating disadvantages respectively. As shown in Figure 5, the oil-air lubrication system is that high-pressure air and tiny oil droplet are fed from bearing side face to bearing inside with the use of oil feeding nozzle. In this system, the air curtain which is generated by high-speed rotation (the air curtain in this case means the wall of circumferential high-speed air stream generated by the friction between the air and high-speed rotating outside surface of inner ring.) blocks the oil flow from the nozzle. As the result, the lubrication oil was not fed into the bearing inside certainly, it was likely the cause of seizure. There was the lack of stability in the range where the $d_m n$ value exceeding (200–250) × 10^4.

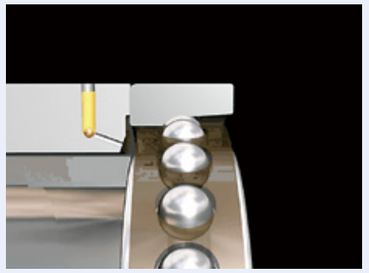

Fig. 5 Conventional oil-air system

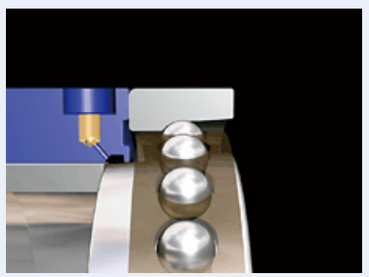

Fig. 6 Spinshot system

(2) Spinshot bearing

New bearing “Spinshot II”[2] as shown in Figure 6, was developed to solve the problem described above, and it has the design specification of improved temperature robust performance described in the section 2.2 and special bearing structure additionally that the width of inner ring is wider than that of outer ring and the outside surface of inner ring is tapered configuration. By this configuration, the lubrication oil assisted with air, is sprayed from the outer ring spacer to the tapered surface of outside surface of inner ring, as shown in Figure 7, the lubrication oil is moved on the tapered surface by centrifugal force of rotation and guided to the inside of bearing and fed to the rolling elements certainly. And since the structure is that the air is not blown to the inside of bearing directly, it is able to control harsh air noise of high frequency due to the air generated by high-speed rotation. In addition, as it is free from the blocking of oil by the air curtain, it is not necessary to speed up the flow rate of air and it was possible to reduce the air pressure. For the amount of air and oil, it is 10 L/min (Normal) per one nozzle, in comparison to conventional oil-air lubrication, about 60 % reduction in air consumption was attained. And in case that the lubrication oil is fed externally, to realize the stable rotation at ultrahigh-speed rotation, it is important to attach the sensor, which is monitoring whether the lubrication oil is fed from lubrication equipment to spindle side certainly or not.

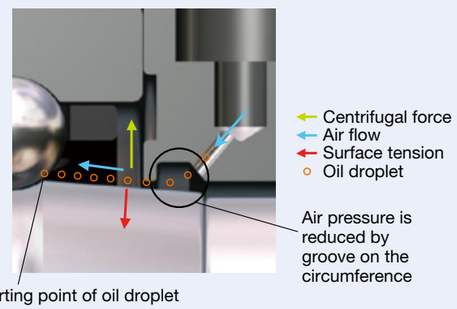

Fig. 7 Lubrication principle of Spinshot II

(3) Development of super lean oil-air lubrication

In order to make further speeding up of oil-air lubrication, as the lubrication method feeding much less quantity of lubrication oil, the super lean oil-air lubrication was developed. The super lean oil-air lubrication is the system feeding lubrication oil by use of air as well as oil-air lubrication, but it is possible to control the discharge rate of 0.001 cc or less for one shot. As the spindle adopted the super lean oil-air lubrication, the spindle of the highest speed in the world was developed. The specification is that the taper of spindle end is HSK-E50, spindle diameter is 60 mm, the maximum rotating speed is 50 000 rpm ($d_m n$ 380 × 10^4).

Table 1 50 000 rpm Spindle specification

Spindle end taper	HSK-E50
Maximum rotating Speed ($d_m n$ value)	50 000 rpm (dmn 380 × 10^4)
Bearing bore diameter	Front side ⌀ 60 mm, Rear side ⌀ 50 mm
Lubrication	Super lean oil-air lubrication
Preload type	Constant pressure preload (DT+DT arrangement)
Preload shifting	3 steps preload shifting

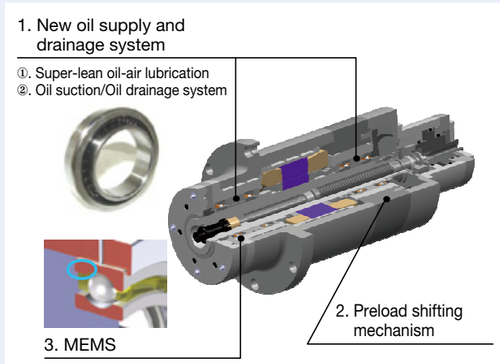

Fig. 8 Features of 50 000 rpm Spindle

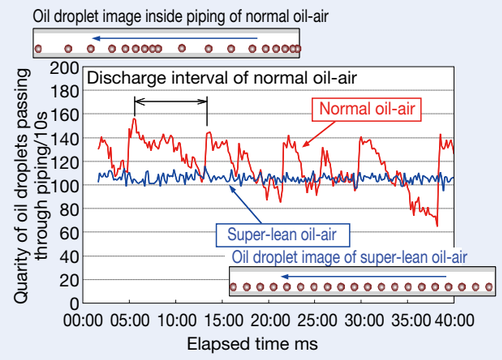

Fig. 9 Comparison result of oil droplet quantity passing through piping

In Table 1, the specification is listed and the features of this spindle are shown in Figure 8[3]. As the first feature, new oil supply and drainage system was adopted. For the oil supply side, by using the super lean oil-air lubrication described above, as shown in Figure 9, in comparison with the oil-air lubrication, the flow of oil droplet inside piping is able to be stabilized and it is possible to control the heat generation of bearing and the change of temperature rise. Also, for the drainage side, newly oil suction and oil drainage system was adopted. By this mechanism, even if the spindle goes up and down or turns, the lubrication oil does not stay inside the bearing and to be drained easily the change of heat generation inside spindle is controlled and it is possible to stabilize the temperature rise. Figure 10 shows the flow pattern of lubrication oil supply and drainage inside the bearing.

As the second feature, by using tandem duplex bearings (DT + DT) with constant pressure preload, the preload shifting mechanism (Figure 11) that can control the preload such as heavy preload at low speed, medium preload at medium to high speed, and light preload at high to ultra-high speed, was adopted. By this preload shifting system, it can bring about the realization of heavy cutting at low speed to ultrahigh-speed cutting. As the third feature, by attaching MEMS (Micro electro mechanical

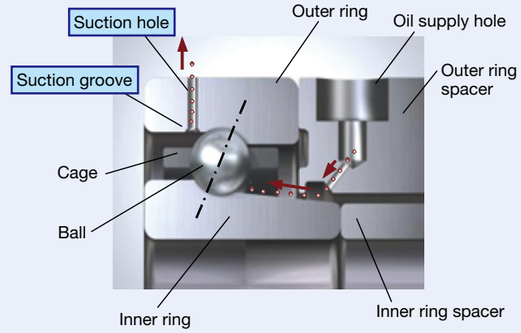

Fig. 10 Flow of lubrication oil inside bearing

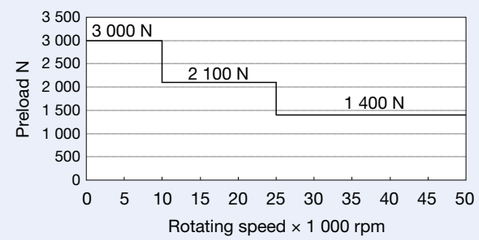

Fig. 11 3 steps change of constant pressure preload

System) temperature sensor inside of the bearing, the temperature around heat source of bearing was measured. By adopting MEMS temperature sensors, it was able to improve the responsiveness of temperature measurement. And for the needs of speeding up and high rigidity of spindle, the higher speed spindle, the more technologically advanced measures are required such as multi balance control at high-speed rotation and high accuracy of bearing etc. In addition, in the case of built-in motor, when the channel of stator cooling oil is not line symmetry channel to the shaft center of spindle, the thermal displacement in radial direction occurs easily, and the shaft elongation affects heavily the quality of finished surface, so that it is looking forward to the arrival of high-speed bearing and motor with excellent heat generation properties, and material of low linear expansion coefficient.

3.2 Measures for high rigidity

Meantime, for the aluminum processing profiler as represented by aircraft components, since the aluminum material has a good machinability. Then the spindle needs the performance of high rigidity as well as higher speed conflicting each other. In addition, this type of machine generally has the turning type spindle because the work size tend to be bigger. In this case, in order to achieve the fine processing profile with a complex and small circular arc, the downsizing of spindle is more advantageous, but to ensure the compatibility with high rigidity, higher technology level is required.

3.3 Measures for 5-axis machine and multitasking machine

(1) Required function in case of tool side turning

For the machine tool with a turning tool head, the required characteristics for spindle, as shown in Table 2, are classified by two keypoints such as (1) how to shorten the overall spindle length, and (2) reliability of bearing lubrication structure that is able to respond to the change of attitude. The needs of item (1) come from the four matters; the oscillation space of turning is reduced by shortening the spindle length, the effect on the linear motion shaft is controlled, the increasing in size of the machine should be avoided and the capacity of turning motor should be reduced by down sizing the spindle. For the position change of item (2), is it designed that the reliability of bearing lubrication is not damaged by the position change?

Table 2 Required characteristics for turning spindle and the problems

(1) Shortening of overall length	(2) Reliability of bearing lubrication structure
• Selection of number of bearing row • Downsizing of bearing system • Downsizing of built-in motor • Shortening of tool clamping mechanism	• Smooth drainage of lubrication oil • User friendliness of piping • Control of grease drop out • Prevention of ingress of coolant

(2) Shortening of overall spindle length

To increase the load capacity of spindle, by increasing the number of bearing row and reducing the load per a bearing row is common practice, but the spindle is lengthened and it is difficult to use for 5-axis machine of turning spindle type. As far as the angular contact ball bearing, the matched back-to-back arrangement (DB) is shorter than the four-row back-to-back arrangement (DBB), and for the cylindrical roller bearing, the single-row is shorter than the double-row, but the load capacity is smaller in each case. Especially in case of multitasking lathe in comparison to 5-axis machining center, the case that it is forced to make compromise this point is found here and there. In case of the machining center, if 2-axis turning are equipped at work side, this point does not become something of a problem. And though the machine adopting turning spindle system in such composition, since the machine itself is large mostly, the problem is hard to become obvious. However, when it is considered that the deployment and expansibility of 5-axis machine to various processes in the future, it is necessary to take measures to shorten the overall length as much as possible by composing compact bearing system including lubrication mechanism and by optimizing bearing arrangement inside the spindle.

And recently since the built-in motor is used in the spindle, and the spindle itself becomes compact, for turning spindle system 5-axis machine, the built-in motor spindle is optimum. In such case, since the motor is the factor determining the overall length of spindle in many cases, the commercialization of smaller size and higher output motor is desired.

(3) Measures for change of attitude

For the oil-air lubrication which is now perfectly established as the lubrication system of high-speed spindle, the smooth drainage of lubrication oil which is fed continuously is an important point to realize the stability in the aspect of lubrication. In case of the composition of turning spindle, it is necessary to pay full attention for the design of drain channel in response to the turning angle.

Also, for the units performing turning motion, it should be free from wiring and piping as much as possible. If possible, to adopt grease lubrication is the one of solutions. However, in such case, there is a concern about the deterioration of life due to dropping out of grease in comparison with the spindle without position change. In addition, as the big challenge which the spindle has, there is the problem that how to prevent the ingress of coolant inside the spindle. In this point, the risk of ingress increases from the vertical type, the horizontal type, and the turning type in order.

3.4 Measures for grease lubrication

(1) Sealed angular contact ball bearing

For the machine tool spindle bearing, the environment friendly clean technology attracts a lot of attention, as the bearing in response to such requirement, the precision sealed angular contact ball bearing (refer to Figure 12) is come into use. In this bearing, compact non-contact seals are adopted, while it is holding the interchangeability with conventional bearing, and the workability improvement by prelubricated grease, splash prevention of grease, and improvement of high-speed rotation are striven. Also, by using this bearing, it is not only the extension of grease life is able to be striven but also it is possible to prevent the drop of grease in case of the vertical type spindle.

(2) Grease replenishing lubrication bearing

Since the grease lubrication can be used for a long time only to be filled the specified amount of grease when the bearing is mounted, it is very easy and it is widely used as the most common lubrication method. However, in case of the built-in motor spindle, the continuous running at high speed with urgent acceleration and deceleration is increasing, though it is possible to rotate for a short time with conventional grease lubrication, the failure case that the grease is deteriorated or depleted by high-speed continuous running and it causes the occurrence of seizure begins to increase.

Consequently, when the grease life is considered, for existing grease lubrication the maximum rotating speed is limited. As well as the oil lubrication, the grease replenishing lubrication is that by supplying the lubricant externally, the grease life was improved spectacularly, and it attained the maximum rotating speed 20 000 rpm though it is grease lubrication.

Figure 13 illustrates the structure of new grease replenishing lubrication system developed by NSK Ltd. For the application except the area of machine tool spindle, until recently, there were the methods to grease into bearings with use of grease replenishing piping or grease nipple etc. However, in this new system, there are the biggest features such as the quantity of supplied lubricant is extremely small amount, in addition the grease is fed directly into the bearing which is rotating at high speed. In case of the oil-air lubrication, as the oiling quantity, the lubrication oil of about 1–3 cm^3 is consumed by single row of bearing for 24 hours. In the meantime, the grease quantity of grease replenishing lubrication is extremely small such as less than 0.1 cm^3, and it is not necessary to drain the lubricant to outside.

In addition, since the consumption of air to supply the lubrication oil is not necessary; as a result, it is free from splashing the oil to atmosphere, as ecological point of view, the grease replenishing lubrication is superior to the oil-air lubrication or the oil mist lubrication. Figure 14 shows the grease replenishing unit “Fine-Lub II” used for the grease replenishing lubrication system.

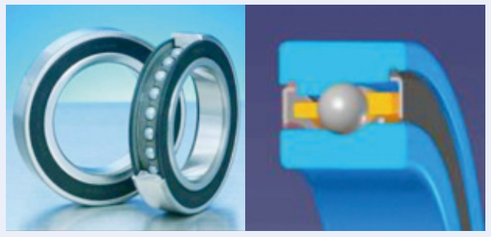

Fig. 12 Sealed angular contact ball bearing

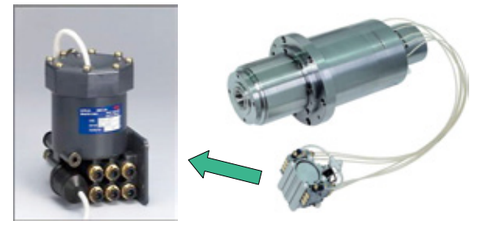

Fig. 14 Grease replenishing unit Fine-Lub II

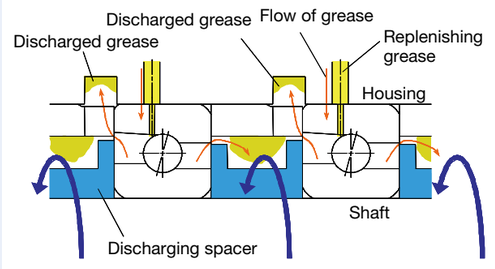

Fig. 13 Grease replenishing lubrication system

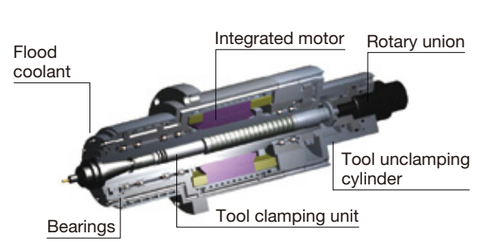

Fig. 15 High-speed built-in motor spindle

NSK Ltd. has developed “High-speed built-in motor spindle”[4] as the standard spindle of NT40 Class adopted grease replenishing lubrication (Refer to Figure 15). This spindle adopted the world’s first new lubrication system saying that grease replenishing lubrication, it attained the maximum rotating speed 20 000 rpm though it is grease lubrication. The main specifications of this spindle are listed in Table 3[4].

3.5 Measures for intelligent spindle

As the direction of machine tool spindle in the future, the demand of intelligent spindle is increasing, but there is not yet the intelligent spindle which comes into practical use in the market. NSK Ltd. has developed the spindle[5] in which the load displacement sensor and the encoder were integrated to detect the axial displacement during cutting process in addition to MEMS sensor described above. The rotation of this spindle was demonstrated in JIMTOF2010.

The purposes of development of this spindle were the control of tool life by detecting the load change at cutting process, the automatic process shutoff by detecting abnormal load, the review of process conditions, and the preventive measures of bearing failure by detecting the preload of bearing etc. Figure 16 illustrates the image of load change at cutting process. It is possible to detect the increase of cutting load or emergent cutting defect. Figure 17 shows the mounting arrangement of the load displacement sensor in the spindle. The shape of sensor is like nozzle top of oil-air lubrication, and the encoder is the inner ring spacer of bearing.

This spindle was mounted on the actual machining center; a work (cast iron) was put on the Kistler dynamometer, and when the drilling process was operated as shown in Figure18, the cutting process test was conducted by comparing the output of displacement sensor and the input load. The comparison result of the test is shown in Figure 19. Including other end mill cutting etc., the almost same values are obtained between the input load and the output of displacement sensor.

Table 3 B1 Spindle specification (L type)

Spindle end taper	NT40/HSK-A63 (Op)
Maximum rotating speed	20 000 rpm
Maximum output	22/18.5 kW (15 Minutes/Continuous)
Maximum torque	118 N·m (25 % ED)
Bearing bore diameter	⌀ 70 mm
Preload type	Position preload (DBB arrangement)

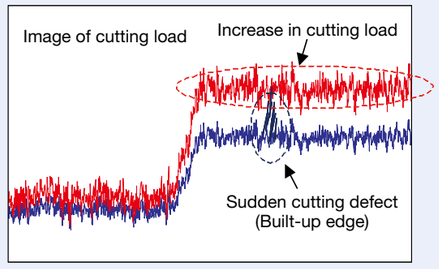

Fig. 16 Image of cutting load

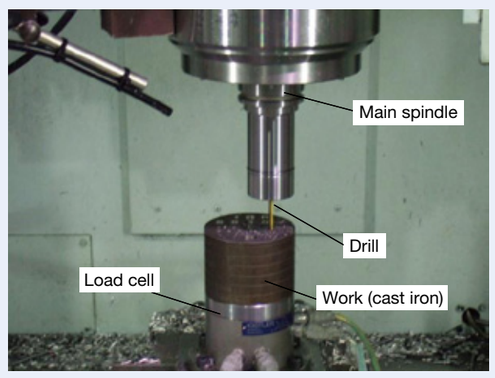

Fig. 18 Cutting process test by actual machine

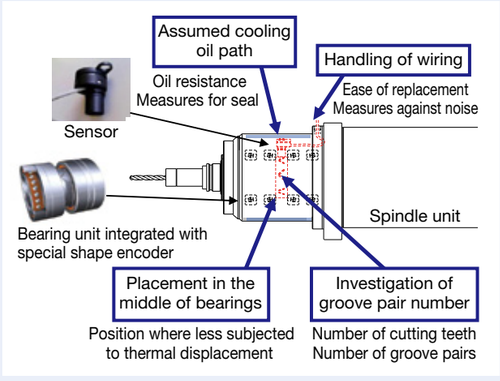

Fig. 17 Spindle integrated load displacement sensor

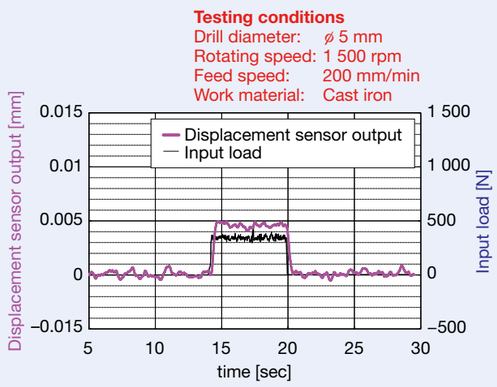

Fig. 19 Comparison of cutting process test results

4. Conclusion

With a focus on the speeding up of machine tool spindle, the technology development of spindle over last 35 years was explained, but the speeding up is standstill in recent years, the market requirement is changing from high speed and high accuracy to high stiffness and improvement of reliability, and nowadays environmental responsiveness, saving energy and intelligent spindle.

In this year, JIMTOF2012 is scheduled to be held, it is considered that Japanese machine tool industry aims saving energy and ecology-conscious directivity in the future, and the high value-added machine tools are increasing by adopting new material such as CFRP and by performing processing of 3 dimensional curved surface. Above all, it is considered that the technology aiming further speeding up of spindle along with the life enhancing and improvement of reliability of grease lubrication will be revived newly[6].

Continuously I hope to take the lead in the spindle technology and intend to advance new research and development aiming the improvement of unique machine tool technology in Japan.

References

1) S. Sugita, Y. Katsuno and Y. Oura, Ultrahigh-speed angular contact ball bearings for machine tool spindle, Technical Journal 673: (2003) 54–56.
2) M. Aoki and S. Nakamura, Technology trend and new technology of machine tool bearings, Journal of The Japan Society for Precision Engineering Vol. 74 No. 9 (2008) 913–916.
3) M. Aoki and Latest trend of spindle and ultrahigh-speed spindle technology, Text of 39th Machine tool associated engineers’ conference (2009).
4) M. Aoki and Y. Morita, Development of grease replenishing lubrication built-in motor spindle NSK Technical Journal 676 (2003) 16–25.
5) Y. Inagaki, Technological trend of spindle and intelligent technology Text of 40th Machine tool associated engineers’ conference (2011).
6) H. Kawamura, The latest technology trend of the machine tool bearing, Machine Design (Kikai Sekkei) Vol. 57 No. 3 (2013) 29–33.

Shinya Nakamura

Hisashi Kawamura

Yoshiaki Katsuno

Electrical Erosion of Motor Bearings

Keiji Yasunaga (Current Enrollment : European Technology Centre)
Industrial Machinery Bearing Technology Center

ABSTRACT

In this paper, we explain the electrical erosion of bearings used in motors and describe measures that can be taken to prevent it. When voltage is applied to the motor due to high-frequency electrical noise from nearby equipment, electric current passes from one bearing ring to the other through the rolling elements and lubricant films. As a result, minute sparks are emitted from the contact areas within the bearing, resulting in electrical erosion damage. Vibration and sound from the bearing get worse due to electrical erosion damage, and surface flaking of the bearing rings may occur as conditions further worsen.

As a result of researching this type of electrical erosion and carrying out various tests, we discovered measures that can be taken against it. One measure is to increase the insulating breakdown voltage of the bearings to be higher than the voltage of the electrical noise. Another is to enlarge the insulation resistance value of bearings through the use of ceramic balls.

1. Introduction

With the recent increase in consciousness of the need to save energy and reduce global warming, the efficiency of motors has greatly increased. Inverter control is one method of achieving higher efficiency, and increasing the control frequency (carrier frequency) enables the motor to operate more efficiently. With the increase in carrier frequency, however, there are cases of bearing electrical erosion generated by high-frequency electric current flow into a bearing. NSK calls such damage “high-frequency electrical erosion.” High-frequency electrical erosion scarcely occurred before 2004, but since then it has been occurring with increasing frequency in inverter control motors for home electronics and industrial equipment.

This introduces how NSK deals with high-frequency electrical erosion.

2. What is High-frequency Electrical Erosion?

“High-frequency electrical erosion” is a term coined by NSK which basically refers to the same phenomenon as conventional electrical erosion; that is, it is the phenomenon in which electrical current flows within the contact area between the bearing ring and rolling element during rotation, partially melting the surface and making it uneven. However, in a remarkable phenomenon, the result occasionally may be a satin-like surface or the wavy wear referred to as “ridge marks” or “fluting” (hereinafter called ridge marks).

“High-frequency electrical erosion” means the damage of bearing that arising from a high-frequency noise occured by an inverter device. It is defined as a phenomenon generated in bearings that are mounted to rotating equipment (the motor, etc.) with inverter control, or bearings that are mounted to rotating equipment near the inverter control equipment.

Photo 1 shows the ridge mark caused by high-frequency electrical erosion on a bearing mounted to the fan motor driven by the inverter.

The roughness known as ridge marks occurs at the integral multiple of the number of rolling elements in a bearing. It causes very loud noise and extreme vibration because the rolling elements roll on such a rough surface, resulting in more noise and less reliability of the rotating equipment.

Photo 2 shows ridge marks photographed by a scanning electron microscope (SEM). A lot of minute discharge marks were observed, and it has been confirmed that some evidence was crushed by rolling elements passing over discharge marks.

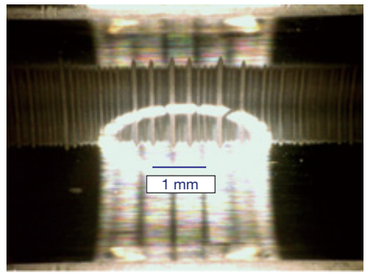

Photo 1 Ridge marks (Fluting) on 6201 ball bearing inner ring raceway

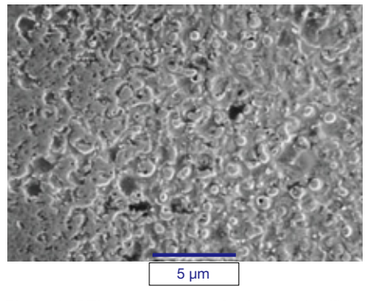

Photo 2 SEM photograph of ridge marks (fluting) on a 6201 ball bearing inner ring raceway

3. Reproduction of High-frequency Electrical Erosion and Various Tests

It is possible for NSK to reproduce the damage by high-frequency electrical erosion that has occurred at customer sites, by forcibly flowing high-frequency electrical current (electrical voltage and frequency control) into bearings. Here are the results of some of these tests.

3.1 Formation process of ridge marks

Photo 3 shows the phases of the forming of ridge marks, in chronological order, as recorded by reproduction test equipment. A 6201 bearing (bore diameter: 12 mm, outside diameter: 32 mm) was used as the test bearing, and the ridge marks forming on the same position of the inner ring raceway were observed at certain times. Fluting was caused by the minute discharge marks at the initial stage of operation. The process of forming ridge marks has been confirmed to occur over the course of a machine’s operation.

3.2 Relationship between insulation breakdown voltage and oil film parameters in a bearing

A rotating bearing possesses a certain level of insulation resistance from the lubricant oil film. When the applied voltage exceeds the insulation breakdown voltage of the oil film, electrical current flows into the bearing and discharge occurs. Figure 1 shows test results regarding the relationship between oil film generated on a rotating bearing and insulation breakdown voltage, using reproduction test equipment.

A sine wave voltage of 16 kHz was applied between a bearing’s inner ring and outer ring for testing, and the voltage was gradually raised while checking the waveform of the electrical current using an oscilloscope. The voltage value where electrical current started to flow into the bearing due to insulation breakdown was defined.

Six sizes of bearings, from the 608 bearing (bore diameter: 8 mm, outside diameter: 22 mm) to the 6204 bearing (bore diameter: 20 mm, outside diameter: 47 mm), were used. The oil film parameter Λ was obtained by calculating the parameters of lubricant type and rotational speed.

As shown in Figure 1, it was confirmed that insulation breakdown voltage was not influenced by bearing size and increased with the increase of oil film parameter Λ (in proportion to oil film thickness).

Test conditions

Bearing:	ø 12 mm × ø 32 mm ×10 mm
Speed:	1 000 rpm
Lubricant:	Lithium soap grease (synthetic oil)
Load:	F_a = 40 N
Frequency:	16 kHz
Waveform:	Sine wave

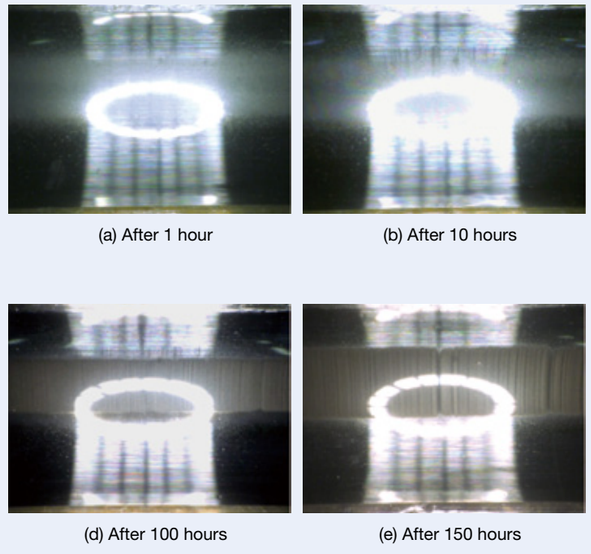

(a) After 1 hour (b) After 10 hours

(c) After 50 hours (d) After 100 hours (e) After 150 hours

Photo 3 Change in ridge marks (fluting) phase on a 6201 ball bearing inner ring raceway at certain times

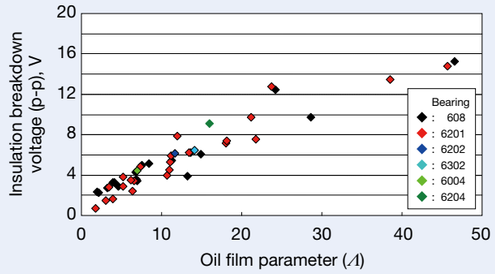

Fig.1 Measured results of insulation breakdown voltage in bearings

3.3 Relationship between bearing vibration and oil film parameters

The relationship between insulation breakdown voltage and oil film parameters in bearings was described in the previous section. A test of the influence rate (rise of bearing vibration) of oil film parameters on high-frequency electrical erosion generated in a bearing was carried out, where high-frequency electrical current passed through the bearing after voltage that exceeded the insulation-breakdown voltage of oil film was applied[1]. Figure 2 shows a plotted chart of bearing vibration rises at certain amounts of time after applying a constant voltage (a sine wave of 16 kHz frequency) between a bearing's inner ring and outer ring with controlling oil film parameter Λ. From this result, it was determined that the smaller the oil film parameter, the smaller the rise of bearing vibration level. That is, it is believed that in the case of thin oil film, the generation of minute discharge marks decreases because high-frequency electrical current passing through the bearing is kept at a low level, resulting in a decrease in the bearing damage level caused by high-frequency electrical erosion.

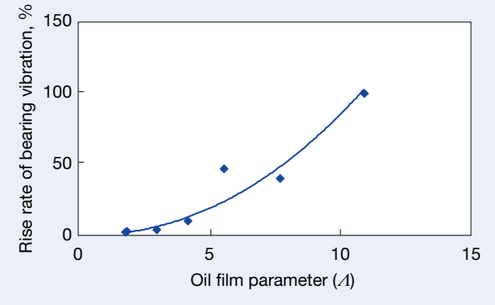

Fig.2 Relationship between oil film parameter and rise of bearing vibration caused by electrical erosion[1]

3.4 The relationship between high-frequency electrical current and bearing vibration

Next, tests to confirm the influence of high-frequency electrical current magnitude passing through a bearing were carried out; that is, the bearing damage level caused by high-frequency electrical erosion due to bearing vibration.

The 608 bearing (bore diameter: 8 mm, outside diameter: 22 mm) was used and continuously operated with an applied voltage of a sine wave of 16 kHz frequency so that the electrical current passing through the rotating bearing reached the desired value. The Anderon value of the bearing was measured every 24 hours, and the test was stopped when high band value exceeded 10.

Figure 3 shows the test results. The horizontal axis shows the electrical current value, and the vertical axis shows the cumulative operational time when the Anderon high band value reached 10.

As can be seen from Figure 3, it was confirmed that the damage level caused by high-frequency electrical erosion increased in accordance with the increase in electrical current passing through the bearing, and the increase in bearing vibration value accelerated.

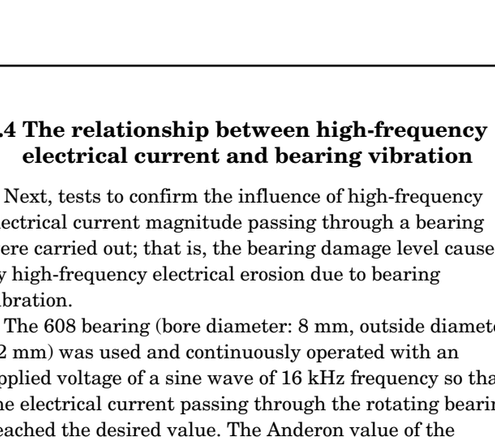

Fig. 3 Measured results over time for the increase in Anderon Value, caused by high-frequency electrical erosion

4. Measures for Suppressing and Preventing High-frequency Electrical Erosion

Experimental knowledge about several parameters for high-frequency electrical erosion was described in the previous section. With this knowledge, methods for suppressing or preventing the generation of high-frequency electrical erosion were considered.

The methods for suppressing or preventing the generation of high-frequency electrical erosion were categorized into two groups, as described below.

(1) Measures related to the power distribution
- Make oil film parameter Λ smaller
- Use conductive grease
- Use a conductive seal

(2) Measures related to insulation
- Increase oil film parameter Λ
- Insulate bearing rings or rolling elements

4.1 Minimization of oil film parameters (Measures related to power distribution)

As stated in section 3.3, it is possible to suppress the rise of bearing vibration by keeping oil film parameter Λ at a low level. However, it is difficult to control this oil film parameter in actual rotating equipment because it varies by lubricant, rotational speed, temperature, and load. Additionally, when this oil film parameter is low, the risk of direct contact of the bearing ring with rolling elements increases and causes failure due to wear or seizure. It will not be a perfect preventive measure, though it can achieve life-extending effectiveness against high-frequency electrical erosion.

4.2 Adoption of conductive grease (Measures related to power distribution)

Conductive grease is prepacked in bearings that support the rotors in types of office equipment, acting as a ground to prevent an electrostatic charge.

Figure 4 shows the measured electrical resistance of a bearing that has been prepacked with conductive grease made by mixing carbon powder with lithium soap grease. It is found that the resistance value is about 100 kΩ at the initial stage of operation, but the electrical resistance increases to about 10 MΩ when total testing time exceeds 4 000 hours. This is because of the degradation of carbon powder over time. Even if conductive grease is used, it is difficult to maintain long-term conductivity, and it will not be a perfect preventive measure.

4.3 Adoption of a conductive seal (Measures related to power distribution)

When a bypass circuit is created between the inner ring and outer ring, giving the bearing conductivity by adding carbon to the rubber in the contact-type seal, it is possible to suppress current passage through the bearing.

Figure 5 shows the measure of electrical resistance in a conductive seal. It has been found that electrical resistance increases with the passage of time, just as it does when conductive grease is used. It is believed that this is because the contact area of the conductive seal with a rotating ring gradually wears out, resulting in the failure of secure electrical conductivity, or an oil film is formed by leakage of the bearing's prepacked lubricant, resulting in a loss of conductivity. Therefore, maintaining long-term conductivity by using a conductive seal is difficult, and it is not a perfect preventive measure.

4.4 Maximization of oil film parameter (Measures related to insulation)

From the results in Figure 1, it is obvious that oil film's insulation breakdown voltage becomes greater if film parameter Λ is increased. As described in section 4.1, however, it is difficult to control this oil film parameter in actual rotating equipment because it varies by lubricant, rotational speed, temperature, and load.

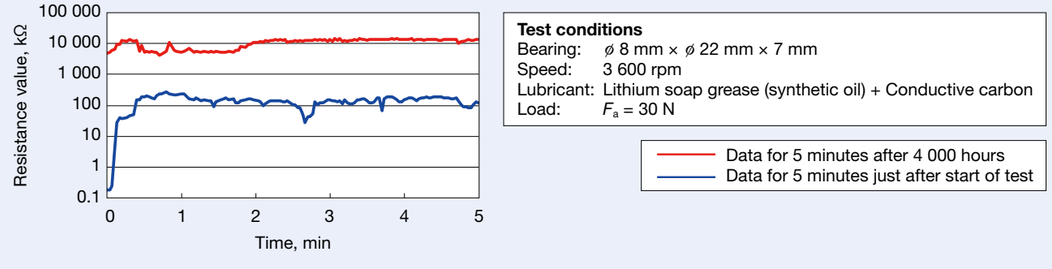

Fig. 4 Variation over time in resistance value of a bearing packed with electrically-conductive grease

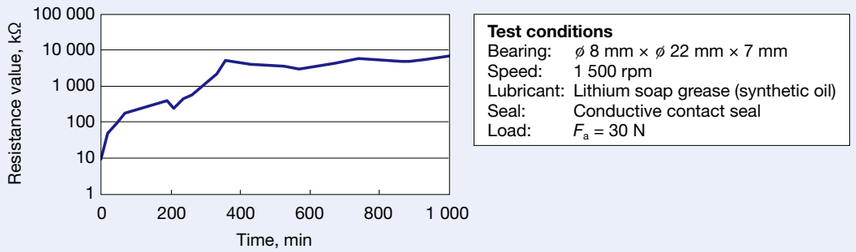

Test conditions
Bearing: ø 8 mm × ø 22 mm × 7 mm
Speed: 1 500 rpm
Lubricant: Lithium soap grease (synthetic oil)
Seal: Conductive contact seal
Load: F_a = 30 N

Fig. 5 Variation over time in the resistance value of bearings fitted with electrically conductive seals

4.5 Adoption of insulation material (Measures related to insulation)

Ceramic material is believed to have both high insulation properties and mechanical properties as a bearing component.

Since ceramic has a very high insulation resistance and is not unstable like oil film, using this material as a countermeasure is most effective and is the only method that enables the prevention of high-frequency electrical erosion.

In the case of relatively small-diameter ball bearings used for general-purpose motors and home appliance motors, it is common to use ceramics for the rolling element from the point of view of handling, workability, and cost.

4.6 Verification of the effects of various measures

Figure 6 shows the experimentally-verified results of the effects on countermeasures for suppressing or preventing high-frequency electrical erosion, described in sections 4.2, 4.3, and 4.5.

As is obvious from Figure 6, for a bearing filled with conductive grease, or a bearing with a conductive seal, damage caused by high-frequency electrical erosion is reduced, as is the increase in vibration, but it is difficult to prevent the damage completely compared to a bearing containing normal steel balls. Also, when bearing interiors were inspected after testing, damage by high-frequency electrical erosion was observed.

On the other hand, because a bearing that contains ceramic balls does not conduct high-frequency electric current, the bearing vibration level rarely rises. Also, when the bearing interior was examined after testing, no damage by high-frequency electrical erosion was observed at all (Photo 4).

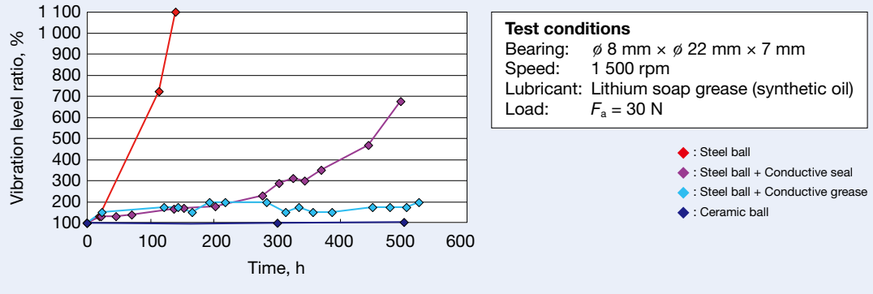

Test conditions
Bearing: ø 8 mm × ø 22 mm × 7 mm
Speed: 1 500 rpm
Lubricant: Lithium soap grease (synthetic oil)
Load: F_a = 30 N

Fig. 6 Measured results of rise in bearing vibration caused by high frequency electrical erosion

Test conditions
Bearing: ø 8 mm × ø 22 mm × 7 mm
Speed: 1 500 rpm
Load: F_a = 30 N

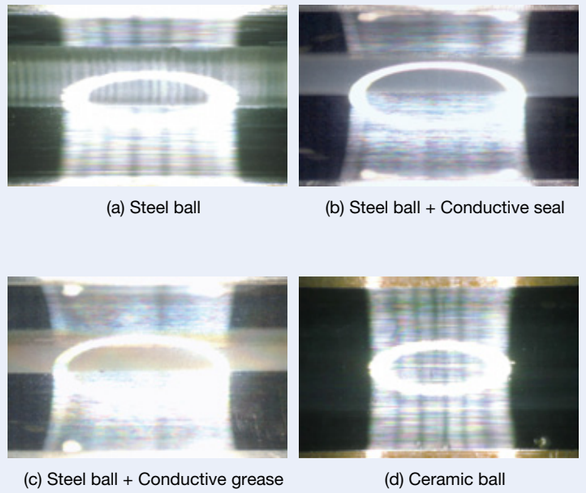

(a) Steel ball (b) Steel ball + Conductive seal

(c) Steel ball + Conductive grease (d) Ceramic ball

Photo 4 Inner ring raceways after high-frequency electrical erosion testing

5. Conclusion

This paper introduced the characteristics of, and examples of countermeasures against, high-frequency electrical erosion. The occurrence of high-frequency electrical erosion has recently been increasing in motors for various applications, and it is believed that this will further increase as inverter control also increases in the future.

We will further promote research because some aspects of high-frequency electrical erosion have not yet been thoroughly explained.

Keiji Yasunaga

Reference

1) A. Yamamoto and H. Ishiwada “Technological Trends of Ball Bearings for Household Electrical Appliances,” NSK Technical Journal, 683 (2009) 32 (in Japanese).

Development of Long-Life Planetary Shaft (SHX3 Steel) for Planetary Gears of Automotive Transmissions

Kouichi Yamamoto and Hiromichi Takemura
Automotive Bearing Technology Center

ABSTRACT

There has been ongoing demand in recent years for more compact and lightweight bearings for use in transmissions, as a way to deliver better fuel efficiency. There has also been demand for the use of low-viscosity AT fluids with lower agitation resistance, which leads to lower friction loss. Another challenge is meeting the needs of demanding transmission operating conditions, such as the very sparse bearing lubrication that occurs when the oil pump shuts down during travel in the electric-motor-only mode in HEVs. Other demands include the need for a wider gear range as a way to reduce gear shifting shock, and for improved efficiency of power transmission in ATs, which require AT bearings capable of operating at higher rotations. This article describes NSK's long-life planetary shaft for automotive transmissions, which is 40 % smaller and lighter.

1. Introduction

Demand has been growing for automotive transmissions that can reduce friction loss, due to increasing environmental consciousness and strengthening of global fuel consumption regulations for automobiles.

Making transmissions more compact and lightweight, and using low-viscosity AT fluid, have been held up as possible methods for increasing the efficiency of transmissions.

For example, low-viscosity AT fluid is widely used for AT bearings to reduce agitation resistance, which has a negative effect on transmission efficiency, and bearings for planetary gears are used under severe lubrication conditions. Additionally, transmission bearings for hybrid electric vehicles (HEVs) must perform well at high speed, and the motors have been downsized to improve fuel efficiency. Moreover, bearings for planetary gears are used in severe environments, such as the very sparse bearing lubrication that occurs in an HEV when the oil pump shuts down in the electric-motor-only mode.

Because of these demands for more compact and lightweight bearings and responsiveness to a severe environment, it is increasingly necessary to lengthen the life of the planetary shaft, the weakest part of the planetary gear bearing[1].

In the 1970s through the 1990s, when three-speed to five-speed ATs were mainstream, through-hardened or high-frequency specifications of JIS SUJ2 steel or JIS SK85 steel were adopted for planetary shafts. In the 2000s, operating conditions and environment became severe with the advent of 6-speed and 8-speed ATs, and HEVs. Therefore, NSK's special heat-treatment specification[2] (UR specification), and special high-frequency heat treatment specification, started to be adopted as the specifications for longer life. The UR specification is that JIS SUJ2 steel is special carbonitrided in NSK's proprietary process, while adding moderate retained austenite, carbonitride, and compressive residual stress on rolling surfaces, resulting in increasing fatigue durability as it is superior in terms of high rigidity, wear resistance and textual stability. With the UR specification, however, there are sometimes problems with generating heat plastic (permanent) curvature deformation from the influence of thermal decomposition of the retained austenite inside the planetary shaft, when the bearing is being used in a high-temperature environment. That is, premature flaking sometimes occurs with the increase in contact surface pressure caused by the edge load of the shaft on the needle roller[3]. To solve this problem, a special high-frequency specification was developed for suppressing heat plastic curvature deformation. The rolling surface in the special high-frequency specification has the same features as those of the UR specification, having superior fatigue durability. For the shaft core, resident-retained austenite is reduced beforehand by special heat treatment, and heat plastic curvature deformation is suppressed.

In recent years, demand has been increasing for planetary gear trains to be compact and lightweight and respond to a severe environment, due to the coming of multi-speed ATs and HEVs. The problems that shortened durability life and increased heat plastic curvature deformation came about when the temperature of the bearing operating environment was further increased, even in the case of special high-frequency specifications, and cases of premature failure were increasing.

This long-life planetary shaft improved fatigue durability, in comparison with special high-frequency specifications, by employing a dedicated heat treatment on SHX3 steel (NSK's proprietary material: case-hardened high chromium steel), and also achieved more than 2.5 times longer life than a conventional shaft because premature failure caused by heat plastic curvature deformation was suppressed.

This paper describes features and application examples of this long-life planetary shaft for planetary gears of transmissions.

Here the long-life planetary shaft is referred to as the "newly-developed planetary shaft," and the special high-frequency specification is referred to as the "conventional planetary shaft."

2. Features of the Long-life Planetary Shaft (SHX3 steel)

The newly-developed planetary shaft has the following features.

Photo 1 shows the appearance of standard planetary shafts.

Figure 1 and Table 1 show the features of both the newly-developed planetary shaft and the conventional planetary shaft specifications.

In both the newly-developed planetary shaft and the conventional planetary shaft, fatigue durability is increased by properly controlling retained austenite under the shaft surface, and expansion or heat plastic curvature deformation is suppressed by preventing the structure change that is caused by resolving retained austenite; this is accomplished by reducing retained austenite at the core.

On the surface layer of the newly-developed planetary shaft, the density of both carbon (C) and nitrogen (N) is higher compared with that of the conventional planetary shaft, due to NSK's exclusive carbonitriding treatment, and fatigue durability is increased by stabilizing the material structure and causing the amount of retained austenite to increase. At the core of the newly developed planetary shaft, heat plastic curvature deformation is suppressed by causing the amount of retained austenite to decrease using a dedicated tempering treatment.

2.1 Compact and lightweight

The fatigue durability of the newly-developed planetary shaft is increased by NSK's exclusive heat treatment on the company's proprietary SHX3 steel (case-hardened high chromium steel), and bearing life is lengthened by more than 2.5 times compared to a conventional bearing (newly developed planetary shaft/special high frequency) (Figure 2). This long-life technology enables a reduction of 40 % in size and weight, compared to a conventional bearing, by downsizing under the same bearing life conditions.

Photo 1 Standard planetary shafts

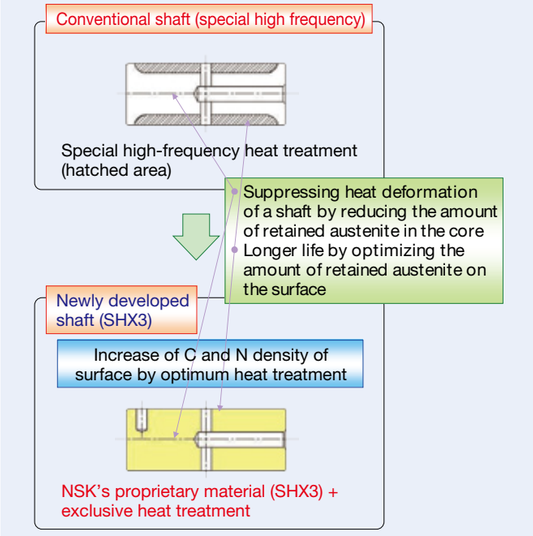

Fig. 1 Comparison between conventional and newly-developed planetary shafts

Table 1 Comparison between conventional and newly-developed planetary shafts

Items		Conventional shaft	Newly developed shaft	Target of newly developed shaft
Material	Grade	SUJ2 (JIS)	SHX3	NSK's proprietary material suitable for a severe lubrication environment, Higher amount of chromium than SUJ2, Other elements adjusted, Then, improved fatigue durability (longer life)
	Quality of material	Through hardened high chromium steel	Case-hardened high chromium steel	
Heat treatment		Special high frequency	Carbonitriding	Dedicated heat treatment, Retained austenite adjusted, Then, suppressing premature failure by heat plastic curvature deformation

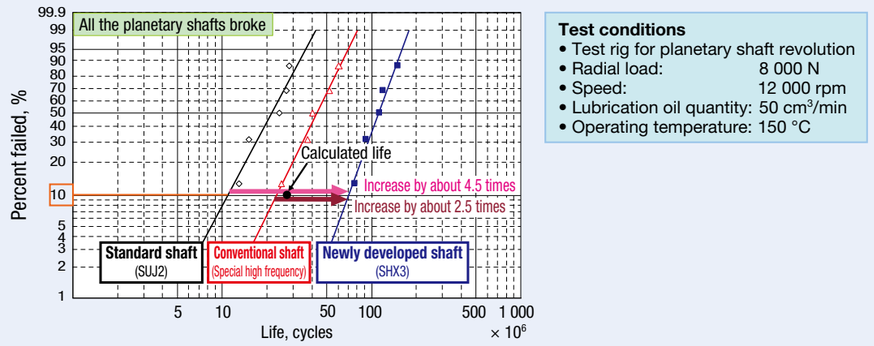

Fig. 2 Results of bearing life test comparing conventional and newly-developed planetary shafts

2.2 Torque reduction

Because bearing life has been lengthened by 2.5 times, as shown in Figure 3, a bearing that is about 40 % smaller and lighter than a conventional bearing is now possible, or a cage and roller (C&R) type with the same size as a conventional bearing. Therefore, it is possible to reduce torque by more than 50 % (analysis value).

2.3 Use in low lubrication and a high-temperature environments

As shown in Figure 4, the newly-developed planetary shaft aims at the structural stability of the surface layer by increasing carbon (C) and nitrogen (N) on the surface of SHX3 steel and can be used in low-lubrication and high-temperature environments because fatigue durability is improved and high-temperature softening resistance is increased.

- Minimum quantity of supply oil: 50 cm³/min (conventionally 300 cm³/min)
- Maximum operating temperature: 150 °C (conventionally 120 °C)

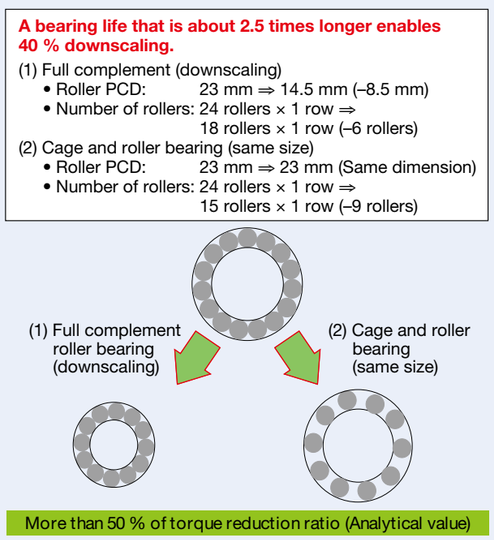

Fig. 3 Effect of reducing torque by downscaling the bearing or using a cage and rollers

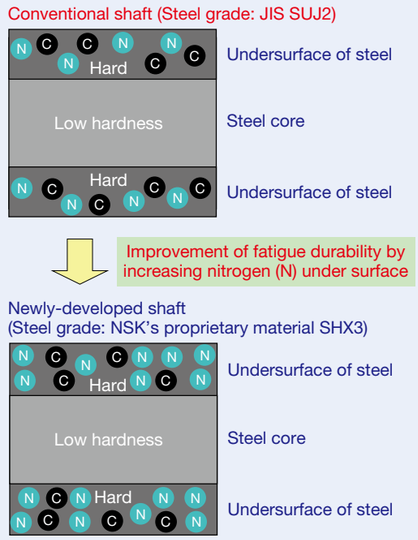

Fig. 4 Conceptual diagram of carbonitriding for conventional and newly-developed planetary shafts

2.4 Correspondence to higher speed

The SHX3 steel planetary shaft has made it possible to replace the full complement type, which gets extended life when used with this shaft with the C&R type (Figure 5), thereby increasing the maximum operating speed by more than three times. While it is possible to increase speed by replacing the full complement type with the C&R type using a conventional planetary shaft, bearing life would then be decreased by the influence of load capacity reduction. In contrast, the newly developed planetary shaft can maintain bearing life as well as achieve higher speed with the C&R, and further lengthen bearing life.

2.5 Suppressing heat plastic deformation

The higher revolution speed of the planetary carrier and the higher load to the pinion gears increases the amount of elastic deformation on the planetary shaft, and heat plastic curvature deformation caused by resolving retained austenite increases because the operating environment is likely to become very hot. If this curvature of the shaft increases, shaft durability decreases due to the increase of contact surface pressure caused by an edge load between the shaft and the needle roller.

Figure 6 is an illustration of longer life brought about by suppressing the heat plastic curvature deformation of both conventional and newly-developed planetary shafts. The heat plastic curvature deformation of the newly-developed planetary shaft (3 µm) is less than half that of a conventional planetary shaft (12 µm) under the same conditions, and the newly-developed planetary shaft makes it possible to suppress bearing failure (flaking or seizure by the increase of partial surface pressure) caused by heat plastic curvature deformation.

Figure 6 shows the analysis results of the relationship between heat plastic curvature deformation and life ratio as an example. Heat plastic curvature deformation of 10 µm sometimes reduces durability life to almost half.

3. Application Examples for Transmissions

Planetary shafts for automobile transmissions must have high fatigue strength with higher speed of carrier revolution, higher speed of pinion gears, usage in a high-temperature environment, and usage under severe lubrication conditions[4].

Figure 7 shows an application example of planetary shaft to planetary gears for a multistage AT. The planetary shaft is fixed at both ends of the carrier, and carrier and planetary shaft rotate together (revolution). The pinion gear is maintained by the pinion shaft and needle roller and revolves. The planetary shaft is used as the equivalent to the inner ring for maintaining the pinion gear (equivalent to the outer ring) and C&R.

The reason why the planetary shaft is strengthened is as follows: Centrifugal force from the weight of the pinion gear, when the pinion gear revolves due to the rotation of the carrier, acts on the loaded zone of the planetary shaft through needle rollers. Whereas the loaded zone of the planetary shaft receives the repeated loads from needle rollers, needle rollers revolve while shifting a number of needle rollers from the C&R's loaded zone to its non-loaded zone (Figure 8). Among the components (pinion gear, planetary shaft, needle roller) of planetary needle roller bearings, the planetary shaft (equivalent to the bearing inner ring) is the weakest component with the most severe load condition, due not only to high contact stress but also to a lot of repeated stress cycles.

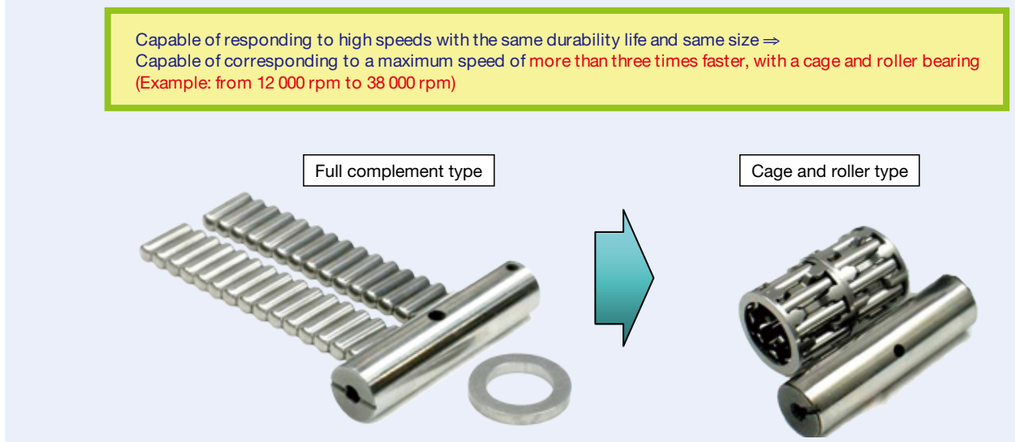

Fig. 5 Comparison of full-complement and cage and roller type bearings

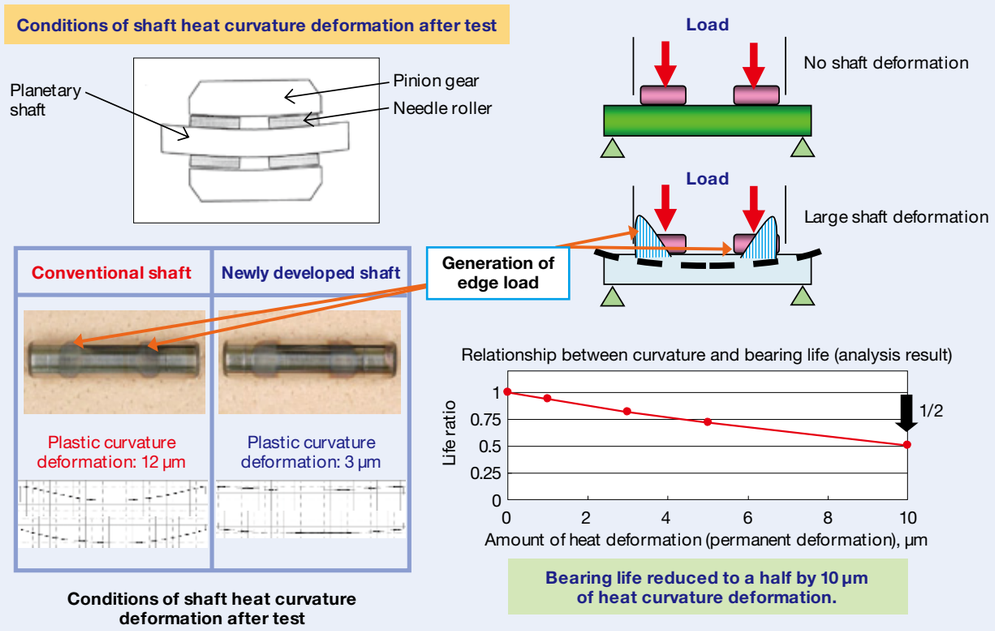

Fig. 6 Long-life technology used to reduce heat plastic curvature deformation

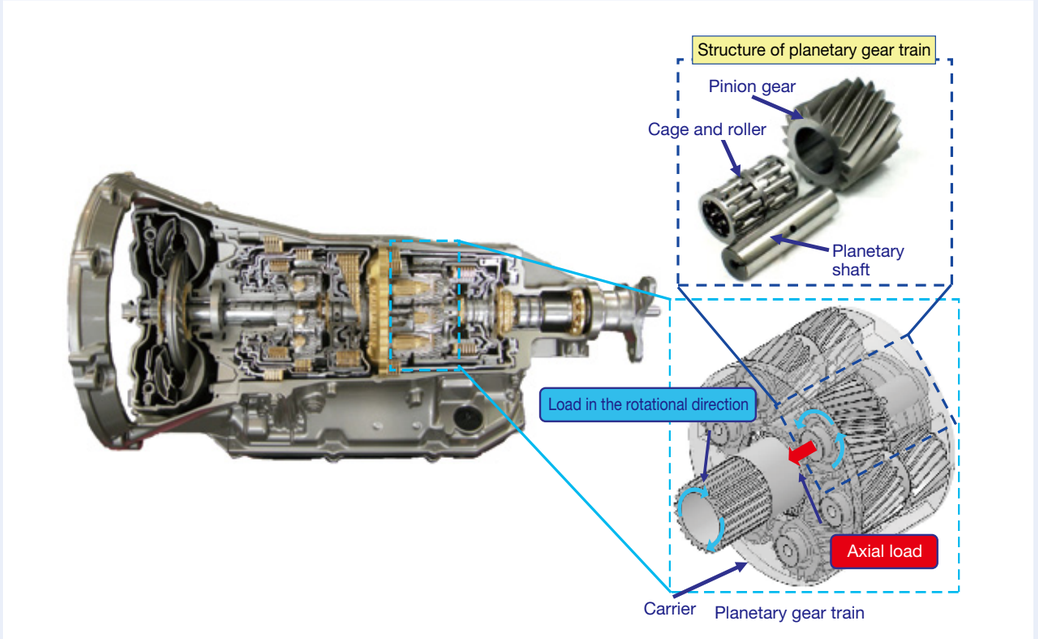

Fig. 7 Example of usage in a planetary gearset of an automotive automatic transmission

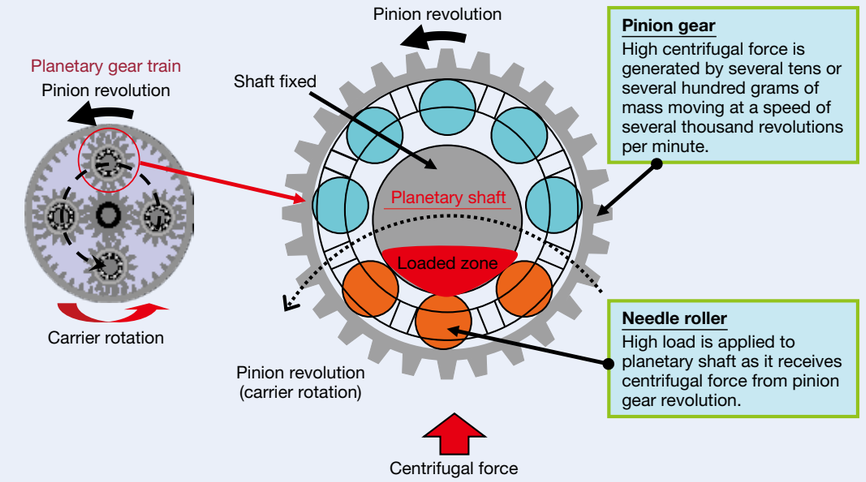

Fig. 8 Position of load acting on a planetary needle roller bearing

4. Conclusion

This product is a high-function planetary shaft that is not deformable by heat with improved fatigue durability and heat resistance compared to conventional long-life products (UR specification, special high-frequency) due to the dedicated heat treatment of SHX3 steel (case-hardened high chromium steel, developed by NSK). The longer life of this planetary shaft dramatically lengthens the life of planetary needle roller bearings. We believe that the product can be used to achieve a reduction in the size and weight of automobiles and contribute to an improvement in fuel efficiency and lower torque.

Also, it can be applied not only to automotive ATs or planetary gears for HEVs but also to any other part with life-extension needs. Especially, many shafts that are similar to this product are used paticularly in tappet rollers for automotive engines to increase efficiency, with some likelihood of success.

We hope to aggressively carry out new product development to respond to a lot of user needs in the future.

References

1) H. Takemura and K. Kitamura, “Development of needle roller bearings for high-speed miniature planetary gears,” Collection of papers in Society of Automotive Engineers of Japan, 42–4 (July 2011) 897–901.
2) Y. Murakami, “Long Life Bearing Technology by Carbonitriding,” NSK Technical Journal, 673 (2002) 3–6.
3) T. Ootsubo and S. Kadokawa, “Trends and New Technologies of Automatic Transmission,” NSK Technical Journal, 677 (2004) 46–53.
4) S. Urakami, J. Liu and Y. Matsumoto, “Development of Ultrahigh-Speed Planetary Needle Roller Bearings,” NSK Technical Journal, 680 (2006) 36–41.

Kouichi Yamamoto

Hiromichi Takemura

Shinkansen Axle Cylindrical Roller Bearings for E5 Series Bullet Train

NSK has received 100 % of JR's orders for Shinkansen Axle Cylindrical Roller Bearings for the E5 Series bullet train (as of June 2013). The maximum speed of the E5 series bullet train has been highly improved to 320 km/h, compared with the conventional bullet train (E2 and E3 series bullet train for Tohoku Shinkansen line) speed of 275 km/h. This is because it was a challenge to reduce the heat generation of the bearings in accordance with the speed increase, and NSK solved the problem. This article describes the cylindrical roller bearing that reduces heat generation.

1. Structure of the Cylindrical Roller Bearing

Figure 1 and Photo 1 show the cylindrical roller bearing.
The Shinkansen axle bearing for the E5 Series bullet train is a double-row cylindrical roller bearing with oil-bath lubrication.

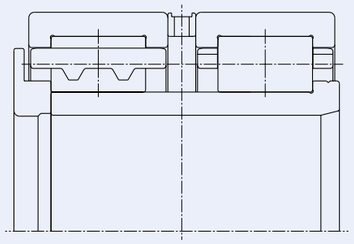

Fig. 1 Shinkansen Axle Cylindrical Roller Bearing for the E5 Series bullet train

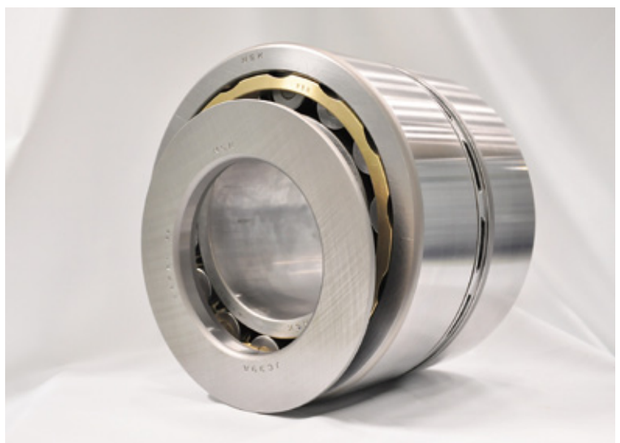

Photo 1 Shinkansen Axle Cylindrical Roller Bearing for the E5 Series bullet train

2. Features

The following three points are improvements for reducing heat generation over the conventional bearing. Figure 2 shows the details.

(1) Shape of loose rib ring
An advancement in oil draining, via the slinger

(2) Shape of cage
An advancement in oil draining, via outside slots

(3) Shape of spacer
An advancement in oil circulation by changing the shape of the oil holes from circular to elongated

The maximum speed of the conventional Shinkansen (E2 and E3 series bullet trains for the Tohoku Shinkansen line) is 275 km/h, and the maximum speed of the Hayabusa in the E5 Series bullet trains is 320 km/h. Figure 3 shows the results of temperature rise tests for a conventional bearing and the newly developed bearing, conducted at NSK.

Comparing the temperature rises at each maximum speed, the temperature rise of the newly developed bearing could be lowered by 6.5 ºC compared to the conventional bearing, when measured at the housing surface.

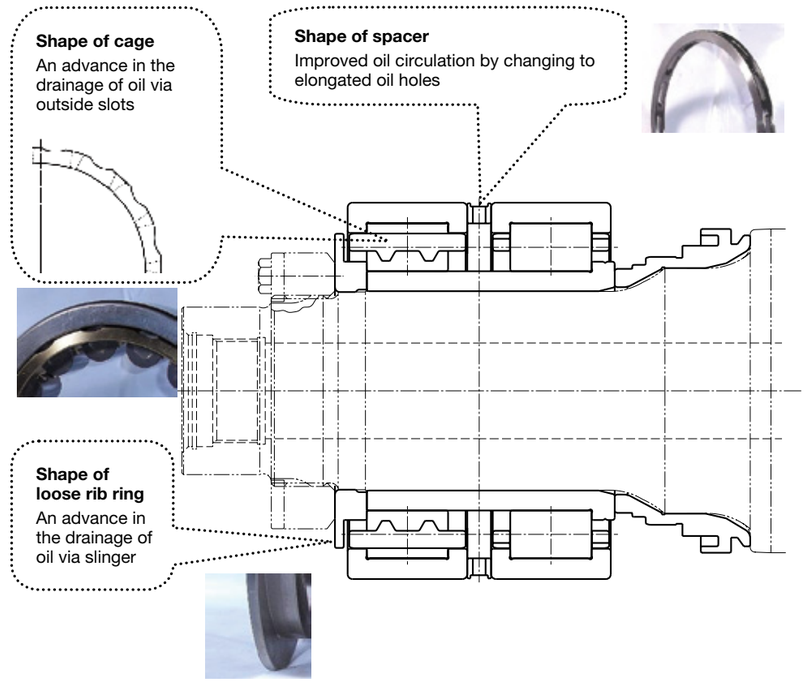

Fig. 2 Features of the Shinkansen Axle Cylindrical Roller Bearing for the E5 Series bullet train

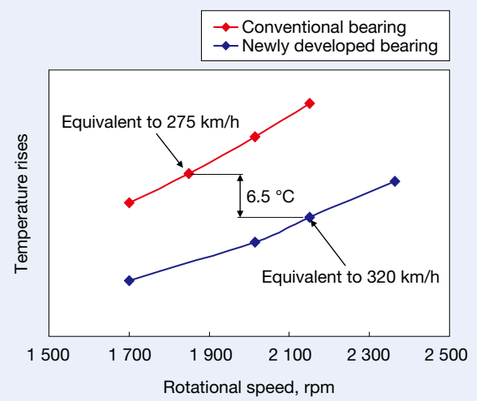

Fig. 3 Temperature increases at the housing surface

3. Applications

This type of bearing was adopted for use in the E5 Series bullet train, which began operating in March 2011. In addition, this type of bearing was also adopted for use in the E6 Series bullet train, which began operating in March 2013.

4. Summary

We really hope to contribute to the future of high-speed rail, employing our vast experience with the high-speed operation of the above-mentioned bullet trains.

High-Performance Standard NSKHPS Large-Size Spherical Roller Bearings

Souety has recently expected a lot of industrial machinery, such as steel-making machines, papermaking machines, construction machines, and mining machines, to have increased power, compactness, and lower maintenance costs, to save energy, and to be environmentally friendly, in addition to being highly reliable. Because of this, the bearings used in the industrial machinery are required to have longer life and higher reliability under high load conditions in high-temperature environments and within a limited space.

NSK has developed the high-performance standard NSKHPS Large-Size Spherical Roller Bearings for industrial machinery (Photo 1), which can address these needs, and has made a sevies lineup.

Photo 1 High-performance standard NSKHPS Large-Size Spherical Roller Bearing

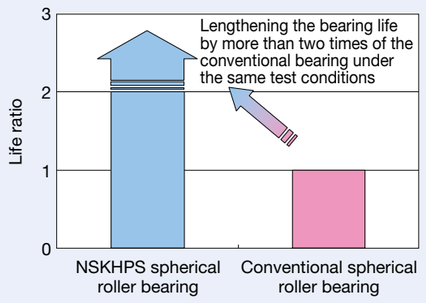

Fig. 1 Life test results

1. Bearing Features

The following are the features of the high-performance standard NSKHPS Large-Size Spherical Roller Bearings for industrial machinery.

(1) Improving the bearing life to more than twice that of the conventional bearing

A spherical roller bearing rotates while sliding between the inner and outer-ring raceway surfaces and the roller rolling contact surfaces. It has been clarified by analysis and testing that the tangential force (friction force) generated on the raceway surfaces due to this sliding affects the bearing's fatigue life. With these results, we achieved a longer bearing life by reducing the tangential force with a special coating on the outer-ring raceway surface (Figure 1).

(2) Standard adopting the high-temperature dimensional stability treatment

If the bearing is used under a high temperature of over 100 ºC (in a high temperature environment), a dimensional change occurs. NSK has adopted a bearing having a dimensional stability of up to 200 ºC by the high degree of heat treatment technology as a standard.

2. Specifications

The series of the bearing lines up 180 mm to 400 mm of bearing outside diameter. Table 1 shows the boundary dimensions and the basic load ratings of the typical bearing examples lined up.

3. Summary

The high-performance standard NSKHPS Large-Size Spherical Roller Bearings for industrial machinery can significantly contribute to reducing maintenance cost, downsizing, energy saving, and improving machine performance. In addition, the bearings can be used in various environments, or for wider application, because of their brass cage with superior strength.

Table 1 Specifications of high-performance standard NSKHPS Large-Size Spherical Roller Bearings

Bearing numbers		Boundary dimensions (mm)				Basic load ratings (N)	
Cylindrical bore	Tapered bore	*d*	*D*	*B*	*r* min.	C_r	C_{0r}
21319CAME4	21319CAMKE4	95	200	45	3	430 000	435 000
23220CAME4	23220CAMKE4	100	180	60.3	2.1	525 000	605 000
21320CAME4	21320CAMKE4		215	47	3	495 000	485 000
23024CAME4	23024CAMKE4	120	180	46	2	395 000	525 000
24024CAME4	24024CAMK30E4		180	60	2	480 000	680 000
23124CAME4	23124CAMKE4		200	62	2	580 000	720 000
24124CAME4	24124CAMK30E4		200	80	2	695 000	905 000
23224CAME4	23224CAMKE4		215	76	2.1	790 000	970 000
23028CAME4	23028CAMKE4	140	210	53	2	525 000	715 000
24028CAME4	24028CAMK30E4		210	69	2	635 000	905 000
23128CAME4	23128CAMKE4		225	68	2.1	725 000	945 000
24128CAME4	24128CAMK30E4		225	85	2.1	835 000	1 160 000
22228CAME4	22228CAMKE4		250	68	3	835 000	945 000
23228CAME4	23228CAMKE4		250	88	3	1 040 000	1 300 000
22328CAME4	22328CAMKE4		300	102	4	1 450 000	1 590 000
23030CAME4	23030CAMKE4	150	225	56	2.1	590 000	815 000
24030CAME4	24030CAMK30E4		225	75	2.1	740 000	1 090 000
23130CAME4	23130CAMKE4		250	80	2.1	905 000	1 180 000
24130CAME4	24130CAMK30E4		250	100	2.1	1 070 000	1 450 000
22230CAME4	22230CAMKE4		270	73	3	955 000	1 120 000
23230CAME4	23230CAMKE4		270	96	3	1 220 000	1 560 000
22330CAME4	22330CAMKE4		320	108	4	1 530 000	1 690 000
23932CAME4	23932CAMKE4	160	220	45	2	450 000	675 000
23032CAME4	23032CAMKE4		240	60	2.1	675 000	955 000
24032CAME4	24032CAMK30E4		240	80	2.1	845 000	1 260 000
23132CAME4	23132CAMKE4		270	86	2.1	1 070 000	1 400 000
24132CAME4	24132CAMK30E4		270	109	2.1	1 240 000	1 670 000
22232CAME4	22232CAMKE4		290	80	3	1 140 000	1 320 000
23232CAME4	23232CAMKE4		290	104	3	1 370 000	1 770 000
22332CAME4	22332CAMKE4		340	114	4	1 700 000	1 900 000
23936CAME4	23936CAMKE4	180	250	52	2	590 000	890 000
23036CAME4	23036CAMKE4		280	74	2.1	935 000	1 270 000
24036CAME4	24036CAMK30E4		280	100	2.1	1 210 000	1 750 000
23136CAME4	23136CAMKE4		300	96	3	1 320 000	1 760 000
24136CAME4	24136CAMK30E4		300	118	3	1 490 000	2 040 000
22236CAME4	22236CAMKE4		320	86	4	1 280 000	1 540 000
23236CAME4	23236CAMKE4		320	112	4	1 620 000	2 110 000
22336CAME4	22336CAMKE4		380	126	4	2 170 000	2 340 000
23940CAME4	23940CAMKE4	200	280	60	2.1	710 000	1 060 000
23040CAME4	23040CAMKE4		310	82	2.1	1 180 000	1 700 000
24040CAME4	24040CAMK30E4		310	109	2.1	1 420 000	2 120 000
23140CAME4	23140CAMKE4		340	112	3	1 700 000	2 330 000
24140CAME4	24140CAMK30E4		340	140	3	1 960 000	2 660 000
22240CAME4	22240CAMKE4		360	98	4	1 620 000	2 010 000
23240CAME4	23240CAMKE4		360	128	4	2 070 000	2 750 000
23944CAME4	23944CAMKE4	220	300	60	2.1	785 000	1 240 000
23044CAME4	23044CAMKE4		340	90	3	1 360 000	1 980 000
24044CAME4	24044CAMK30E4		340	118	3	1 640 000	2 490 000
23144CAME4	23144CAMKE4		370	120	4	1 960 000	2 710 000
24144CAME4	24144CAMK30E4		370	150	4	2 250 000	3 200 000
22244CAME4	22244CAMKE4		400	108	4	1 960 000	2 430 000
23244CAME4	23244CAMKE4		400	144	4	2 520 000	3 400 000
23948CAME4	23948CAMKE4	240	320	60	2.1	795 000	1 300 000
23048CAME4	23048CAMKE4		360	92	3	1 450 000	2 140 000
24048CAME4	24048CAMK30E4		360	118	3	1 730 000	2 730 000
23148CAME4	23148CAMKE4		400	128	4	2 230 000	3 100 000
24148CAME4	24148CAMK30E4		400	160	4	2 660 000	3 800 000
23952CAME4	23952CAMKE4	260	360	75	2.1	1 170 000	1 870 000

Note: This table shows the specifications of a bearing series with a bore diameter range of between 95 mm and 260 mm.

Energy-Saving HALFRICTION Ball Bearings for High-Efficiency Motors

Recently, efforts to reduce CO_2, or increase energy saving in various types of machine and equipment have been promoted as countermeasures to global warming. For motors that are said to account for about 75 % of industrial power consumption at manufacturing plants, efforts to increase efficiency have been accelerating such as energy-saving laws and regulations being enacted in many countries. The International Electrotechnical Commission (hereinafter called IEC) has been promoting unification of the international regulations for controlling motor efficiency since 2008, and the efficiency regulations for level IE1 up to level IE4*) are being defined.

Motor losses include iron loss, copper loss, circuit loss, windage loss, and mechanical loss, and motor efficiency can be improved by reducing these losses (Figure 1). Mechanical losses, including bearing friction loss, is said to be about 12 % of the overall loss, and the motor manufactures have been mainly working to reduce the high ratio of losses such as iron loss and copper loss. It is anticipated that the requirement to reduce bearing friction loss will increase more in order to achieve the motor efficiency required by level IE3 and level IE4.

NSK has developed an energy-saving bearing for high-efficiency motors; this article provides the details (Photo 1).

Photo 1 Energy-saving HALFRICTION Ball Bearings for high-efficiency motors

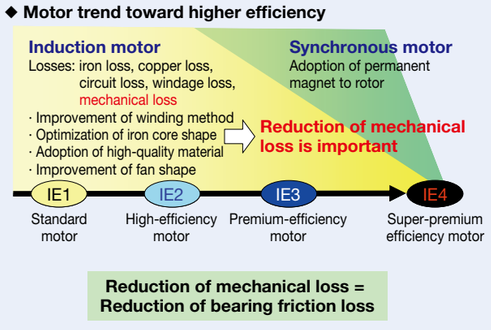

Fig. 1 Motor trend toward greater efficiency

1. Features

(1) The friction resistance in the rolling area could be reduced by optimizing the bearing internal design (Figure 2), and the friction loss could be reduced by half of the conventional bearing (Figure 3). This bearing can contribute to efficiency improvements in energy-saving products that are designed to meet severe efficiency regulation levels, such as level IE3 level IE4 in the international standard IEC, in addition to the JIS standard.

(2) It has become possible to restrict the temperature rise of a bearing by reducing its friction loss, resulting in reliability improvements in motors and equipment.

(3) Fretting resistance (false brinelling) performance against the external vibration when there is no rotation is improved by optimizing the bearing internal design.

2. Applications

This type of bearing may be used with high-efficiency or general industry motors, for the application of a relatively light load.

3. Summary

In addition to the bearings in Table 1, we will also offer a lineup of bearings of the size normally used for general industry motors.

*: Levels IE1 to IE4 are the efficiency levels defined by the IEC. The efficiency levels are, in ascending order by efficiency level, IE1 (standard), IE2 (high efficiency), IE3 (premium efficiency), and IE4 (super-premium efficiency).

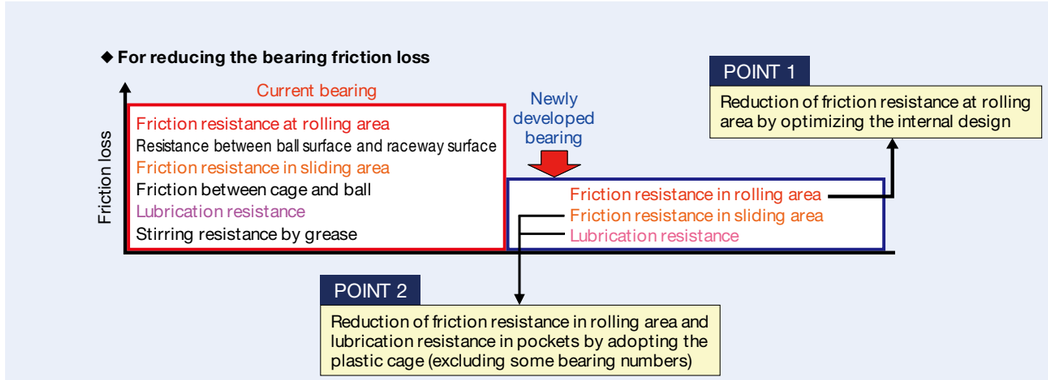

Fig. 2 Concept of development

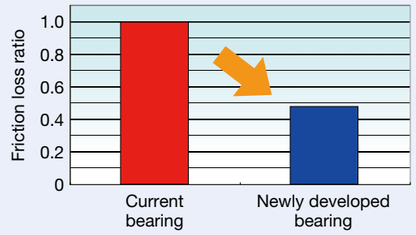

Fig. 3 Measurement results of friction loss

Table 1 Series deployment of the Energy-Saving HALFRICTION Ball Bearings

	Boundary dimensions (mm)		
	Bore diameter	Outside diameter	Width
6200A50	10	30	9
6201A50	12	32	10
6202A50	15	35	11
6203A50	17	40	12
6204A50	20	47	14
6205A50	25	52	15
6206A50	30	62	16
6207A50	35	72	17
6208A50	40	80	18
6209A50	45	85	19
6210A50	50	90	20
6211A50	55	100	21
6212A50	60	110	22

	Boundary dimensions (mm)		
	Bore diameter	Outside diameter	Width
6300A50	10	35	11
6301A50	12	37	12
6302A50	15	42	13
6303A50	17	47	14
6304A50	20	52	15
6305A50	25	62	17
6306A50	30	72	19
6307A50	35	80	21
6308A50	40	90	23
6309A50	45	100	25
6310A50	50	110	27
6311A50	55	120	29
6312A50	60	130	31
6313A50	65	140	33
6314A50	70	150	35
6315A50	75	160	37
6316A50	80	170	39

High-Performance, Shielded Double-Row Angular Contact Ball Bearings for Industrial Water Pumps

High efficiency, high reliability and the reduction of environmental load are in demand for industrial water pumps. Therefore, the compatibility of both downsizing and high load capacity are in demand for bearings used in these pumps. To respond to these needs, NSK has commercialized high-performance, shielded double-row angular contact ball bearings for industrial water pumps (Photo 1) with the dimensions (bore diameter, outside diameter and width) complying with ISO standards. This article introduces them and their excellent features.

1. Features

The following shows the features of the high-performance, shielded double-row angular contact ball bearings for industrial water pumps.

(1) Improvement of bearing life up to approximately three times (compared to a conventional bearing)

Bearing life was improved up to approximately three times (Figure 2), compared to a conventional bearing owing to the optimized design (Figure 1) of the shielded bearing. This makes it possible to downsize the bearings and can contribute to the reduction of running cost.

The bearing can also contribute to the simplification of pump design and the improvement of productivity, because it is the bearing of the grease-prelubricated type.

(2) Improvement of axial load resistance, up to approximately three times (compared to a conventional bearing)

Axial load resistance was improved by up to approximately three times (Figure 3), compared to a conventional bearing owing to by the optimized design of the bearing. The bearing can respond to high axial load and contribute to improved pump reliability.

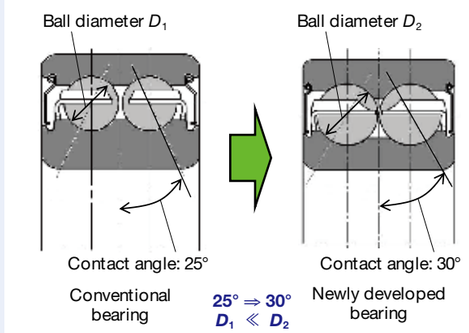

Fig. 1 Comparison of cross-sectional views for a conventional bearing and the newly developed bearing

Photo 1 High-performance, shielded double-row angular contact ball bearings for industrial water pumps

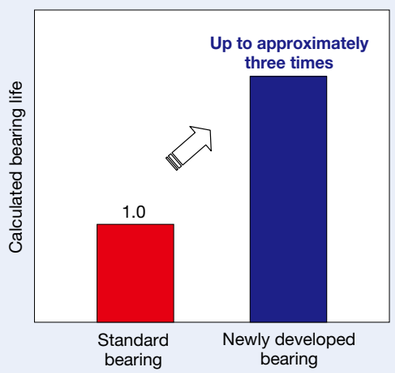

Fig. 2 Comparison of calculated life for a standard bearing and the newly developed bearing

(3) Expansion of the acceptable working temperature range This bearing can be used at a temperature of up to 150 °C by adopting the high-temperature dimensional stability treatment, and contributes to reliability improvements for operating at high temperature.

2. Specifications

This series lines up bore diameter from 25 mm to 65 mm (Table 1).

3. Summary

High-performance, shielded double-row angular contact ball bearings for industrial water pumps can contribute to the reduction of running costs and the improvement of axial load resistance because of their optimized design, as well as improved reliability of the pump, by expanding the acceptable working temperature range. Additionally, this bearing can contribute to the simplification of pump design and the improvement of productivity, because it is the bearing of the grease-prelubricated type.

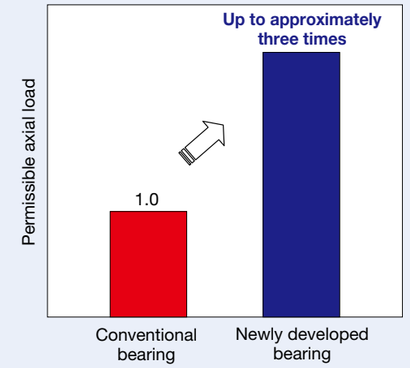

Fig. 3 Comparison of permissible axial load for a conventional bearing and the newly developed bearing

Table 1 Dimensions and basic load ratings

Bearing number	Boundary dimensions (mm)			Basic load ratings (N)	
	Bore diameter	Outside diameter	Width	Dynamic load rating	Static load rating
	d	*D*	*B*	C_r	C_{0r}
3305FZZ	25	62	25.4	30 500	20 400
3306FZZ	30	72	30.2	39 500	27 300
3307FZZ	35	80	34.9	49 500	35 000
3308FZZ	40	90	36.5	60 500	44 000
3309FZZ	45	100	39.7	66 500	49 500
3310FZZ	50	110	44.4	85 500	64 500
3311FZZ	55	120	49.2	106 000	82 000
3312FZZ	60	130	54.0	122 000	95 500
3313FZZ	65	140	58.7	138 000	109 000

NSKROBUST Series Type E of Angular Contact Ball Bearings for Machine Tools

In recent years, the needs for higher speed and higher efficiency have been heightened by the rapid increase in the amount of work to be processed by machine tools for the rapidly growing EMS markets. Additionally, machine tools used to process automotive components are improving productivity by downsizing, and high load resistance has been in demand even for small spindle bearings.

Furthermore, with the growing needs to save energy and reduce environmental load, demand for grease lubrication is increasing. To respond to these needs for higher speed and higher load, NSK has developed the NSKROBUST Series Type E of angular contact ball bearings for machine tools (Photo 1). This article introduces them.

Photo 1 Type E of the NSKROBUST Series of angular contact ball bearings for machine tools

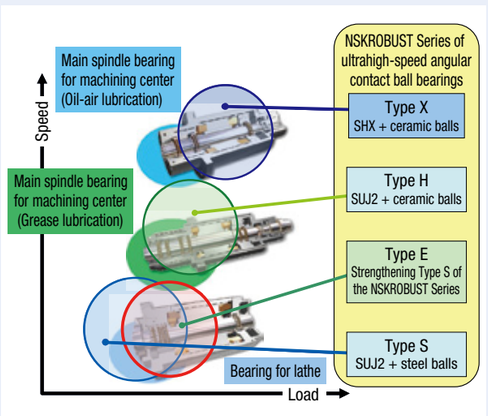

Fig. 1 NSKROBUST Series lineup

1. Bearing Specifications

The NSKROBUST Series of angular contact ball bearings for machine tools includes a variety of types S, H, and X (Figure 1), according to application.

NSKROBUST Series Type E offers improved handling of Type S functions and is applied to the NSKROBUST Series of bore diameter from 30 mm to 140 mm (Table 1).

2. Features

(1) Product quality of the bearing is improved for the purpose of improving durability under severe conditions, such as high speed and high load.

(2) NSK's originally developed material technology is applied to the bearings for machine tools for the purpose of controlling the age deterioration that occurs under severe lubrication conditions.

This product could achieve more than 20 times normal durability under severe lubrication conditions compared to the conventional Type S (Figure 2), thanks to the above-mentioned features. Additionally, this product could improve its seizure-resistant PV value by approximately 40 % compared to the conventional Type S and based on evaluation results using the position-preload type of spindle, and it could achieve seizure resistance improvement and high reliability (Figure 3 and Figure 4).

Table 1 Bearing dimensions of NSKROBUST Series Type E

Bearing type	Dimension series	Contact angle (°)	Bearing bore diameter (mm)
NSKROBUST Series Ultrahigh-speed angular contact ball bearings	BNR10 BNR20	18	30–140
	BER10 BER20	25	
	BNR19 BNR29	18	
	BER19 BER29	25	
NSKROBUST Series High-speed angular contact thrust ball bearings	BAR10	30	
	BTR10	40	

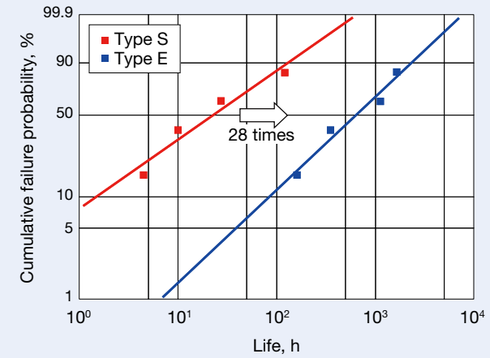

Bearing number	50BNR10
Cooling conditions	External cylinder cooling Constant at 24 °C
Rotational speed/$dm{\cdot}n$	18 000 rpm/115 × 10^4
Preload	1 400 N (constant pressure preload)
Lubrication	NSK MTE grease
Prepacked amount of grease	5 % of free internal space

Fig. 2 Durability against surface damage (wear and seizure) under severe lubrication conditions

Test conditions	
Bearing number	50BNR10 (DB matching)
Cooling conditions	External cylinder cooling Constant at 24 °C
Rotational speed	Step-up by 1 000 rpm/20 h
Preload when assembled	1 180 N (position preload)
Lubrication	NSK MTE grease
Prepacked amount of grease	15 % of free internal space

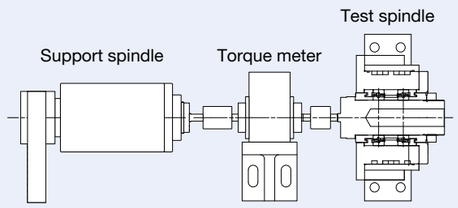

Fig. 3 Test machine and test conditions for evaluation of seizure resistance

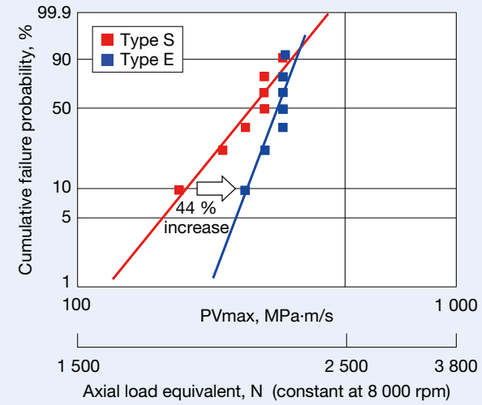

Fig. 4 Test results of seizure resistance

3. Applications

This product is the main spindle bearing for machine tools and can be used on machining centers and lathes. This can be especially effective under severe grease lubrication conditions.

4. Summary

This product is upward compatible with the conventional NSKROBUST Series Type S. Bearing reliability, seizure resistance, and bearing life have been improved. These functions can improve the rigidity and cutting load resistance of main spindles. This product also contributes to improving the environmental performance and production efficiency of machine tools.

SPACEA Series—Highly Corrosion Resistant and High-Hardness Stainless Steel ESZ Bearings

Bearings for the manufacturing facilities of various types of high-function films used in solar panels or liquid crystal TV screens need to be resistant to corrosion since they are used in corrosive environments such as water, alkali, and acid. Recently, with increases in TV screen size and demand for smartphones, the manufacturing facilities of high-function films have become larger, but there is demand for lengthening the maintenance intervals and simplifing the maintenance. To respond to these needs, NSK has developed ESZ bearings made from highly corrosion-resistant and high-hardness stainless steel and available in several series (Figure 1 and Figure 2).

This article introduces the features and specifications of ESZ bearings.

1. Features

ESZ bearings feature:

(1) Durability

ESZ bearings' inner and outer rings are made of ESZ steel with a hardness of approximately 30 % higher than conventional precipitation-hardened stainless steel (JIS SUS630). Balls are made of ceramic and are superior in corrosion resistance and wear resistance. Thus, ESZ bearings achieve approximately. ten times the durability of conventional stainless steel bearings made to the standard of JIS SUS630, in corrosive environments such as underwater (Figure 3).

(2) Corrosion resistance

ESZ steel is a high-hardness stainless steel that is as highly corrosion resistant as the conventional stainless steel JIS SUS630 in an acid or alkali environment.

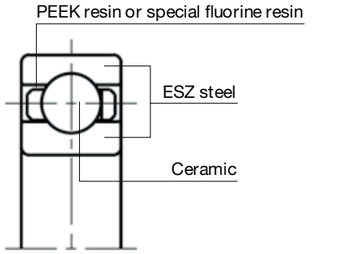

Fig. 1 ESZ bearings made of highly corrosion-resistant, high-hardness stainless steel (deep-groove ball bearing type)

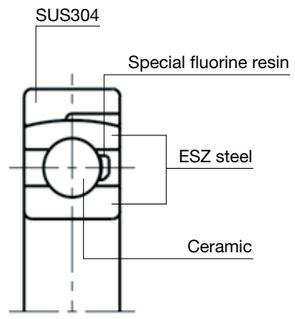

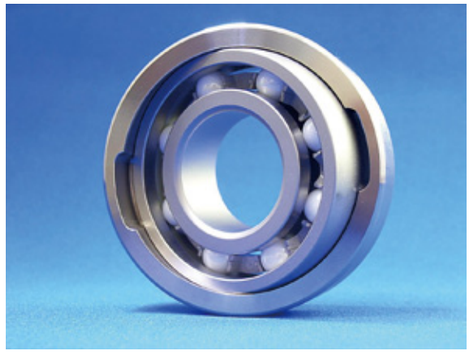

Fig. 2 ESZ bearing made of highly corrosion-resistant, high-hardness stainless steel (aligning-ring type)

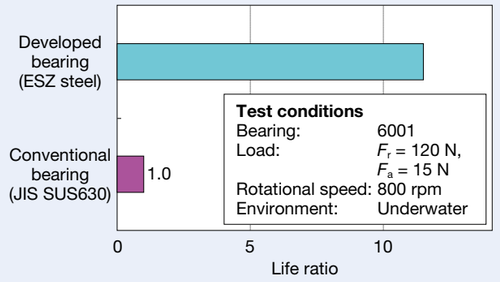

Fig. 3 Operating life test results

(3) Self-aligning

The aligning ring on this type of bearing is made of austenitic stainless steel (JIS SUS304) outside the outer ring. The bearing can achieve smooth aligning by optimizing the spherical shape of its fitting surface with the outer ring, surface roughness and clearance when the inclination between the shaft and housing (misalignment) is generated. This could simplify the responses to the deflection of the roller itself due to the increase in size (lengthening) of carrier rollers for high-function films, or a mounting error at the time of maintenance.

2. Specifications

Table 1 shows the boundary dimensions.

For the size of bearing with the bearing bore diameter of 35 mm or more, PEEK (polyether ether ketone) resin, which is superior in strength and corrosion resistance, has been adopted for the cage as a standard. On the other hand, for a bearing size with a bore diameter of less than 35 mm, the cage is made of a special fluorine resin that is low frictional and highly corrosion-resistant.

3. Applications

ESZ bearings are applicable to equipment used in a wide range of corrosive environments such as food machinery and carrier devices for medical equipment-related fields as well as cleaning equipment for various types of chemical films and film-stretching equipment.

4. Summary

ESZ bearings have been gaining recognition on the market.

We will continuously promote new product development to respond to all environments as well as to the needs for greater sophistication and diversity in the future.

Table 1 Boundary dimensions of ESZ bearings made of highly corrosion-resistant, high-hardness stainless steel

Deep groove ball bearing type — Unit: mm

Basic number	Boundary dimensions		
	Bore diameter	Outside diameter	Width
6000	10	26	8
6200		30	9
6001	12	28	8
6201		32	10
6002	15	32	9
6202		35	11
6003	17	35	10
6203		40	12
6004	20	42	12
6204		47	14
6005	25	47	12
6205		52	15
6006	30	55	13
6206		62	16
6007	35	62	14
6207		72	17
6008	40	68	15
6208		80	18
6009	45	75	16
6209		85	19
6010	50	80	16
6210		90	20
6011	55	90	18
6211		100	21
6012	60	95	18
6212		110	22

Aligning-ring type — Unit: mm

Basic number	Boundary dimensions		
	Bore diameter	Outside diameter	Width
CD200	10	35	9
CD201	12	37	10
CD202	15	40	11
CD203	17	46	12
CD204	20	54	14
CD205	25	60	15
CD206	30	72	16

Ultrahigh-Speed, Large-Diameter Ball Bearing for Hybrid Car Motors

To increase motor-driven power performance as well as fuel economy performance, the hybrid system has become more and more diverse. For bearings used for hybrid car motors, there is an increasing need for a larger-diameter bearing corresponding to the larger motor and also for correspondence to ultrahigh-speed for higher motor power.

NSK has developed an ultra-high-speed, large-diameter ball bearing (Photo 1) that can achieve the ultrahigh speed of over two million $d_m \cdot n$ (pitch circle diameter × maximum rotational speed), which is the highest level in the world for automotive applications. This is a large-diameter bearing with a bore diameter of up to 160 mm and outside diameter of up to 190 mm, as the bearing for hybrid car motors.

Photo 1 Ultrahigh-speed, large-diameter ball bearing for hybrid car motors

1. Structure and Specifications

Figure 1 shows the cross-sectional view of the newly developed bearing. Corresponding to the high centrifugal force generated by high-speed rotation of a large-diameter bearing, the cage durability has been highly improved by adopting a carbon fiber-reinforced PEEK as a cage material, for the first time in automotive bearings. In addition, regarding the ball-guided snap cage, the bearing durability in the ultrahigh-speed rotation has been dramatically improved by controlling the vibration with cage wobbling and the skidding damage by using the inner ring's outside surface as the riding surface (Figure 2).

Seizure caused by friction or heat generation can be prevented under ultrahigh-speed rotation by optimizing the groove dimensions, ball diameter, number of balls, and clearance in the bearing interior. As for the inner and outer rings, the dimensional change when used and the aging variation of radial clearance can be controlled, and the durability can be improved by using the materials and heat treatment technologies that are superior in dimensional stability.

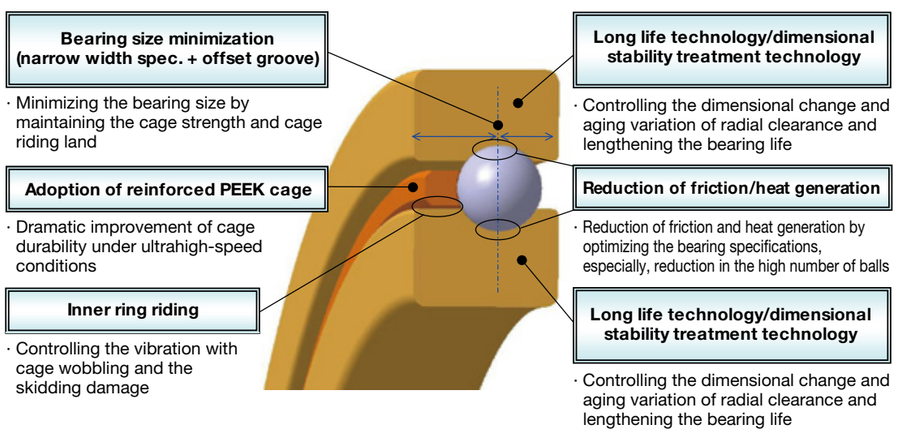

Fig. 1 Cross-sectional view of the newly developed bearing

2. Features

This bearing is notable for its excellent high-speed performance.

The high-speed performance of a $d_m \cdot n$ over two million can be achieved by adopting the carbon-fiber-reinforced PEEK cage, adopting the cage riding type of the inner ring outside surface, optimizing the bearing internal design, and using longer-life technology.

3. Summary

The developed bearing enables ultrahigh-speed rotation and an increase in the size of the motor, and is believed to contribute to the improvement of fuel efficiency and improvement in travelling performance of hybrid cars. We hope to develop new function bearings to meet market needs because improvement of fuel efficiency in hybrid cars is certain to continue.

Test conditions	
Load	No load (unbalance load only by rotational load)
Outer ring rotational speed	10 080 rpm
Inner ring rotational speed	4 255 rpm
$d_m \cdot n$ (pitch circle diameter × rotational speed)	Equivalent to 2.6 million (cage orbital speed equivalent)
Lubrication	ATF: 0.35 L/min
Lubrication oil temperature	90 °C
Test time	60 h

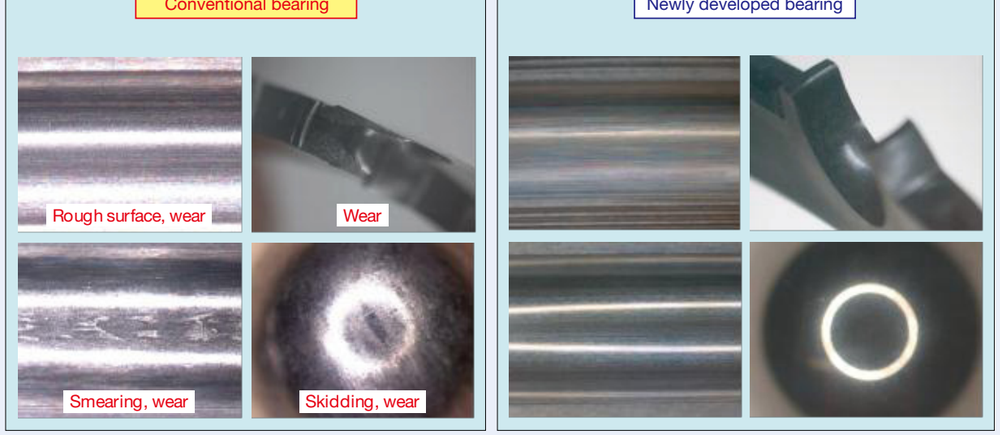

Fig. 2 High-speed test results of a conventional bearing and the newly developed bearing

Highly Reliable, Lower Frictional Torque Ball Bearings for Belt-Type CVTs

Recently, belt type CVTs have been gaining market share in Japan and China, as a transmission that delivers both excellent fuel economy and a smooth ride.

On the other hand, CVT pulley support bearings have been facing severe conditions and require higher performance compared to general transmission bearings, so users are demanding high reliability and high efficiency.

NSK has developed highly reliable, lower-frictional-torque ball bearings (Photo 1) for belt-type CVTs that could highly improve durability in addition to controlling torque loss.

Photo 1 Highly reliable, lower frictional torque ball bearing for belt-type CVTs

1. Features

(1) CVT-specific design for longer bearing life

Figure 1 shows the features of the bearing.

The newly developed bearing controls the generation of surface damage (peeling) under the low-viscosity oil and diluted or contaminated lubrication putting some technology (the unique special heat treatment acquired by NSK, anti-creep technology and design technology combined in the fiber-reinforced plastic cage), and can achieve a durability of 2.5 times higher than that of a conventional bearing (Figure 2).

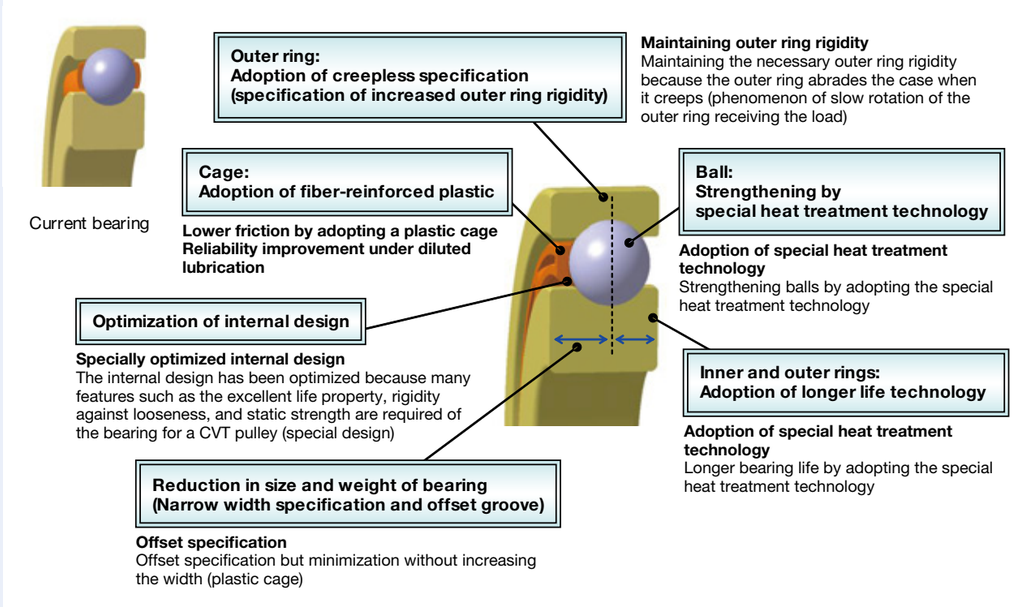

Fig. 1 Cross-sectional view of newly developed bearing

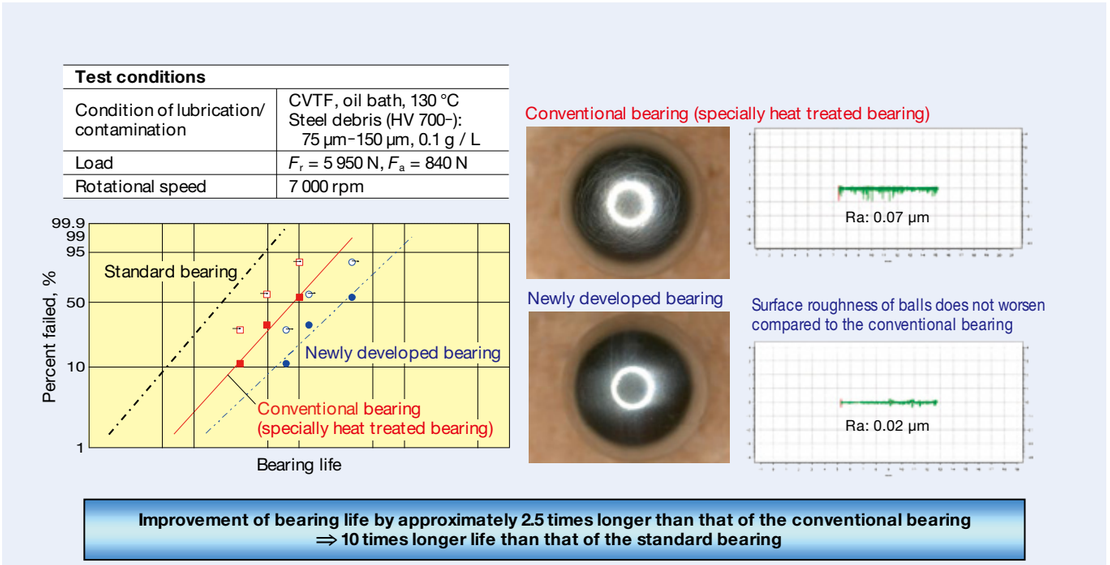

Fig. 2 Durability test results of a conventional bearing and newly developed bearing

(2) Fiber-reinforced plastic cage for lower torque

The agitation torque of lubrication oil by the bearing rotation could be reduced by 30 % without greatly changing the load rating capacity or bearing size by adopting a fiber-reinforced plastic cage. Additionally, further reduction in size and weight could be achieved by offsetting the raceway groove (Figure 3).

2. Summary

Highly reliable, lower-frictional-torque ball bearings for belt-type CVTs are believed to contribute to the high reliability and improvement in efficiency of belt-type CVTs. This type of bearing will soon be supplied from global ball bearing production sites, with further expansion of this application in the future.

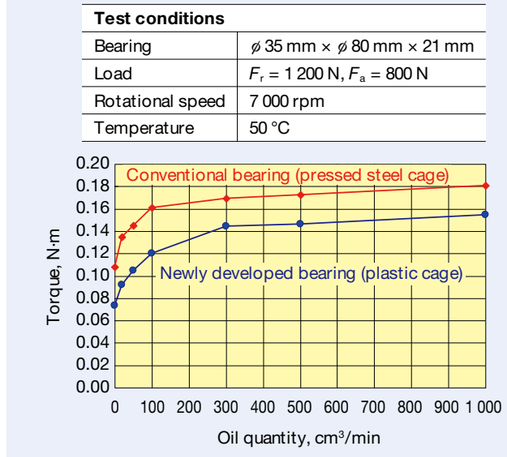

Fig. 3 Relationship between oil quantity and torque

Silent Needle Roller Bearing for Automotive Electrical Components

Recently, the operating noise from the automotive electrical component, although it may not be outstanding, can irritate passengers, a sound that is more noticeable in cars with greatly reduced engine noise such as electric vehicles (hereinafter called EVs) and hybrid electric vehicles (hereinafter called HEVs). One source of noise in this otherwise quiet environment is the bearing; thus, demand is increasing for quieter bearings.

NSK has carried out a review of component precision considering the impact of noise and what would be required to develop a high-precision processing method for needle roller bearings used for driving, and it has developed a quiet-running needle roller bearing (Photo 1) that is most suitable for use in automotive electrical components, as described below.

Photo 1 Silent Needle Roller Bearings for automotive electrical components

1. Background of Development

For needle roller bearings used for automotive electrical components, the crowning (Figure 1) — in other words, the smooth inclination at both ends of the roller (rolling element) surface — is added to support the high load. The out-of-roundness of the end position of the rolling surface, as it is usually built, had less accuracy than that of the center position, and sometimes this led to the degradation of the sound level under conditions of a large roller tilt (Figure 2).

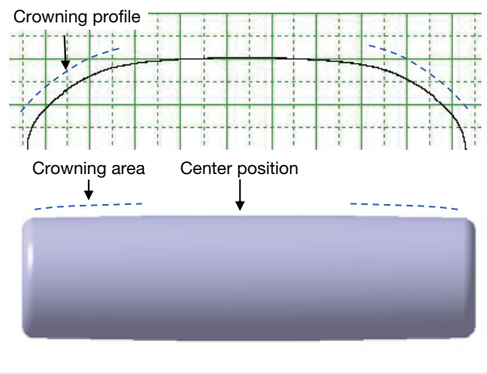

Fig. 1 Crowning profile of a needle roller

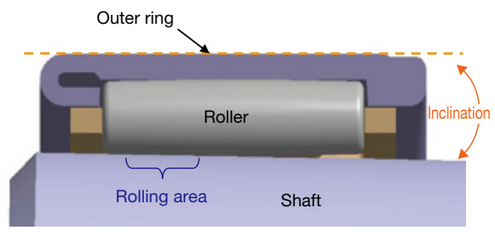

Fig. 2 Rolling area of the roller under conditions of a large tilt

2. Features

The conventional processing method of crowning for large-diameter rollers of cylindrical roller bearings was applied and adjusted to the needle roller (less than Φ 5 mm) of needle roller bearings. The out-of-roundness level of the roller crowning area was improved to approximately 1/4 compared to a conventional roller (Figure 3).

3. Effect of the Developed Bearing

The sound level was measured with the bearing forced to tilt, after offsetting the weight from the bearing center, as shown in Figure 4 and Table 1. The sound level (sound pressure ratio) generated by the bearing was less than 1/3 of that of the conventional bearing (Figure 5).

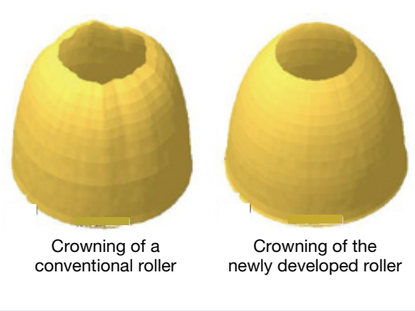

Fig. 3 Comparison of the accuracy of the roller crowning area

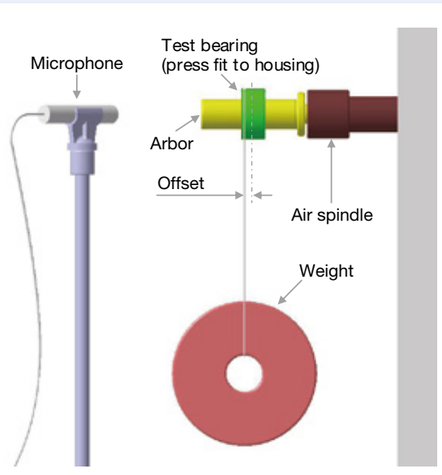

Fig. 4 Layout of measuring device for sound level

4. Applications

(1) Automotive electrical components for EVs, HEVs, and luxury cars that require low noise levels

(2) Rotary support part of the products that must run quietly, such as domestic washing machines and air conditioners

5. Summary

The need for silent needle roller bearings is anticipated to increase in the future due to an increase of electric operation of automobiles, and new value-added proposals will be required for home appliances. We hope to continuously develop new products, meet market needs and contribute to the improvement of product performance.

Table 1 Test conditions

Bearing type	Drawn cup needle roller bearing
Mass of weight	2 kg
Offset amount	7 mm
Position of microphone	200 mm from bearing center, 45°
Measuring frequency	10 Hz–10 kHz
Averaging time	10 s

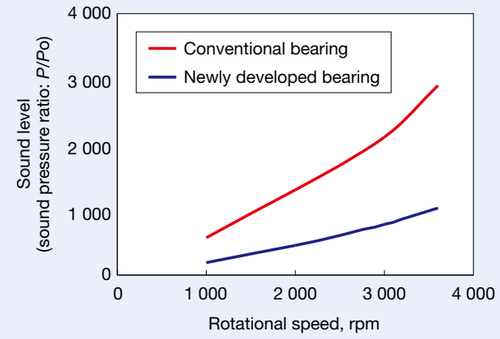

Fig. 5 Comparison of sound levels

Automotive Transmission Thrust Needle Roller Bearings with Integrated Washer and Oil-Flow Control

With the rise of environmental consciousness, demand for improvement of fuel efficiency for automobiles has increased, as has the need for more efficient transmissions—such as reductions in size and weight and torque loss. If the oil flow circulating into the transmission is to be controlled, the oil pump can be downsized, contributing to higher efficiency. Because the transmission is assembled with many thrust needle roller bearings, the need to integrate the bearing components (roller, bearing washer (bearing ring of thrust bearing), and cage) has been increasing, with the goal of reducing man-hours. NSK has thus developed a new product (Photo 1) with the added function of distributing the most suitable amount of oil into the unit to the thrust needle roller bearing, which improves the mounting capability of the unit. This article describes the newly developed thrust needle roller bearings with integrated washer and oil-flow control.

Photo 1 Thrust needle roller bearing with integrated washer and oil-flow control

1. Specifications

Enlarging the opening area of the bearing washer is possible by changing its profile, if a lot of oil is expected to flow into the bearing interior. It is also possible to achieve an increase in the oil-flow amount by narrowing the cage width or making holes in the cage (Figure 1). When controlling the ingress of oil, controling the oil flow is possible by making the profile of the bearing washer fully curled or widening the cage width.

In addition, the new product has a curled profile, as shown in Figure 2, which improves the accuracy of the internal clearance because it partially holds the bearing components (roller, bearing washer, and cage). This enables improvement of the resistance to eccentricity (shaft dislocation), which had been the problem of thrust needle roller bearings with integrated washers.

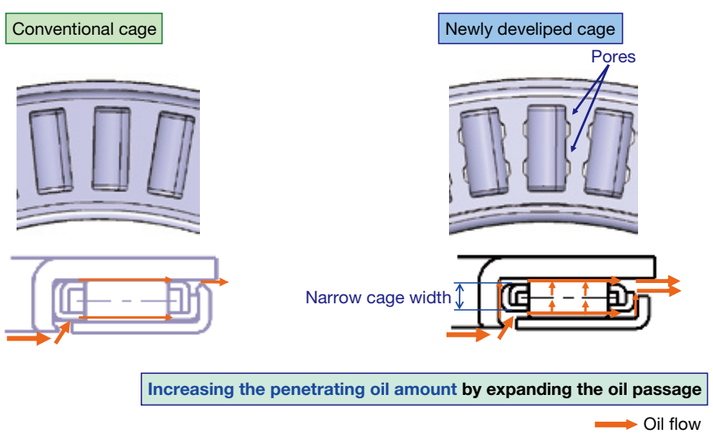

Fig. 1 Comparison of oil amount penetrating through a conventional cage and the newly developed cage

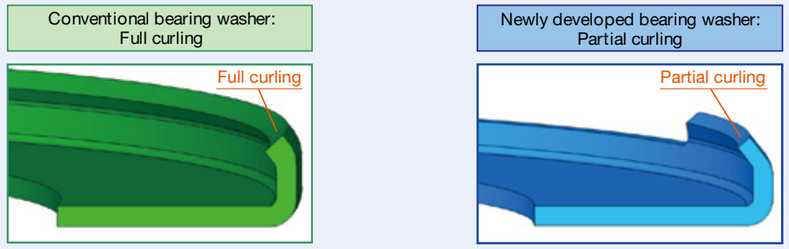

Fig. 2 Partial curling of newly developed bearing washer and full curling of a conventional bearing washer

2. Features

(1) Control of oil flow by optimizing the design of the bearing washer and cage (Figure 3)

(2) Improvement of resistance to eccentricity by improving the accuracy of the bearing's internal clearance

3. Summary

The addition of the oil-flow control function to the thrust needle roller bearing with an integrated washer is believed to contribute to downsizing the oil pump or improving the unit assembling. In future, we hope to further promote product developments that meet market needs.

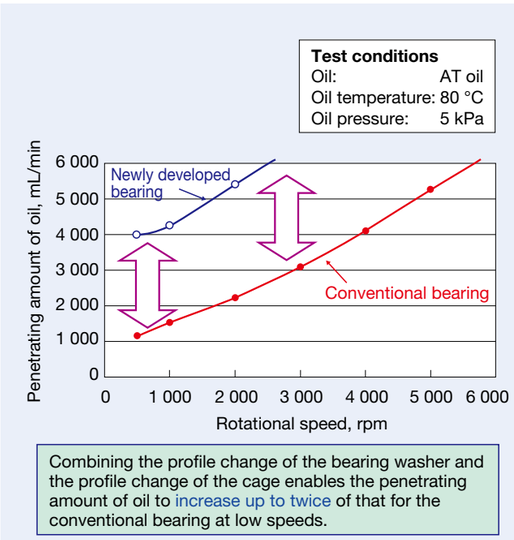

Fig. 3 Test results of penetrating amount of oil

HMS Series of Ball Screws for High-Speed Machine Tools

Recently, machine tools targeted at machining centers have been polarized into featuring either higher speed or higher precision. Since a high feed speed has been required to improve the productivity of machine tools for automotive components, NSK has commercialized the medium-lead HMD series of ball screws for high-speed machine tools in addition to high-speed and low-noise technologies. On the other hand, fine-lead ball screws have been used for the high-precision machine tools for die machining, but there has been demand for a higher speed to improve the productivity in these applications.

NSK has developed and commercialized the HMS series of ball screws for high-speed machine tools (Photo 1) and to meet the needs mentioned above. This article provides an overview of this series.

Photo 1 HMS series of ball screws for high-speed machine tools

1. Structure and Specifications

The HMS series uses the SRC (Smooth Return Coupling) recirculation system (Figure 1) that enables smooth ball recirculation, and also uses small-lead ball screws for higher-precision requirements.

The product specifications are as follows:

- Ball recirculation system: SRC recirculation circuit
- Permissible $d \cdot n$ value: 160 000
  (d: shaft diameter (mm), n: rotational speed (rpm))
- Accuracy: JIS C5
- Combination of shaft diameter and lead: Series lineup in Table 1

2. Features

(1) High-speed performance

This product enables an increase of approximately 20 % in the permissible $d \cdot n$ value (that is, 160 000) and achieves a maximum feed speed of 48 m/min (for a 40 mm shaft diameter and 12 mm lead) compared to the conventional return tube recirculation system, by adopting the SRC recirculation system utilizing NSK's original high-speed and low-noise technologies.

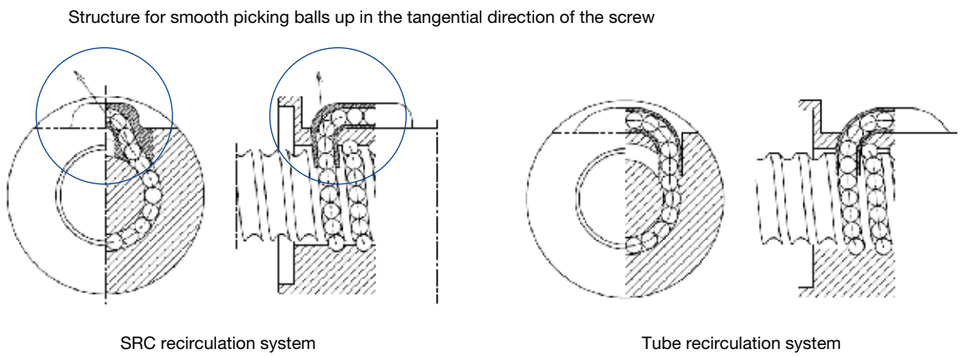

Fig. 1 Comparison of a conventional return tube recirculation system and an SRC recirculation system

Table 1 Series lineup

Models	Shaft diameter (mm)	Lead (mm)	Basic load rating (N)		Maximum feed speed (m/min)
			Dynamic load rating (C_a)	Static load rating (C_{0a})	$d \cdot n$ = 160 000
ZFRC4010-10	40	10	52 000	137 000	40
ZFRC4012-10		12	61 000	155 000	48
ZFRC4508-10	45	8	37 300	118 000	28
ZFRC4510-10		10	54 200	155 000	35
ZFRC5010-10	50	10	57 700	175 000	32
ZFRC5012-10		12	77 600	214 000	38

(2) Low noise and low vibration

By using the SRC recirculation circuit, the noise level was reduced by up to 6 dB (A) and the vibration level was reduced by up to half compared to a conventional product.

Figure 2 shows the measurement results of the noise level compared to the conventional product. Figure 3 shows the measurement results of the vibration acceleration level.

(3) Interchangeability

This product is designed for easy replacement by maintaining the interchangeability of nut outside diameter and nut flange mounting deimensions with the conventional tube-type ball screws.

3. Applications

This product is suitable for the feed axis of machine tools for which high load capacity and high rigidity are needed, such as for die machining and heavy cutting.

4. Summary

We are planning to expand the lineup of this HMS series for fine lead and the HMD series for medium lead, We hope that these contribute higher function of machine tools in the future.

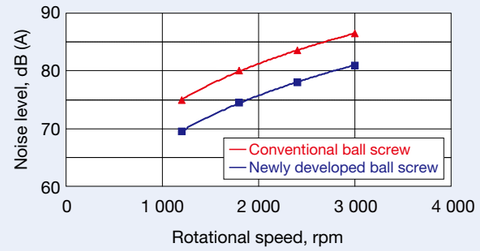

Fig. 2 Noise levels

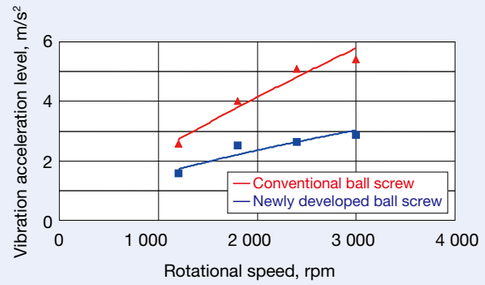

Fig. 3 Vibration acceleration levels

Miniature Large-Lead Series of High-Speed, Low-Noise Ball Screws

The need to improve productivity of machine equipment, such as the mounting equipment of electronic components to the board or the array apparatus of components, has been increasing. Downsizing the machine and shortening the cycle time are two methods of doing this. In addition, component mounting accuracy has been improving, and there is more demand for accurate positioning.

In 2003, NSK began sales of high-speed and low-noise ball screws, facilitating both high-speed rotation and low noise. NSK has also been developing the most suitable series for the various types of industrial machinery, such as machine tools, semiconductor manufacturing equipment, carrier devices, and injection molding machines. It has developed the small-diameter Miniature Large-Lead Series of ball screws (Photo 1), which is most suitable for the mounting equipment or the array apparatus of components, by applying the technology of high-speed and low-noise ball screws.

This article explains the structure and of these ball screws specifications.

Photo 1 Miniature Large-Lead Series of high-speed, low-noise ball screws

1. Structure and Specifications

The specifications of Miniature Large-Lead Series ball screws are:

(1) Accuracy class and clearance
JIS standard: Class C5, Ct7
Axial clearance: less than 0.005 mm

(2) Rotational speed and feed speed
Maximum rotational speed: 5 000 rpm
Maximum feed speed: 1 250 mm/s (in the case of BSS0815)

2. Features

(1) Smaller diameter

Inertia can be decreased by making the shaft diameter of the ball screw as small as possible, and the motor load can be reduced at a high speed and high acceleration or deceleration.

(2) Larger lead

The lead of small-diameter ball screws can be made larger by introducing a new processing technology that can achieve a high-speed feed, even at the same rotational speed.

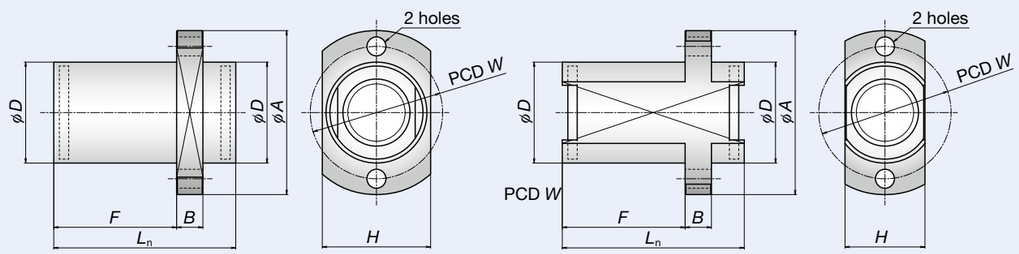

Standard nut profile

Low-profile (minimum width of flange) nut profile
Low-profile nut is an option.

Fig. 1 Ball screw nuts of Miniature Large-Lead Series

Table 1 Ball screw nut specifications of the Miniature Large-Lead Series

Nut models	Shaft diameter	Lead	Basic load rating, N		Ball screw nut dimensions							Mounting hole dimensions		Maximum feed speed, mm/s
			Dynamic	Static	D	A	B	L_n	F	H		W	X	
			C_a	C_{0a}						Standard	Minimum			
BSS0608-2E	6	8	550	715	14	27	4	16	8	15	10	21	3.4	660
BSS0608-4E			1 180	1 760				24	16					
BSS0612-2E		12	550	715				20	12					1 000
BSS0612-4E			1 180	1 760				32	24					
BSS0810-2E	8	10	910	1 260	18	31	4	18	10	19	13	25	3.4	830
BSS0810-4E			1 950	3 080				28	20					
BSS0815-2E		15	910	1 260				22	14					
BSS0815-4E			1 950	3 080				37	29					

Note: All right turn screws

(3) Adoption of End-deflector recirculation system

High-speed rotation up to 5 000 rpm can be achieved by adopting the end-deflector recirculation system, which has received high praise in the market as a high-speed and low-noise ball screw.

(4) Narrowing the flange width

Flange and nut widths are reduced by up to 33 %, and this can contribute to the downsizing of equipment.

(5) Maintenance-free for the long term

The machine can go without maintenance for extended periods if an NSK K1 lubrication unit is installed. (optional)

Owing to these improvements, the Miniature Large-Lead Series of ball screws enables a high-speed and high-acceleration/deceleration operation that exceeds that of the linear motor for the use of mounting equipment where the ball screw is used within a relatively short stroke and makes it easy to shorten the machine's cycle time. In addition, the ball screws enable the high-speed and high-accuracy multipoint positioning that had seemed difficult for the small air cylinder to achieve.

3. Applications

The main application is production equipment for electric and electronic components and for small carrier devices.

Taking the mounting equipment for electronic circuit boards as an example, the high-speed and high-acceleration/deceleration drive is needed to shorten the cycle time for the head drive shaft, in order to mount the components to the board. In addition, making the drive shaft compact is also needed to meet demand for a high-density arrangement of components. This series enables the high-speed feed by a larger lead, and cycle time is likely to be shortened. Though the motor load increases if the lead is made larger, the influence of the larger lead is minimized by the low-inertia specifications of making the screw shaft diameter smaller. Additionally, the smaller diameter of the screw shaft and the narrower width of the flange enables a high-density arrangement.

The other example is the small carrier device. The concrete example is the replacement of the ball screw from the small air cylinder used in the array apparatus of components. A number of air cylinders with different strokes are needed for multipoint positioning using the air cylinder, and it is difficult to adjust the speed and acceleration/deceleration. Using this series enables the accurate multipoint positioning with a shaft, and it is easy to adjust the speed and acceleration/deceleration. In addition, compactness of the device can be expected because no compressor or air pipe arrangement is necessary and the screw shaft and nut flange are small.

4. Summary

The small-diameter Miniature Large-Lead Series of ball screws, most suitable for mounting equipment and component aligning machines, can contribute to the shortening of machine cycle time, machine downsizing, and high-speed and high-precision multipoint positioning for the application of mounting equipment.

Precision-Grade, Medium-Preload, Random-Matching NSK Linear Guides

The LH, SH, LS, and SS series—the main series of NSK linear guides—have been widely used in general industry, such as semiconductor manufacturing equipment, liquid crystal manufacturing equipment, car manufacturing facilities, transfer devices, and machine tools. Also, the rails and sliders that make up the random-matching linear guides have usually been set aside and sold together in accordance with the required specifications. NSK is marketing standard-grade and light-preload versions of these series of parts in response to the customer requirements for quick turnaround.

NSK has developed precision-grade, medium-preload, random-matching linear guides (Photo 1) that improve the running parallelism and the rigidity by improving the accuracy of the rail and slider in response to demand. This was done because quick turnaround was also required for high-precision and high-rigidity products in the sales and small markets as well as the Chinese and other Asian markets.

Photo 1 Ball screw for motorcycle brake systems

1. Features

(1) Improvement of running parallelism and rigidity

By improving the processing accuracy of the rail raceway surface and reference plane for mounting, half of the running parallelism target can be achieved compared to the conventional standard grade of random-matching linear guides (Figure 1). In addition, twice the rigidity of the conventional light-preload type can be achieved by controlling the proper preload (Figure 2).

(2) Extensive lineups

Addition of the precision grade and medium-preload type resulted in an increase in the combination of model numbers, accuracy, slider models, and preloads from 44 conventional types to 122 types. The lineup of random-matching types has been greatly expanded, enabling us to meet a larger variety of market needs. Table 1 shows the lineup of random-matching types. In addition, Figure 3 shows the profile shapes of slider models.

(3) Long-term free maintenance

Lubrication unit NSK K1 can be mounted and can achieve long-term maintenance-free operation.

(4) Extensive optional components

Optional components for dust prevention such as a double seal, protector, and rail cap are available, and these make it possible to respond to situations involving contamination.

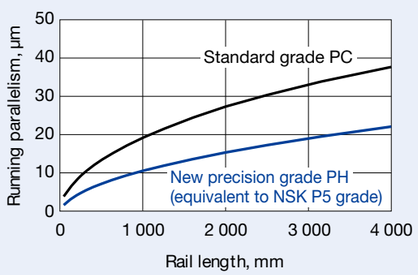

Fig. 1 Running parallelism of random matching types

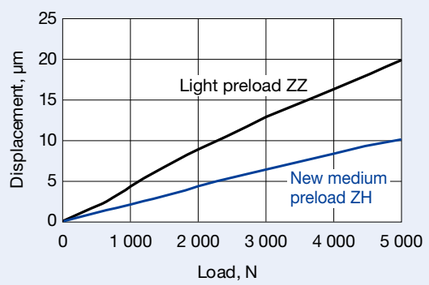

Fig. 2 LH35AN rigidity in the direction of compression

Table 1 Lineup of random-matching types

Series	Size	Slider models								Accuracy		Preload		Grease selection surface treatment
		AN	AL	BN	BL	CL	EM	GM	JM	Precision grade PH	Standard grade ZH	Medium preload ZH	Light preload ZZ	
LH	15	○		○			○	○		○	○	○	○	○
	20	○		○			○	○		○	○	○	○	○
	25	○	○	○	○		○	○		○	○	○	○	○
	30	○	○	○	○		○	○		○	○	○	○	○
	35	○	○	○	○		○	○		○	○	○	○	○
	45	○	○	○	○		○	○		○	○	○	○	○
	55	○	○	○	○		○	○		○	○	○	○	○
	65	○		○			○	○		○	○	○	○	○
SH	15	○		○			○	○		○	○	○	○	○
	20	○		○			○	○		○	○	○	○	○
	25	○	○	○	○		○	○		○	○	○	○	○
	30	○	○	○	○		○	○		○	○	○	○	○
	35	○	○	○	○		○	○		○	○	○	○	○
	45	○	○	○	○		○	○		○	○	○	○	○
	55	○	○	○	○		○	○			○		○	○
LS	15		○			○	○		○	○	○	○	○	○
	20		○			○	○		○	○	○	○	○	○
	25		○			○	○		○	○	○	○	○	○
	30		○			○	○		○	○	○	○	○	○
	35		○			○	○		○	○	○	○	○	○
SS	15		○			○	○		○	○	○		○	○
	20		○			○	○		○	○	○		○	○
	25		○			○	○		○	○	○		○	○
	30		○			○	○		○	○	○		○	○
	35		○			○	○		○	○	○		○	○

2. Applications

This type is available for a broad range of applications such as semiconductor manufacturing equipment, liquid crystal manufacturing equipment, car manufacturing facilities, transfer robots, and machine tools.

3. Summary

Because random-matching products can combine the rail and the slider randomly, it is possible to keep a stock of the rails and the sliders individually. Adding the precision-grade, medium-preload, random-matching types to NSK's original workshop system—which combines the slider to the rail after cutting in accordance with user specifications—has allowed for the short-time turnaround of high-precision and high-rigidity products globally.

We are planning to promote higher-precision random-matching products in the future.

Model	Cross-sectional profile	Slider length
AN AL	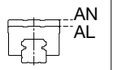	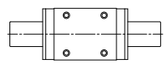
BN BL	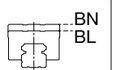	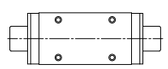
CL	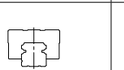	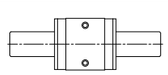
EM		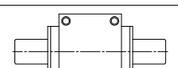
GM		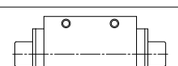
JM		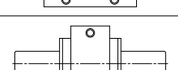

Fig. 3 Slider models of random-matching types

Random-Matching, Miniature PU and PE Series of NSK Linear Guides

The miniature PU/PE series of NSK Linear Guides launched in 2003 as a miniature linear guide offers outstanding features including a high motion performance that ensures a smoother motion and a design that ensures easier assembly by preventing balls from dropping out of the ball slide. Not only that, it is lightweight and has a low inertia suited to providing high acceleration and deceleration rates. The PU series is the narrow-width type and the PE series is the wide-width type suited to the usage of a single guide.

The lineup has been enhanced by commercializing the high-load type of 1.5 times the load capacity.

Additionally, NSK has commercialized the random-matching linear guides (Photo 1) that enable any combination of the rail and the ball slide. This article introduces the features of the series.

Photo 1 Random-matching, miniature PU and PE series of NSK Linear Guides

1. Features

(1) Improved processing accuracy results in high-precision random matching

Table 1 shows the assembly accuracy standards of the random-matching miniature PU and PE series. The accuracy standards of the preloaded assembly type are also described.

Improved accuracy in the processing of the raceway and datum surfaces for the rails and ball slides has resulted in dimensional tolerances being reduced to half the levels of the normal grade of the preloaded assembly type, PN.

Consequently, any random combination of rails and ball slides can enjoy approximately the same levels of precision as the precision grade, P6.

(2) Single-unit inventory control and sales result in shorter delivery times

These rails and ball slides are inventory-controlled and sold on a single-unit basis. This allows for immediate delivery. Prompt delivery is also possible if customers place additional orders for ball slides or request replacements, as well as when ball slide shapes or other specifications are changed.

2. Lineup and Reference Numbers

Table 2 shows the product lineup of miniature PU and PE series.

The random-matching type provides three sizes of size numbers 9, 12 and 15 for both the PU series and the PE series. In addition, a standard type and high-load type are provided, and the high-load type improved the load capacity to approx. 1.3 to 1.5 times more than that of the standard type by lengthening the ball slide to approx. 1.4 to 1.7 times (differ by size) longer than that of standard type. This enables us to greatly improve the product life (a life 2 to 3 times longer than that of standard type).

Additionally, the high-load type has an especially high moment load capacity (1.5 to 2.7 times higher than that of the standard type) in the directions of pitching and yawing, and is suitable for an application receiving a moment load, like a cantilever.

Figure 1 shows the examples of reference numbers for the random-matching type. The ball slides and rails are treated individually from the random-matching type, but it is possible to sell the assembly in an assembled condition if needed.

Table 1 Accuracy standards of miniature PU and PE series

unit: μm

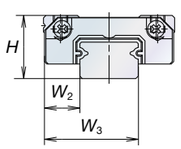

Items	Accuracy grade				
	Preloaded assembly type				Random-matching type
	Super precision P4	High precision P5	Precision P6	Normal PN	Normal PC
Tolerance of mounting height *H*	± 10	± 15	± 20	± 40	± 20
Variation of mounting height *H* (all ball slides on a set of rails)	5	7	15	25	15/30*
Tolerance of mounting width W_2 or W_3	± 15	± 20	± 30	± 50	± 20
Variation of mounting width W_2 or W_3 (all ball slides on reference rail)	7	10	20	30	20

Note*: On the same rail/on multiple rails

Pitching is the direction of rotating around the horizontal axis perpendicular to the guide.
Yawing is the direction of rotating around the vertical axis perpendicular to the guide.

Table 2 Product lineup of miniature PU and PE series

Series	Size number	Rail width (mm)	Standard type		High-load type	
			Ball slide shape code	Lineup*	Ball slide shape code	Lineup*
Miniature PU series	5	5	TR	○	–	–
	7	7	AR	○	–	–
	9	9	TR	○ ★	UR	○ ★
	12	12	TR	○ ★	UR	○ ★
	15	15	AL	○ ★	BL	○ ★
Wide miniature PE series	5	10	AR	○	–	–
	7	14	TR	○	–	–
	9	18	TR	○ ★	UR	○ ★
	12	24	AR	○ ★	BR	○ ★
	15	42	AR	○ ★	BR	○ ★

Note*: ○ = Preloaded assembly type is available; ★ = Random-matching type is available.

3. Applications

For a wide range of applications, these products can be used with semiconductor production equipment, liquid crystal production equipment, medical equipment, inspection equipment, and various types of compact precision stages.

4. Summary

The miniature PU and PE series of NSK linear guides have lined up the random-matching types to enable any combination of rail and ball slide, in addition to the preloaded assembly type. It has become possible to quickly supply a linear guide suitable for any application and usage environment.

Random-matching types of sizes 5 and 7 will be developed in accordance with future market demand.

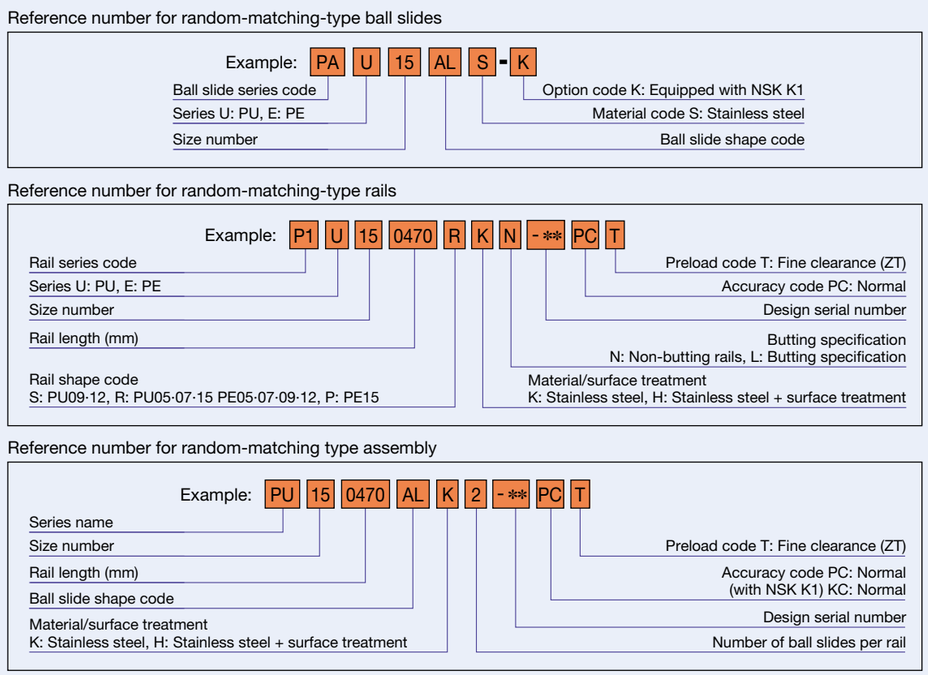

Fig. 1 Examples of miniature PU and PE series nomenclatures

Highly Durable, Highly Rigid, Slidable Intermediate Shaft for EPS

As automobiles have become more commonplace in emerging nations, the use of electric power steering (EPS) has also increased in order to improve fuel economy. In these markets, there are still many rough roads, which present the challenge of improving durability and suppressing the vibration and noise that is transmitted to the steering wheel.

EPS employs a motor to assist the steering force of drivers as they turn the steering wheel in the direction they wish to go. EPS also transmits that steering force onto the suspension via the intermediate shaft. The intermediate shaft not only transmits the rotational movement (steering angle and steering force), but it also helps to absorb deflection and vibration of the vehicle body by expanding and contracting (Figure 1).

Since there are still many rough roads in emerging nations—roads that cause a lot of vibration—the intermediate shaft must frequently expand and contract to a significant degree. As a result, the slide joint of the shaft will wear out over time, resulting in the generation of unpleasant vibration and noise. The rigidity of the intermediate shaft also affects the “feel” of steering. In response to this, NSK has developed a high durability, high rigidity, slidable intermediate shaft, PQUS24, for EPS, with the following superior features for improved durability and steering “feel” (Photo 1).

Photo 1 Newly developed, highly durable, slidable intermediate shaft: PQUS24

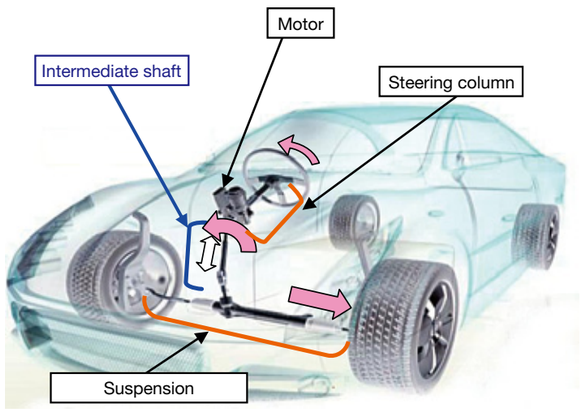

Fig. 1 Column-type electric power steering system

1. Structure

This product consists of the hollow inner shaft with outer meshing teeth, coated by resin and an outer tube with inner meshing teeth (Figure 2 and Figure 3).

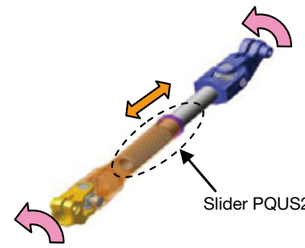

Slide action for smooth transmission of rotational movement

1. Transmits steering rotation angle and force to the suspension.
2. Sliding action absorbs vibration and deflection of vehicle body.
3. Does not loosen or rattle.

Fig. 2 Roles of the intermediate shaft

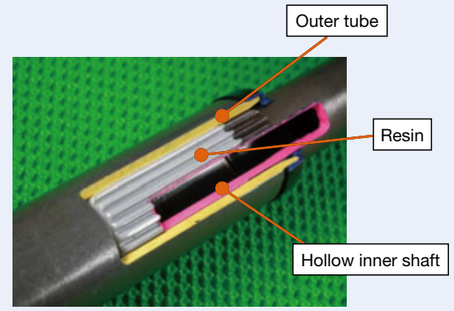

Fig. 3 Cutaway view of the newly developed PQUS24

2. Features

(1) Improved durability in the slide joint

By increasing the size of the slide joint and the number of meshing teeth, NSK has reduced the amount of force exerted on the tooth surface, thereby improving wear resistance and durability.

(2) Improved steering feel

By increasing the size of the slide joint, increasing the number of meshing teeth, and increasing the size of the inner shaft, NSK has increased the rigidity of the slide joint, resulting in an improvement in steering feel. In addition, as a world’s first for high-output column-type EPS, NSK hollowed out the inner shaft to achieve weight reduction while maintaining the same size of outer tube as a conventional part.

(3) Suppressed steering wheel vibration

By applying an optimum thickness of resin coating on the inner shaft surface and applying grease that has superior lubrication performance, NSK has reduced the wear on the slide joint. Additionally, by increasing the size of the slide joint and the number of meshing teeth, NSK has reduced the amount of force exerted on each tooth surface, thereby greatly reducing slide resistance. In this way, the intermediate shaft can slide more smoothly for better vibration absorption and a reduction in the amount of unpleasant vibration and noise that can be transmitted from the road to the steering wheel when driving on rough roads.

3. Summary

This product not only features improved durability on rough roads, but it also makes for a steering “feel” that allows the driver to “be as one with their automobile.” This product can also suppress the vibration and noise that is transmitted to the steering wheel on rough roads. NSK will introduce this product in emerging nations and then expand its application to the global automobile market.

Wedge Gear of New Positive-Lock Mechanism for Steering Column

The steering column is an important component that is used for three major functions of automobiles; running, turning, and stopping. The steering column also has key safety functions: Not only must it support an air bag; it must also absorb the impact of the driver by shortening itself in the event of a collision. In addition, the steering column provides drivers with the ability to adjust the steering wheel to the desired position in their vehicle. It is a component that requires the contradictory functions of providing both the stability needed for the steering wheel in the event of a collision and the operability for adjusting the position of the steering wheel.

NSK has developed a new mechanism of a positive-lock Wedge Gear that can provide these contradictory functions. This article introduces the gear.

1. Structure and Operating Principle

Photo 1 shows the column-type electric power steering (EPS) with the Wedge Gear mounted. Photo 2 shows a gear lever and a v-gear that are main components.

The cross-section of the gear lever tip is wedged and the minute teeth are formed on both surfaces of the wedge. The same minute teeth are formed on the surfaces of the v-portion of receiving v-gear. When the teeth of both components are engaged, they lock firmly (Photo 3 (a)). When the engagement is released by unlocking the gear lever, it becomes possible to smoothly change the tooth cross-phase, that is, the vertical position of the steering wheel, without any interference (Photo 3 (b)). Figure 1 shows this schematically.

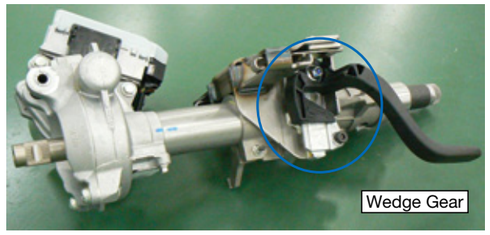

Photo 1 An EPS with the newly developed, positive-lock, Wedge Gear mechanism

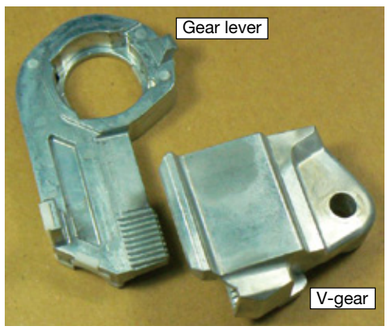

Photo 2 Gear lever and V-gear for the Wedge Gear of the new positive-lock mechanism

(a) Locked position of gear lever

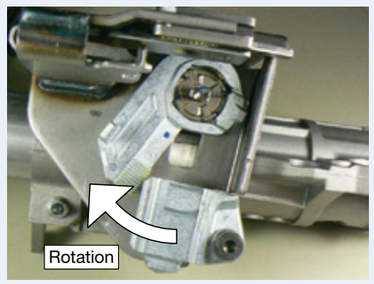

(b) Released condition of gear lever

Photo 3 Wedge Gear of the new positive-lock mechanism

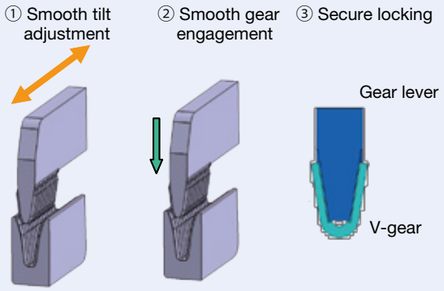

Fig. 1 Gear lever and V-gear for the Wedge Gear of the new positive-lock mechanism

2. Features

Conventional positive-lock mechanisms include the multi-plate method and the plain gear method.

(1) Multi-plate method

The multi-plate method maintains holding force by the friction between several steel plates, but the frictional feel occurs due to the insufficient clearance between steel plates when adjusting the position of the steering wheel, that is, when being released. The method has drawbacks such as the instability of the frictional force. By increasing the number of plates to obtain the desired holding force, the number of components also increases.

(2) Plain gear method

Because the plain gear method has opposing plain gears and it sometimes causes the teeth-and-teeth engagement, the method has the drawbacks of operability and certainty.

Table 1 shows a comparison of these features.

In addition, Figure 2 shows the vertical holding forces at the position of the steering wheel. This force is the most important. The holding force of the Wedge Gear increases by more than three times compared to the mechanism without a positive lock. If a driver is thrown forward at the time of a crash, the Wedge Gear can suppress the vertical change of the steering wheel position, resulting in a more effective operation of impact absorption.

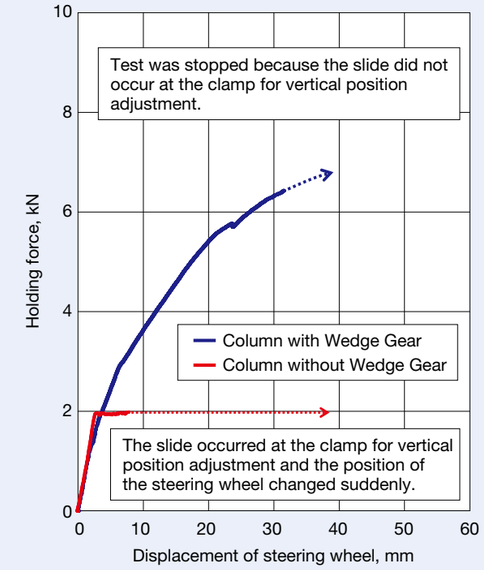

Fig. 2 Holding force comparison of steering wheels on columns with and without the Wedge Gear

3. Summary

Mass production of the new positive-lock mechanism, introduced here, has already started. We will promote the use of this developed product to contribute to further improving the safety of automobiles in the future.

Table 1 Comparison of various positive-lock mechanisms

Items	Wedge Gear	No positive-lock mechanism	Multi-plate method	Plain gear method
Tilt operability	◎	◎	○	◎
Lever operability for tightening	◎	◎	◎	△
Positive-lock performance	◎	△	○	◎

Megapositioner of Highly Rigid, Ultralarge-Torque-Output, Rotary Positioning Units

Manufacturing equipment for liquid crystal display TVs and solar cells has been getting larger in recent years with increases in panel size. Additionally, improvements in large component manufacturing facilities for automobiles have made them faster and more accurate.

NSK has developed the Megapositioner (Photo 1) to respond to needs related to high-speed and high-accuracy rotational positioning of such large and heavy equipment. This article introduces the product.

Photo 1 Megapositioner of highly rigid, ultralarge-output-torque, rotary positioning units

1. Structure

Combining the Megatorque Motor and the precision speed reducer without backlash could achieve high torque and high accuracy with a compact size and enable high-speed and high-accuracy rotational positioning of large-size machinery.

2. Features

(1) High-speed positioning of large loads by inertia moment

Combining the Megatorque Motor and the precision speed reducer could achieve the positioning of work having an inertia moment of maximum 700 kg·m². Two types line up for the maximum output torque of 500 N·m and 1 960 N·m.

Figure 1 shows the relationship between a load inertia moment and output torque of the Megapositioner.

(2) High-accuracy positioning

Combining the Megatorque Motor and the precision speed reducer without backlash could achieve the repetitive accuracy of positioning within ± 5 arcseconds (Specifications of precision positioning). Figure 2 shows the measurement results of positioning accuracy per one revolution of the output shaft.

(3) Compact size, but compatibility of high rigidity and through hole of large diameter

Compact design with the low profile of 222 mm (SR6 series), but the permissible moment load of 9 000 N·m (at a single moment load) and high rigidity were achieved.

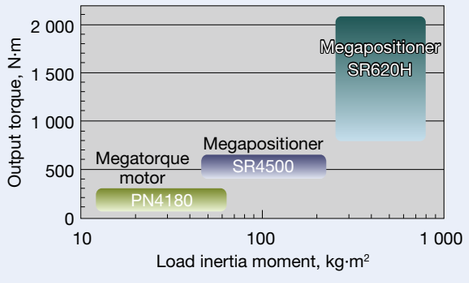

Fig. 1 Applicable ranges of Megapositioners

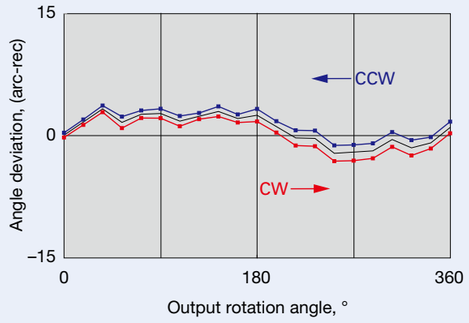

Fig. 2 Positioning accuracy per 1 revolution of output shaft

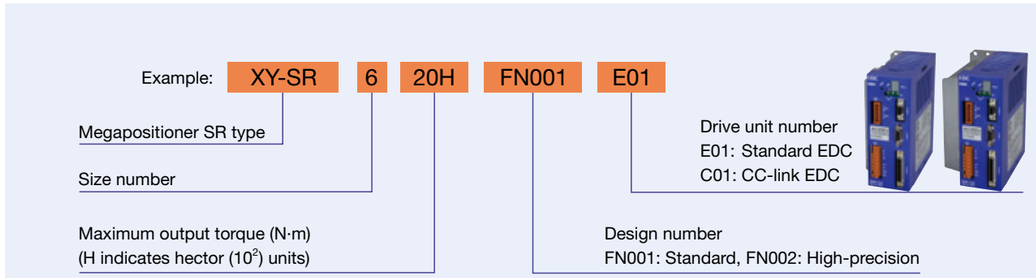

Fig. 3 Example of a Megapositioner nomenclature

(4) Megatorque Motor used as a drive unit

The Megatorque Motor with a built-in controller function is used as a drive unit. Therefore, it is possible to start up and operate in the same way as the Megatorque Motor.

3. Reference Number and Specifications

Figure 3 shows the example of the reference number and Table 1 shows the specifications of Megapositioners.

Table 1 Specifications of Megapositioners

Item \ Model	XY-SR4500FN001	XY-SR4500FN002	XY-SR620HFN001	XY-SR620HFN002
Max. torque (N·m)	500		1 960	
Rated torque (N·m)	80		520	
Max. speed (s^{-1})	0.42		0.21	
Rated speed (s^{-1})	0.25		0.04	
Speed reduction ratio	20		24	
Sensor resolution (counts/rev)	52 428 800		62 914 560	
Accuracy (arc-rec)	60	40	60	40
Repeatability (arc-rec)	± 15	± 5	± 15	± 5
Rotor runout (μm)	10			
Max. axial load (N)	11 600		32 700	
Max. radial load (N)	10 200		28 900	
Max. moment load (N·m)	820		2 770	
Max. load inertia (kg·m²)	200		700	
Weight (kg)	100		240	
Environmental conditions	5 to 40 °C temperature, 20 to 80% humidity. In indoor use, free from dust, condensation and corrective gas.			

4. Summary

Mass production of this Megapositioner has already started. We will promote its development to meet the future needs of users.

PX Series of High-Acceleration Megatorque Motors

Due to increased demand for smartphones and liquid crystal TVs in East Asian countries such as China, Taiwan and South Korea, production of electronic components such as light emitting diodes (LEDs) has increased rapidly. In addition, in Japan, Europe, and America, there is growing demand for automotive ICs for the automotive industry due to the growing need for energy conservation and safety. There is also strong demand for improved throughput and reliability of inspection equipment for such products. To meet these needs, NSK has developed the new PX series of high-acceleration Megatorque Motor (Photo 1), aiming for the dramatic reduction of positioning time and improvement of stopping accuracy when the inertia moment is small (hereinafter called light load).

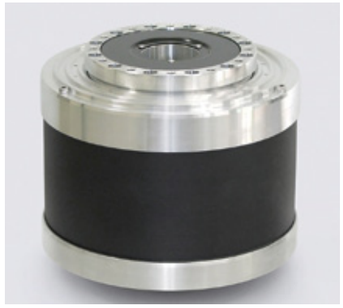

Photo 1 PX series of Megatorque Motor

1. Structure

NSK started mass production of Megatorque Motors in 1985 and has been leading the market for direct drive motors. Presently, two series of Megatorque Motors are available. One is the PS series for high-speed transfer of medium and lightweight items, and the other is the PN series for high-speed transfer of large, heavy items.

NSK lines up the PX series (Figure 1) specific to high-speed positioning of light load. These are for the recent production expansion of electronic components.

2. Features

(1) Reduced positioning time with high acceleration and deceleration

The ratio of output torque against inertia is improved and double acceleration and deceleration are achieved by reducing the rotor diameter of the motor and designing the winding to produce high output, compared to earlier models.

(2) Improved transfer accuracy through enhanced rigidness of structure around bearings

The rigidness of the structure around bearings is enhanced to suppress vibration of the rotary table. The projection structure of the output side surface is designed to prevent the heat generated by the motor from reaching the rotary table, which would affect accuracy.

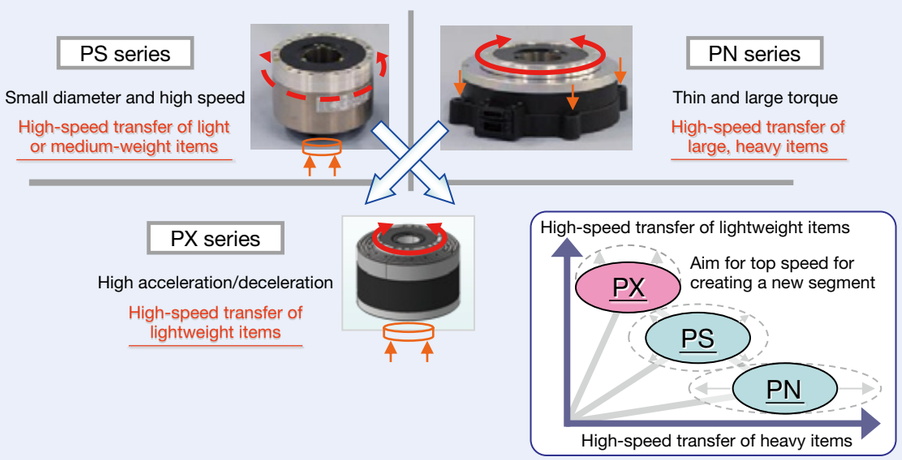

Fig. 1 Product portfolio of Megatorque Motors

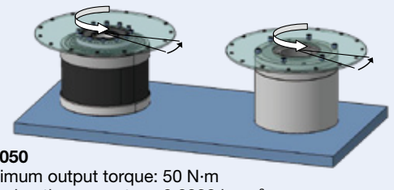

PX3050
Maximum output torque: 50 N·m
Rotor inertia moment: 0.0028 kg·m^2

PS3060
Maximum output torque: 60 N·m
Rotor inertia moment: 0.019 kg·m^2

Fig. 2 Comparison of PX3050 and PS3060

(3) Compact and a large hollow diameter

While the outer diameter size of PX3 remains the same as earlier products at Φ 160 mm, it is possible to replace the earlier model. The hollow diameter is Φ 35 mm to allow room for suction nozzle tubing and signal wiring.

Figure 2 and Figure 3 show the results of the positioning test. The light load item (inertia moment: 0.005 kg·m^2) was mounted on PX3050 (new series) and the positioning angle was 15° for the test. The same test was carried out using PS3060 (current series) for comparison. Figure 2 shows the rotor inertia moments of both motors.

Rotational acceleration was improved from 320 s^{-2} to 770 s^{-2}, and the positioning time was shortened from 29.8 ms to 19.6 ms, as shown in Figure 3. The superiority of the PX motor in light load positioning is also shown.

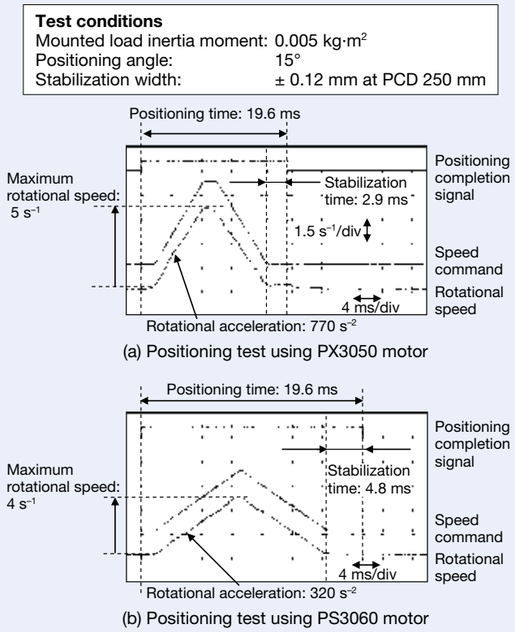

Fig. 3 Comparison of positioning times of PX3050 and PS3060 under light loads

3. Applications

An automatic inspection and selection device called the handler is used in the final process of assembling electronic components such as LEDs and ICs. Among the devices, “turret type” means the system to allocate the several inspection processes radially and transfer the components to be inspected on the rotary table (Figure 4).

Mechanical indexes were used in the past, but it was difficult to meet the needs for both higher acceleration/deceleration and precise positioning at the same time, and the results of its replacement by the Megatorque Motor have been increasing. It is expected to improve the throughput and line operating ratio, improve inspection accuracy, and improve the selecting ratio.

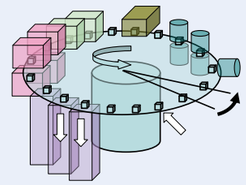

Fig. 4 Turret-type test handler system

4. Summary

The market for Megatorque Motors has been growing while steadily catching the large evolution flows of industry, such as the mounting to the assembly machines (starting with the automotive industry), the maturation of the semiconductor manufacturing equipment industry, and diffusion of the media of CDs and DVDs.

East Asia is becoming a major manufacturing cluster for electronic components such as LEDs, and direct-drive motors have been getting considerable attention as a means of achieving an easier, speedier, and higher-precision rotation mechanism.

The industrial structure of smartphones and liquid crystal TVs has been changing. We will continue to evolve the PX series while identifying the diversified needs, and we hope to support the industries from below.

Worldwide Sales Offices

P: Phone F: Fax ☆: Head Office

NSK LTD.-HEADQUARTERS, TOKYO, JAPAN

Nissei Bldg., 1-6-3 Ohsaki, Shinagawa-ku, Tokyo 141-8560, Japan

INDUSTRIAL MACHINERY BUSINESS DIVISION-HEADQUARTERS
P: +81-3-3779-7227 F: +81-3-3779-7644

AUTOMOTIVE BUSINESS DIVISION-HEADQUARTERS
P: +81-3-3779-7189 F: +81-3-3779-7917

●Africa

South Africa:

NSK SOUTH AFRICA (PTY) LTD.

SANDTON 27 Galaxy Avenue, Linbro Business Park, Sandton 2146, South Africa
P: +27-11-458-3600 F: +27-11-458-3608

●Asia and Oceania

Australia:

NSK AUSTRALIA PTY. LTD.

MELBOURNE ☆ 11 Dalmore Drive, Scoresby, Victoria 3179, Australia
P: +61-3-9765-4400 F: +61-3-9764-8304

SYDNEY Unit 10, 24-28 River Road West, Parramatta, New South Wales, 2150, Australia
P: +61-2-8843-8100 F: +61-2-9893-8406

BRISBANE 1/69 Selhurst Street, Coopers Plains, Queensland 4108, Australia
P: +61-7-3347-2600 F: +61-7-3345-5376

PERTH Unit 1, 71 Tacoma Circuit, Canning Vale, Western Australia 6155, Australia
P: +61-8-9256-5000 F: +61-8-9256-1044

New Zealand:

NSK NEW ZEALAND LTD.

AUCKLAND 3 Te Apunga Place, Mt. Wellington, Auckland 1060, New Zealand
P: +64-9-276-4992 F: +64-9-276-4082

China:

NSK (SHANGHAI) TRADING CO., LTD.

JIANGSU No.8 NSK Rd., Huaqiao Economic Development Zone, Kunshan, Jiangsu, China (215332)
P: +86-512-5796-3000 F: +86-512-5796-3300

NSK (CHINA) INVESTMENT CO., LTD.

JIANGSU ☆ No.8 NSK Rd., Huaqiao Economic Development Zone, Kunshan, Jiangsu, China (215332)
P: +86-512-5796-3000 F: +86-512-5796-3300

BEIJING Room 2116, Beijing Fortune Bldg., 5 Dong San Huan Bei Lu, Chao Yang District, Beijing, China (100004)
P: +86-10-6590-8161 F: +86-10-6590-8166

TIAN JIN Room 06, 09F The Exchange Tower 2, No. 189 NanJing Road, Heping District, Tianjin, China (300050)
P: +86-22-8319-5030 F: +86-22-8319-5033

CHANGCHUN Room 2311, Building A, Zhongyin Building, 727 Xi'an Road, Changchun, Jilin, China (130061)
P: +86-431-8898-8682 F: +86-431-8898-8670

SHENYANG Room 1101, China Resources Building, No. 286 Qingnian Street, Heping District, Shenyang Liaoning, China (110004)
P: +86-24-2334-2868 F: +86-24-2334-2058

DALIAN Room 1805 Xiwang Tower, No.136 Zhongshan Road, Zhongshan District, Dalian, Liaoning, China (116001)
P: +86-411-8800-8168 F: +86-411-8800-8160

NANJING Room A1 22F, Golden Eagle International Plaza, No.89 Hanzhong Road, Nanjing, Jiangsu, China (210029)
P: +86-25-8472-6671 F: +86-25-8472-6687

FUZHOU Room 1801-1811, B1#1A Class Office Building, Wanda Plaza, No.8 Aojiang Road, Fuzhou, China (350009)
P: +86-591-8380-1030 F: +86-591-8380-1225

WUHAN Room 1110, New World International Trade Tower I, No.568 Jianshe Road, Wuhan, Hubei, China (430000)
P: +86-27-8556-9630 F: +86-27-8556-9615

QINGDAO Room 802, Farglory International Plaza, No.26 Xianggang Zhong Road, Shinan District, Qingdao, Shandong, China (266071)
P: +86-532-5568-3877 F: +86-532-5568-3876

GUANGZHOU Room 2302, TaiKoo Hui Tower 1, No.385 Tianhe Road, Tianhe District, Guangzhou, China (510620)
P: +86-20-3817-7800 F: +86-20-3786-4501

CHANGSHA Room 1048, 10/F, Zhongtian Plaza, No.766 WuyiRoad, Changsha, Hunan, China (410005)
P: +86-731-8571-3100 F: +86-731-8571-3255

LUOYANG Room 1108, Fangda Hotel, 6 XiYuan Road, LuoYang HeNan, China (471003)
P: +86-379-6069-6188 F: +86-379-6069-6180

XI'AN Room 1007, B Changan Metropolls Center88 Nanguanzheng Steet, Xi'an, Shanxi, China (710068)
P: +86-29-8765-1896 F: +86-29-8765-1895

CHONGQING Room 2306, Unit B, No.137, Keyuan 2nd Road, Jiulongpo District, Chonqing, China (400039)
P: +86-23-6806-5310 F: +86-23-6806-5292

CHENGDU Room1117, Lippo Tower, No.62 North Kehua Road, Chengdu, Sichuan, China (610041)
P: +86-28-8528-3680 F: +86-28-8528-3690

NSK CHINA SALES CO., LTD.

JIANGSU No.8 NSK Rd., Huaqiao Economic Development Zone, Kunshan, Jiangsu, China (215332)
P: +86-512-5796-3000 F: +86-512-5796-3300

NSK HONG KONG LTD.

HONG KONG ☆ Suite 705, 7th Floor, South Tower, World Finance Centre, Harbour City, T.S.T, Kowloon, Hong Kong, China
P: +852-2739-9933 F: +852-2739-9323

SHENZHEN Room 624-626, 6/F, Kerry Center, Renminnan Road, Shenzhen, Guangdong, China
P: +86-755-25904886 F: +86-755-25904883

Taiwan:

TAIWAN NSK PRECISION CO., LTD.

TAIPEI ☆ 11F., No.87, Song Jiang Rd., Jhongshan District, Taipei City 104, Taiwan R.O.C.
P: +886-2-2509-3305 F: +886-2-2509-1393

TAICHUNG 3F. -2, No. 540, Sec. 3, Taiwan Blvd., Xitun Dist., Taichung City 407, Taiwan R.O.C.
P: +886-4-2708-3393 F: +886-4-2708-3395

TAINAN 5F. No.8, Daye 1st Rd., Southern Taiwan Science Park, Tainan City 741, Taiwan R.O.C.
P: +886-6-505-5861 F: +886-6-505-5061

TAIWAN NSK TECHNOLOGY CO., LTD.

TAIPEI ☆ 11F., No.87, Song Jiang Rd., Jhongshan District, Taipei City 104, Taiwan R.O.C.
P: +886-2-2509-3305 F: +886-2-2509-1393

TAICHUNG 10F-3, No.925, Sec.4, Taiwan Blvd., Xitun Dist., Taichung City 407, Taiwan R.O.C.
P: +886-4-2358-2945 F: +886-4-2358-7682

TAINAN 5F. No.8, Daye 1st Rd., Southern Taiwan Science Park, Tainan City 741, Taiwan R.O.C.
P: +886-6-505-5861 F: +886-6-505-5061

India:

NSK INDIA SALES CO.PVT.LTD.

CHENNAI ☆ 6th Floor, Bannari Amman Towers, No.29 Dr. Radhakrishnan Salai, Mylapore, Chennai-600 004 Tamil Nadu, India
P: +91-44-2847-9600 F: +91-44-2847-9601

GURGAON Unit No-202, 2nd Floor, Block-A, Iris Tech Park, Sector-48, Sohna Road, Gurgaon-122018, Haryana, India
P: +91-124-4104-530 F: +91-124-4104-532

MUMBAI 321, 'A' Wing, Ahura Centre, 82, Mahakali Caves Road, Andheri (East), Mumbai -400 093, India
P: +91-22-2838-7787 F: +91-22-2838-5191

Indonesia:

PT. NSK INDONESIA

JAKARTA Summitmas II, 6th Floor, Jl. Jend Sudirman Kav. 61-62, Jakarta 12190, Indonesia
P: +62-21-252-3458 F: +62-21-252-3223

Korea:

NSK KOREA CO., LTD.

SEOUL Posco Center (West Wing) 9F, 440, Teheran-ro, Gangnam-gu, Seoul, 135-777, Korea
P: +82-2-3287-0300 F: +82-2-3287-0345

Malaysia:

NSK BEARINGS (MALAYSIA) SDN. BHD.

SHAH ALAM ☆ No. 2, Jalan Pemaju, U1/15, Seksyen U1, Hicom Glenmarie Industrial Park, 40150 Shah Alam, Selangor, Malaysia
P: +60-3-7803-8859 F: +60-3-7806-5982

PRAI No.24, Jalan kikik, Taman Inderawasih, 13600 Prai, Penang, Malaysia
P: +60-4-3902275 F: +60-4-3991830

JOHOR BAHRU 88 Jalan Ros Merah 2/17, Taman Johor Jaya, 81100 Johor Bahru, Johor, Malaysia
P: +60-7-3546290 F: +60-7-3546291

IPOH Gr. Floor, 89 Jalan Bendahara, 31650 Ipoh, Perak, Malaysia
P: +60-5-2555000 F: +60-5-2553373

Philippines:

NSK REPRESENTATIVE OFFICE

MANILA 8th Floor The Salcedo Towers 169 H.V. dela Costa St., Salcedo Village Makati City, Philippines 1227
P: +63-2-893-9543 F: +63-2-893-9173

Singapore:

NSK INTERNATIONAL (SINGAPORE) PTE LTD.

SINGAPORE 238A, Thomson Road, #24-01/05, Novena Square Tower A, Singapore 307684
P: +65-6496-8000 F: +65-6250-5845

NSK SINGAPORE (PRIVATE) LTD.

SINGAPORE 238A, Thomson Road, #24-01/05, Novena Square Tower A, Singapore 307684
P: +65-6496-8000 F: +65-6250-5845

Thailand:

NSK BEARINGS (THAILAND) CO.,LTD.

BANGKOK 26 Soi Onnuch 55/1 Pravet Subdistrict, Pravet District, Bangkok 10250, Thailand
P: +66-2320-2555 F: +66-2320-2826

Vietnam:

NSK VIETNAM CO., LTD.

HANOI Techno Center, Room 204-205, Thang Long Industrial Park, Dong Anh District, Hanoi, Vietnam
P: +84-4-3955-0159 F: +84-4-3955-0158

NSK REPRESENTATIVE OFFICE

HO CHI MINH CITY Suite 307, Metropolitan Building, 235 Dong Khoi Street, District 1,HCMC, Vietnam
P: +84-8-3822-7907 F: +84-8-3822-7910

Worldwide Sales Offices

P: Phone F: Fax ☆: Head Office

●Europe

United Kingdom:

NSK EUROPE LTD. (EUROPEAN HEADQUARTERS)

MAIDENHEAD Belmont Place, Belmont Road, Maidenhead, Berkshire SL6 6TB, U.K.
P: +44-1628-509-800 F: +44-1628-509-808

NSK UK LTD.

NEWARK Northern Road, Newark, Nottinghamshire NG24 2JF, U.K.
P: +44-1636-605-123 F: +44-1636-605-000

France:

NSK FRANCE S.A.S.

PARIS Quartier de l'Europe, 2 Rue Georges Guynemer, 78283 Guyancourt, France
P: +33-1-30-57-39-39 F: +33-1-30-57-00-01

Germany:

NSK DEUTSCHLAND GMBH

DUSSELDORF ☆ Harkortstrasse 15, D-40880 Ratingen, Germany
P: +49-2102-4810 F: +49-2102-4812-290

STUTTGART Liebknechtstrasse 33, D-70565 Stuttgart-Vaihingen, Germany
P: +49-711-79082-0 F: +49-711-79082-289

WOLFSBURG Tischlerstrasse 3, D-38440 Wolfsburg, Germany
P: +49-5361-27647-10 F: +49-5361-27647-70

Italy:

NSK ITALIA S.P.A.

MILANO Via Garibaldi 215, Garbagnate Milanese (Milano) 20024, Italy
P: +39-299-5191 F: +39-299-025778

Netherlands:

NSK EUROPEAN DISTRIBUTION CENTRE B.V.

TILBURG De Kroonstraat 38, 5048 AP Tilburg, Netherlands
P: +31-13-4647647 F: +31-13-4647648

Poland:

NSK REPRESENTATIVE OFFICE

WARSAW Ul. Migdalowa 4/73, 02-796, Warsaw, Poland
P: +48-22-645-1525 F: +48-22-645-1529

Russia:

NSK POLSKA SP. Z O.O.

SAINT-PETERSBURG Office I 703, Bldg 29, 18th Line of Vasilievskiy Ostrov, Saint-Petersburg, Russia, 199178
P: +7-812-332-5071 F: +7-812-332-5072

Spain:

NSK SPAIN S.A.

BARCELONA C/Tarragona, 161 Cuerpo Bajo, 2a Planta, 08014, Barcelona, Spain
P: +34-93-289-2763 F: +34-93-433-5776

Turkey:

NSK RULMANLARI ORTA DOGU TIC. LTD. STI.

ISTANBUL 19 Mayis Mah. Ataturk Cad., Ulya Engin Is Merkezi No: 68 Kat. 6, P.K. : 34734, Kozyatagi-Istanbul, Turkey
P: +90-216-477-7111 F: +90-216-477-7174

United Arab Emirates:

NSK BEARINGS GULF TRADING CO.

DUBAI JAFZA View 19, Floor 24 Office LB192402/3, PO Box 262163, DownTown Jebel Ali, Dubai, UAE
P: +971-4-804-8207 F: +971-4-884-7227

●North and South America

United States of America:

NSK AMERICAS, INC. (AMERICAN HEADQUARTERS)

ANN ARBOR 4200 Goss Road, Ann Arbor, Michigan 48105, U.S.A.
P: +1-734-913-7500 F: +1-734-913-7511

NSK CORPORATION

ANN ARBOR 4200 Goss Road, Ann Arbor, Michigan 48105, U.S.A.
P: +1-734-913-7500 F: +1-734-913-7511

NSK PRECISION AMERICA, INC.

FRANKLIN ☆ 3450 Bearing Drive, Franklin, Indiana 46131, U.S.A.
P: +1-317-738-5000 F: +1-317-738-5050

SAN JOSE 780 Montague Expressway, Suite 504, San Jose, California, 95131, U.S.A.
P: +1-408-944-9400 F: +1-408-944-9405

NSK LATIN AMERICA, INC.

MIAMI 3470 NW 82 Avenue Suite 625, Miami FL 33122, U.S.A.
P: +1-305-477-0605 F: +1-305-477-0377

Canada:

NSK CANADA INC.

TORONTO ☆ 5585 McAdam Road, Mississauga, Ontario, Canada L4Z 1N4
P: +1-905-890-0740 F: +1-800-800-2788

MONTREAL 2150-32E Avenue Lachine, Quebec, Canada H8T 3H7
P: +1-514-633-1220 F: +1-800-800-2788

VANCOUVER 3353 Wayburne Drive, Burnaby, British Columbia, Canada V5G 4L4
P: +1-877-994-6675 F: +1-800-800-2788

Argentina:

NSK ARGENTINA SRL

BUENOS AIRES Garcia del Rio 2477 Piso 7 Oficina "A" (1429) Buenos Aires-Argentina
P: +54-11-4704-5100 F: +54-11-4704-0033

Brazil:

NSK BRASIL LTDA.

SAO PAULO ☆ Rua 13 de Maio, 1633-14th Andar-Bela Vista-CEP 01327-905 São Paulo, SP, Brazil
P: +55-11-3269-4786 F: +55-11-3269-4720

BELO HORIZONTE Rua Ceara 1431-4th andar-sala 405-Funcionarios Belo Horizonte-MG, Brazil 30150-311
P: +55-31-3274-2591 F: +55-31-3273-4408

JOINVILLE Rua Blumenau, 178-sala 910-Centro Joinville-SC, Brazil 89204-250
P: +55-47-3422-5445 F: +55-47-3422-2817

PORTO ALEGRE Av. Cristovão Colombo, 1694-sala 202-Floresta Porto Alegre-RS, Brazil 90560 001
P: +55-51-3222-1324 F: +55-51-3222-2599

RECIFE Av. Conselheiro Aguiar, 2738-6th andar-conj. 604-Boa Viagem Recife-PE, Brazil 51020-020
P: +55-81-3326-3781 F: +55-81-3326-5047

Peru:

NSK PERU S.A.C.

LIMA Av. Caminos del Inca 670, Ofic : # 402, Santiago del Surco, Lima, Perú
P: +51-1-652-3372 F: +51-1-638-0555

Mexico:

NSK RODAMIENTOS MEXICANA, S.A. DE C.V.

MEXICO CITY ☆ Av. Presidente Juarez No.2007 Lote 5, Col. San Jeronimo Tepetlacalco, Tlalnepantla, Estado de Mexico, Mexico, C.P.54090
P: +52-55-3682-2900 F: +52-55-3682-2937

MONTERREY Av. Ricardo Margain 575, IOS Torre C, Suite 516, Parque Corporativo Santa Engracia, San Pedro Garza Garcia, N.L. Mexico, C.P.66267
P: +52-81-8000-7300 F: +52-81-8000-7095

<As of January 2015>

For the latest information, please refer to the NSK website.
www.nsk.com

Motion & Control

No. 25 September 2015

Published by NSK Ltd.

Eco-awareness and reliability in motion

NSK

NSK used environmentally friendly printing methods for this publication.

CAT. No. ETJ-0025 2015 C-9 Printed in Japan